A Minimal Nuclear Energy Density Functional

Aurel Bulgac,[1,*] Michael McNeil Forbes,[2,1,†] Shi Jin,[1,‡] Rodrigo Navarro Perez,[3,§] and Nicolas Schunck[3,¶]

[1]*Department of Physics, University of Washington, Seattle, Washington 98195–1560, USA*
[2]*Department of Physics & Astronomy, Washington State University, Pullman, Washington 99164–2814, USA*
[3]*Nuclear and Chemical Science Division, Lawrence Livermore National Laboratory, Livermore, CA 94551, USA*

(Dated: August 30, 2017)

We present a minimal nuclear energy density functional (NEDF) called "SeaLL1" that has the smallest number of possible phenomenological parameters to date. SeaLL1 is defined by 7 significant phenomenological parameters, each related to a specific nuclear property. Even in its present form, which is not yet fully optimized, the SeaLL1 NEDF describes the nuclear masses of 606 even-nuclei from the AME2012 evaluation [1, 2] with a mean energy error of 0.97 MeV and a standard deviation 1.46 MeV, two-neutron and two-proton separation energies with rms errors of 0.69 MeV and 0.59 MeV respectively, and the charge radii of 345 even-even nuclei [3] with an rms error of 0.034 fm. SeaLL1 incorporates the equation of state of pure neutron matter from quantum Monte Carlo calculations with chiral effective field theory two-body (NN) interactions at N3LO level and three-body (NNN) interactions at the N2LO level. Two of the 7 parameters are related to the saturation density and the energy per particle of the homogeneous symmetric nuclear matter; one is related to the nuclear surface tension; two are related to the symmetry energy and its density dependence; one is related to the strength of the spin-orbit interaction; and one is the coupling constant of the pairing interaction. We identify additional phenomenological parameters that have little effect on the previous properties, but can be used to fine tune other nuclear features such as the Thomas-Reiche-Kuhn sum rule, the excitation energy of the giant dipole and Gamow-Teller resonances, the static dipole electric polarizability, and the neutron skin thickness.

CONTENTS

* bulgac@uw.edu
† mforbes@alum.mit.edu
‡ js1421@uw.edu
§ rnavarrop@ugr.es
¶ schunck1@llnl.gov

I. INTRODUCTION

Achieving accurate and precise calculations of nuclear masses, charge and neutron distributions, nuclear matter properties, and dynamics, from a microscopic approach remain one of the most challenging problems in quantum many-body theory. Almost a century ago, Aston [4] realized that a nucleus is not quite the sum of its parts. This lead Eddington [5] to correctly conjecture a link between nuclear masses, the conversion of hydrogen into heavier elements, and the energy radiated by the stars. An accurate theoretical model of nuclear masses, particularly close to the neutron drip line and with an uncertainty of better than 100 keV (an accuracy which has not been achieved yet even for known stable nuclei) will have a great impact on predicting the origin and the abundances of elements in the Universe [6, 7].

When quantum mechanics was first applied to many-body systems, Weizsäcker [8] proposed that an energy density approach could be an effective tool for calculating nuclear binding energies. This was the first instance of an energy density functional being applied in nuclear physics, several decades *before*

a_v	a_s	a_I	a'_I	a_C	a'_C	δ	χ_E
−15.47	16.73	22.87	0	0.699	0	0	3.30
−15.49	16.78	22.91	0	0.700	0	12.29	3.18
−15.32	17.76	24.96	−22.60	0.767	−0.675	0	2.64
−15.34	17.80	25.01	−22.43	0.767	−0.661	11.46	2.50
−15.77	17.50	23.65	0	0.723	0	0	1.87
−15.46	18.29	25.72	−26.00	0.792	−0.773	0	1.53

Table I. Parameters and the energy rms of the mass formulas Eqs. (1) or (2), with or without the even-odd staggering correction Eq. (2b). Here $\chi_E^2 = \sum |E_{N,Z} - E(N,Z)|^2/N_E$ and we fit the $N_E = 2375$ measured (not extrapolated) nuclear masses of nuclei with $A \geq 16$ from Audi *et al.* [1] and Wang *et al.* [2] and an evaluated uncertainty less than 1 MeV with the electronic correction. (All quantities expressed in MeV.) The last two rows show how the mass formulas Eqs. (1) or (2) fit the theoretical nuclear masses computed using the SeaLL1 functional.

the foundation of density functional theory (DFT) [9–11] was formulated. Bethe and Bacher [12] further developed Weizsäcker's ideas and introduced the nuclear mass formula (the Bethe-Weizsäcker formula) for the ground state energies of nuclei with $A = N + Z$ nucleons (N neutrons and Z protons):

$$E(N,Z) = a_v A + a_s A^{2/3} + a_C \frac{Z^2}{A^{1/3}} + a_I \frac{(N-Z)^2}{A}. \quad (1)$$

Unlike electrons in atoms, nuclei are saturating systems with a nearly constant interior density. This yields the terms in Eq. (1) referred to as: a volume energy, a surface tension, a non-extensive Coulomb energy, and a symmetry energy that favors similar numbers of protons and neutrons. (Due to the presence of the long-range Coulomb interaction, the terms "volume" and "surface" do not have a strict thermodynamic meaning.) As shown in the first row of Table I, these four terms alone fit the AME2012 evaluated nuclear masses [1, 2] with a root-mean-square (rms) error of χ_E=3.30 MeV per nucleus. This is a remarkable result: the nuclear binding energy of heavy nuclei can reach 2000 MeV, hence the errors are at the sub-percent level.

A slightly better fit is obtained using a mass formula with surface corrections terms to the symmetry and Coulomb energies, as well as odd-even staggering correction due to pairing:

$$E(N,Z) = a_v A + a_s A^{2/3} + a_C \frac{Z^2}{A^{1/3}} + a'_C \frac{Z^2}{A^{2/3}} + a_I \frac{(N-Z)^2}{A} + a'_I \frac{(N-Z)^2}{A^{4/3}} + \Delta. \quad (2a)$$

$$\Delta = \begin{cases} -\delta A^{-1/2} & \text{even-even nuclei,} \\ 0 & \text{odd nuclei,} \\ \delta A^{-1/2} & \text{odd-odd nuclei.} \end{cases} \quad (2b)$$

This pairing contribution is significantly smaller than the others, with an amplitude $\approx 12\,\mathrm{MeV}/A^{1/2}$. It is also smaller

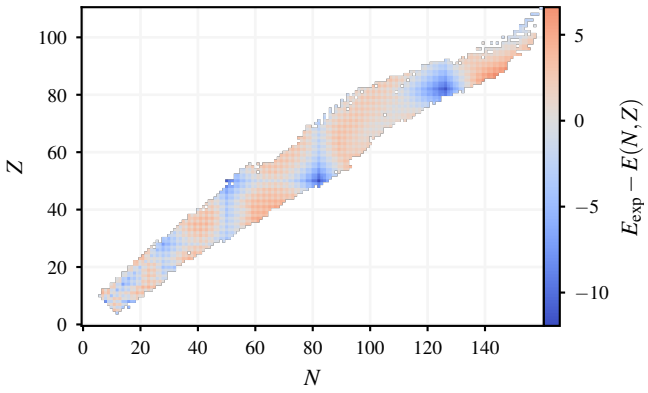

Figure 1. (Color online) The differences $E_{\rm exp} - E_{\rm th}$ in MeVs between the evaluated ground state energies [1, 2] of 2375 nuclei with $A \geq 16$ and fitted with the 6-parameter mass formula Eq. (2) and $\Delta \equiv 0$. One can easily identify the location of closed shells (the blue regions) for protons and neutrons.

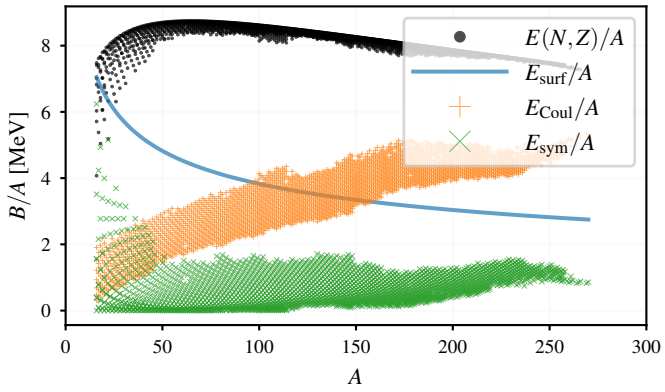

Figure 2. (Color online) The binding energy per nucleon $B/A = |E(N,Z)|/A$ and the Coulomb, surface and symmetry energy per nucleon in Eq. (2) for the measured 2375 nuclei with $A \geq 16$ [1, 2].

than contributions arising from shell-correction energies (discussed below), changing the rms error χ_E by about at most 150 keV. This fit is shown in Table I and the residuals are displayed in Fig. 1. The magnitudes of the various terms are compared in Fig. 2, which shows that the volume, surface, and Coulomb contributions are dominant, while the symmetry energy contribution is roughly at the level of 10%.

There are several possible ways to determine the volume, surface, symmetry, etc. coefficients of (1) or (2). For example, one may turn off the Coulomb interaction, and extract volume, surface, and symmetry energy from the asymptotic behavior of the energy of nuclei with very large numbers of protons and neutrons [13]. This corresponds to considering the thermodynamic limit, which is not realized in real nuclei due to the presence of the long-range Coulomb interaction among the protons. We prefer instead a unified approach, determining the parameters by directly fitting almost all nuclear binding energies, whether experimental or computed. (See last two rows of Table I.)

In a parallel development, properties of many-fermion sys-

tems were understood in mathematical physics by tying together the roles of the geometry and of the periodic trajectories in cavities. As early as 1911, Weyl [14, 15, 16, 17, 18, 19, 20] and others related the wave eigenstate density in boxes of various shapes and boundary conditions to the geometrical shape of the box [21–24]. In a manner similar to the nuclear mass formula Eq. (1), this approach can be applied to saturating systems, relating the ground state energy to the volume (V), surface area (A), and mean curvature radius R of the many-particle system [13]:

$$E = a_V V + a_S S + a_R R + \dots . \tag{3}$$

The similarity between (3) and the nuclear mass formula (1) become apparent after relating the volume to the particle number $n = A/V \approx$ const. (The Coulomb repulsion energy cannot be evaluated separately in a straightforward manner due to the long-range character of the interaction.) The ground state energy can thus be rewritten in terms of particle number A (here for only one kind of particles)

$$E = b_V A + b_S A^{2/3} + b_R A^{1/3} + \dots . \tag{4}$$

The coefficient b_V is the energy per particle in infinite matter and a_S represents the surface tension. These types of expansion are classical in character: Planck's constant plays no explicit role. Their accuracy for many-fermion systems is thus limited by the lack of quantum effects (often referred to as shell effects). It appears that for nuclei, the mass formula Eq. (2) is about as good as one can achieve without introducing the quantum effects.

There is a long debate in literature ,fueled mainly by studies of quantum chaos, about whether an expansion in powers of A can be extended beyond the terms present in Eq. (4). Naïvely, one might expect the next terms to be proportional to A^0, $A^{-1/3}$, and so forth, but a a more careful analysis shows that that is not correct. (See for example Brack and Bhaduri [24].) The next term is instead proportional to $A^{1/6}$ [25–28], arising from the contribution of periodic orbits. Subsequent terms appear to be stochastic, due to the inherent chaotic character of the interacting many-body systems [29].

Gutzwiller [30], Balian and Bloch [25, 26, 27], and Berry and Tabor [31, 32] observed that quantum states in a finite system can be quite accurately reproduced by quantizing the periodic classical trajectories. (See also Brack and Bhaduri [24].) Combining the idea of geometric quantization, with the Thomas-Fermi model, the Pauli principle, and copious empirical evidence that strongly interacting fermionic systems share many similarities with non-interacting systems [33–39], one can quite accurately construct the single-particle density of states and binding energies as a function of the particle number, eventually correcting this by the shape of the system.

The single-particle density of states $n(\varepsilon)$ in a given potential has a smooth and an oscillating components:

$$n(\varepsilon) = n_{\rm TF}(\varepsilon) + n_{\rm osc}(\varepsilon), \tag{5a}$$

$$n_{\rm osc}(\varepsilon) = \sum_{\rm PO} a_{\rm PO}(\varepsilon) \sin\left(\frac{S_{\rm PO}(\varepsilon)}{\hbar} + \phi_{\rm PO}\frac{\pi}{2}\right) + \dots , \tag{5b}$$

where the sum is performed over classical periodic orbits (PO) (diameter, triangles, squares, etc.). Here, $a_{\rm PO}(\varepsilon)$ is the stability amplitude, $S_{\rm PO}(\varepsilon)$ the action, and $\phi_{\rm PO}$ the Maslov index of each orbit at the energy ε [24–27, 40]. The single-particle density of states in the Thomas-Fermi approximation $n_{\rm TF}$ [14–24] has a clear dependence on the size and shape of the system, and leads to Eqs. (3) and (4) for a square-well potential. At the same time, the nature of the periodic orbits also depends on the size and shape of the single-particle potential. Knowing $n(\varepsilon)$, one can calculate the particle number A and shell-corrections (SC) $E_{\rm SC} = E - E_{\rm TF}$ for a many-fermion system by integrating up to the chemical potential μ:

$$A = \int_{-\infty}^{\mu} n(\varepsilon){\rm d}\varepsilon, \qquad E_{\rm SC} = \int_{-\infty}^{\mu} \varepsilon n_{\rm osc}(\varepsilon){\rm d}\varepsilon. \tag{6}$$

The theory of periodic orbits and structure of these shell-corrections has been studied extensively. For example, in a 3-dimensional spherical cavity, quantum effects can be reproduced by including only triangular and square orbits [24–27, 40]. The emergence of magic numbers, and the role of the shapes of many-fermion systems have been tested in theory and validated against experimental results in fermion systems with up to 3000 electrons [41–43]. In particular, in atomic clusters, the emergence of super-shells has been predicted theoretically [40, 42, 44] and confirmed experimentally [41, 43]. (Nuclei are too small to exhibit of super-shells.)

In nuclear physics, a similar line of inquiry is encapsulated in the method of shell-corrections, developed by Strutinsky [45–47] and many others [28, 48–60]. This method shows that $n(\varepsilon)$ has a well defined dependence on the particle number. The smooth part of the density of states is quite well described by the Thomas-Fermi approximation (and by the smoothing procedure introduced by Strutinsky). The leading terms are the volume ($\sim A$), surface ($\sim A^{2/3}$), Coulomb ($\sim Z^2/A^{1/3}$), and symmetry energy ($\sim (N-Z)^2/A$) contributions encoded in the Bethe-Weizsäcker mass formula (1). The oscillating part is dominated by the nuclear shape and the shell effects from the periodic orbits, where the amplitude depends on the particle number as $A^{1/6}$ [28].

The separation of $n(\varepsilon)$ into the smooth and oscillating parts (5a) is a general characteristic of the many fermion systems. Both the macroscopic-microscopic method [28, 45–60] and self-consistent approaches [61–66] lead to the same conclusions about the various contributions described above, and agree with experimental data [67]. In all previous considerations of mass tables, either in self-consistent approaches or in microscopic-macroscopic models, the single-particle spectroscopic factors are modified only by pairing correlations. It is well-known, however, that the coupling between collective degrees of freedom and single-particle degrees of freedom lead to a significant fragmentation of the single-particle occupation probabilities, which are measured in pick-up and knock-out reactions [56, 68]. This fragmentation of the single-particle occupation probabilities is not taken into account in the single-particle density of states Eqs. (5) or in the definition of the single-particle densities Eqs. (10), and is likely to affect the exact magnitude of the shell-effects. The order of magnitude of these effects is perhaps a (small) fraction of the rms error

χ_E = 3.3 MeV of the Bethe-Weizsäcker mass formula (1). All of this this begs the question: To what order can one expand the density of states in powers of the particle numbers and periodic orbits?

There is a reasonable consensus that, beyond the leading contributions from the periodic orbits and shell-corrections, any such an expansion fails due to the effects of quantum chaos – i.e. contributions from classically chaotic trajectories through the many-body phase space [29]. Stable periodic orbits provide the strongest shell effects in quantum systems, evident for example in the magic numbers (see e.g. Fig. 20). Unstable periodic orbits also produce shell effects, but typically with smaller weights. In contrast, chaotic orbits appear to produce irregular oscillations in the single-particle density of states with a rather small amplitude. Various estimates suggest that chaotic fluctuations appear at the level of 0.5 MeV per nucleus [69–77], noticeably smaller than shell effects contributions due to periodic orbits and deformations, which are of the order of several MeVs.

The effect of periodic orbits is not limited to finite systems: the Casimir energy in quantum field theory [78, 79], critical phenomena [80, 81], and strongly interacting infinite inhomogeneous systems, e.g. nuclear pasta phase in neutron stars [82–88], can also be explained and calculated to high precision by evaluating the contributions from periodic orbits. This method has become the standard approach for evaluating the Casimir energy in a variety of fields [89–93].

It is somewhat surprising that shell effects from periodic orbits appear at the same level as deformation effects in the energy of nuclear systems. Naïvely one might expect the deformation energy to be controlled by the surface area of a saturating system, and thus to contribute as a correction to the surface term in nuclear mass formulas like Eqs. (1) and (2). However, the deformation energy in nuclei has a quantum nature, and is determined by a delicate interplay between the change in surface area and the shell effects. A similar behavior has been observed in the case of atomic clusters with up to 3000 electrons [44]. This leads to a leveling of the peaks, which one would otherwise expect in the absence of deformation, leaving in place only the large negative shell-corrections for the magic spherical systems, as seen in Fig. 20 for the case of nuclei.

The shape stability of a many-fermion system is controlled by the single-particle level density at the Fermi level. In an open-shell system this level density is high; the system can thus deform quite easily and single-particle levels can rearrange until the level density is low enough to render the system stable. The stabilization process of the nuclear deformation in the ground state is analogous to the Jahn-Teller effect in polyatomic molecules [94], where the high degeneracy of the ground state is lifted by the deformation of the system. This mechanism leads to new "magic numbers" in deformed systems as Strutinsky discussed in his seminal papers [45–47]. The increase in surface area and the energy penalty incurred (deformation energy) is canceled to a large extent by the shell-corrections (due to periodic orbits in the deformed potential), unless the system is "magic" or "semi-magic". The cancellation between deformation energy and shell effects suggests that open-shell systems should be easier to deform than magic systems. This is consistent with the character of the residuals remaining after fitting the nuclear binding energies with Bethe-Weizsäcker formulas like Eqs. (1) and (2) as shown in Fig. 1 and Fig. 20. The largest residuals appear as large (negative) spikes at the shell closures for spherical nuclei with magic numbers of either protons or/and neutrons, while the expected (positive) peaks in between magic numbers are flattened. From the nature of the residuals $E_{\rm exp} - E_{\rm th}$ in Fig. 1 – sharp negative spikes at the magic numbers, but roughly constant fluctuations in between – one can conclude that mass formulas of the type Eq. (2) do encode the role of the nuclear deformation. For open shell nuclei it thus appears that the deformation energy is roughly compensated by the shell-correction energy, and shell effects only survive near magic and semi-magic nuclei. A sufficiently accurate theory of nuclear masses may even aim to include contributions arising from quantum chaos.

A number of corrective terms might be considered to improve the accuracy of the nuclear mass formulas Eqs. (1) and (2). For example, in the Coulomb term, one might replace Z^2 with $Z(Z-1)$ to correctly count the number of proton pairs, and one might add an additional term proportional to Z to account for the Coulomb exchange interaction and screening [95]. Motivated by Eq. (4), one might also consider including terms proportional to $A^{1/3}$ and A^0. The symmetry energy terms might also be "corrected" by replacing $(N-Z)^2/4$ with $T(T+1)$ where $T = |N-Z|/2$. Finally, one might introduce an additional correction to account for the Wigner energy $\propto |N-Z|$, which appears as a cusp in the nuclear binding energies as a function of $N-Z$ (basically only for nuclei with $|N-Z| \leq 2$) [96]. However, including these corrections lead to very small improvements in the energy rms χ_E below the value 2.64 MeV obtained with the main terms of Eq. (2). These corrections are eclipsed by the shell effects as seen in Fig. 1.

The goal of this paper is to generate a phenomenological NEDF with the minimal number of physically motivated parameters required to describe static bulk nuclear properties. Specifically, we want to follow the spirit of DFT in electronic structure theory and require that our NEDF depend only on the local, intrinsic density of nucleons and gradient terms. We will consider two variants of our NEDF: the first one is in the spirit of Kohn-Sham [10] and requires using orbital-based techniques, that are formally similar to the Hartree-Fock-Bogoliubov (HFB) approximation by design. In nuclear physics such an approach was pioneered by Fayans [97, 98] and later also by Baldo *et al.* [99, 100]. Since working with orbitals is computationally expensive, we also present a second, orbital-free, variant of our NEDF in the spirit of Hohenberg-Kohn [9]. It is obtained from the orbital-based functional by a semiclassical approximation (with some corrections). The orbital-free functional has only 4 parameters that have all a well-defined physical interpretation as in the Bethe-Weisäcker formula. Although the orbital-free theory lacks shell corrections, it still does a remarkable job of describing nuclei on average, reproducing both binding energies and charge radii within a simple calculations framework. The orbital-based functional will be subsequently determined by a fine-tuning of the parameters of the orbital–free functional, and the addition of terms needed to describe the relatively smaller contributions arising from the spin-orbit interaction,

the pairing effects, and the density dependence of the symmetry energy.

There are a variety of many-body approaches based on the Schrödinger equation: the quantum Monte Carlo (QMC) method [101, 102], the self-consistent Green function method [103], the coupled-cluster method [104], and the in-medium renormalization method [105]. In all these approaches one has to specify the two-body (NN), three-body (NNN), etc. interactions between nucleons, the form of which is ambiguous depending on how the theory is regularized. Chiral effective field theory (EFT) [106, 107] provides a framework for organizing these interactions using the symmetries of the underlying theory quantum chromodynamics (QCD) of quarks and gluons with the hope that physical results are independent of the cutoff. There is still no guarantee, however, that this many-body expansion converges.

The DFT approach differs from approaches based on the Schrödinger equation, even though, in the case of many-electron systems, it has been established that there is a mathematical one-to-one correspondence between the number density and the wavefunction of a many-body system [9, 11]. In principle, this one-to-one correspondence leads to the existence of an exact energy density functional. In practice, however, this functional is extremely complicated and establishing a useful form is more of an art than a science. One particularly successful example is the unitary Fermi gas, which shares many properties with dilute neutron matter. In this case, the form of a local energy density functional follows using only dimensional arguments, renormalizability of the theory, Galilean invariance, and symmetries. This functional, called the superfluid local density approximation (SLDA) has been verified and validated against QMC calculations and experiments at the few percent level for a wide range of systems [108, 109]. Our approach here is motivated by similar considerations, leading to a simple and compact functional in which time-dependent phenomena can be computed with a similar computational cost to time-independent phenomena. Thus, unlike approaches based on Schrödinger equation which are primarly limited to static properties, the DFT can be applied to reactions, fission, time-dependent non-equilibrium phenomena, and for very heavy systems with remarkable accuracy.

Section II discusses the various components of both the orbital-based and orbital-free NEDF. Section III discusses a number of nuclear observables that are used as validation of the predictive power of the NEDF, such as global mass tables, density distributions, single-particle spectra, neutron skin, static fission properties, and properties of the neutron start crust. Section IV briefly discusses notable differences between our NEDF and others. Finally, our results are summarized in Section V.

II. FUNCTIONAL FORM OF THE NEDF

The lesson from our brief historical review is that, since nuclei are saturating systems with a rather well defined saturation density, the bulk of the nuclear binding energy should be fixed by the geometry of the nuclei (volume, surface area, curvature radius) to sub-percent accuracy. As demonstrated in Table I, the accuracy of the mass formulas Eqs. (1) and (2) – which both lack shell effects, deformation, spin-orbit effects, pairing, etc. – suggests that such a nuclear energy density functional (NEDF) should be capable of describing at a similar level of accuracy both the nuclear binding energies, and the proton and neutron matter density distribution. Therefore, we might reasonably expect that a NEDF will also describe the nuclear charge radii, for which there is a large amount of accumulated data [3]. Quantum effects enter at the level of a few MeVs per nucleus, reducing the rms energy error χ_E from around 3 MeV to about 0.5 MeV [58–60], and are most pronounced for magic or semi-magic nuclei, see Fig. 1.

We will describe a NEDF that depends on the smallest number of phenomenological parameters needed to account for all the contributions in the nuclear mass formulas Eqs. (1) and (2). First we relate these parameters to various physical quantities relevant for nuclear physics. For a large nucleus, the Coulomb energy can be used to estimate the saturation density n_0 by approximating the nucleus as a uniformly charged sphere with $E_C = 3Z^2e^2/5R = a_C Z^2/A^{1/3}$, where $R = r_0 A^{1/3}$ and $r_0 \approx 1.2\,\text{fm}$ is a nuclear length scale:

$$n_0 = \frac{3}{4\pi r_0^3}, \quad \text{where} \quad r_0 = \frac{3e^2}{5a_C}. \tag{7a}$$

One can further estimate the ground-state energy of infinite nuclear matter per nucleon ε_0, the nuclear surface tension σ, and their dependence on the isospin $(N-Z)/2$:

$$\varepsilon_0 = \frac{E(N,Z)}{A} = a_v + a_I \frac{(N-Z)^2}{A^2}, \tag{7b}$$

$$\sigma = a_s + a_I' \frac{(N-Z)^2}{A^2}. \tag{7c}$$

Finally, one can relate the value of the coefficient a_C' (or of the alternative coefficient of the contribution $a_C'' Z^2/A$ to the mass formula [51]) with the nuclear surface diffuseness.

For a NEDF to be as accurate as the mass formula, one thus expects no more than 5 or 6 significant parameters. As we shall see, such a functional does exist, requiring as few as 4 parameters, and demonstrating better accuracy than the original Bethe-Weizsäcker mass formula, with the additional property of predicting charge radii. That a functional depending on such a small number of phenomenological parameters can go beyond the capabilities of the empirical mass formula and also describe density distributions is truly remarkable.

We postulate a NEDF with three main contributions, which significantly improves on the Weizsäcker's original idea [8]:

$$\mathcal{E}[n_n, n_p] = \overbrace{\mathcal{E}_{\text{kin}}}^{\text{kinetic}} + \underbrace{\mathcal{E}_C}_{\text{Coulomb}} + \overbrace{\mathcal{E}_{\text{int}}}^{\text{interactions}}. \tag{8}$$

The first two terms – the kinetic energy and Coulomb energy – are well motivated and have no free parameters. All phenomenological parameters of the model appear in the interaction term

$\mathcal{E}_{\text{int}}$:

$$\mathcal{E}_{\text{int}} = \overbrace{\mathcal{E}_{\text{homo}}}^{\text{homogeneous}} + \underbrace{\mathcal{E}_{\boldsymbol{\nabla} n}}_{\text{gradients}} + \overbrace{\mathcal{E}_{\text{SO}}}^{\text{spin-orbit}} + \underbrace{\mathcal{E}_{\Delta}}_{\text{pairing}} + \overbrace{\mathcal{E}_{\text{entrain}}}^{\text{entrainment}}, \tag{9}$$

The Kohn-Sham formulation of the functional is specified in terms of the single-particle orbitals $\mathrm{v}_{k\sigma}(\boldsymbol{r}), \mathrm{v}_{k\sigma}(\boldsymbol{r})$ through the number, anomalous, kinetic, spin-density, current, and spin-current densities (for both neutron and protons):

$$n(\boldsymbol{r}) = \sum_{k,\sigma} \mathrm{v}^*_{k\sigma}(\boldsymbol{r})\mathrm{v}_{k\sigma}(\boldsymbol{r}), \tag{10a}$$

$$\nu(\boldsymbol{r}) = \sum_{k} \mathrm{v}^*_{k\uparrow}(\boldsymbol{r})\mathrm{u}_{k\downarrow}(\boldsymbol{r}), \tag{10b}$$

$$\tau(\boldsymbol{r}) = \sum_{k,\sigma} \boldsymbol{\nabla} v^*_{k\sigma}(\boldsymbol{r}) \cdot \boldsymbol{\nabla} v_{k\sigma}(\boldsymbol{r}), \tag{10c}$$

$$\boldsymbol{s}(\boldsymbol{r},\boldsymbol{r}') = \sum_{k,\sigma,\sigma'} v^*_{k\sigma}(\boldsymbol{r})\boldsymbol{\sigma}_{\sigma,\sigma'} v_{k\sigma'}(\boldsymbol{r}'), \tag{10d}$$

$$\boldsymbol{s}(\boldsymbol{r}) = \boldsymbol{s}(\boldsymbol{r},\boldsymbol{r}), \tag{10e}$$

$$\boldsymbol{j}(\boldsymbol{r}) = \sum_{k,\sigma} \frac{\boldsymbol{\nabla} - \boldsymbol{\nabla}'}{2\mathrm{i}} \mathrm{v}^*_{k\sigma}(\boldsymbol{r}') \cdot \mathrm{v}_{k\sigma}(\boldsymbol{r})\Big|_{\boldsymbol{r}=\boldsymbol{r}'}, \tag{10f}$$

$$\boldsymbol{J}(\boldsymbol{r}) = \frac{\boldsymbol{\nabla} - \boldsymbol{\nabla}'}{2\mathrm{i}} \times \boldsymbol{s}(\boldsymbol{r},\boldsymbol{r}')\Big|_{\boldsymbol{r}=\boldsymbol{r}'}. \tag{10g}$$

See [61, 110] and references therein for details. (Note: In nuclear physics literature proton and neutron number densities are typically denoted with the symbols $\rho_{n,p}(\boldsymbol{r})$. In accordance with the wider physics literature, we reserve ρ for mass densities, which are related to number densities by $\rho_{n,p}(\boldsymbol{r}) = m n_{n,p}(\boldsymbol{r})$.)

Developing an orbital-free version of (9) would require expressing all the various terms exclusively in terms of the number density $n(\boldsymbol{r})$. Whether such a NEDF exists and how it should be implemented remains an open question. In this work we will implement an orbital-free functional by approximating all the auxiliary densities (10) as functions of the number density; see section II I for details.

A. Kinetic Terms

The kinetic energy density derives from the energy density of a non-interacting system of protons and neutrons and contains no free parameters:

$$\mathcal{E}_{\text{kin}} = \frac{\hbar^2}{2m}(\tau_n + \tau_p) - \frac{\delta m}{2m}\frac{\hbar^2}{2m}(\tau_n - \tau_p) + O\left(\frac{\delta m}{2m}\right)^2, \tag{11}$$

where $\tau_{n,p}$ are the kinetic densities in the HFB formulation with neutron and proton $m_{n,p} = m \pm \delta m/2$. In principle, one should include an explicit isospin splitting due to the different proton and neutron masses, but we follow here common practice in nuclear theory to use a common average mass $m = (m_n + m_p)/2$ and neglect $\delta m = m_n - m_p$. Note that since we are using the bare masses here, the theory is covariant under Galilean boosts. The consideration of terms with a more complex dependence on the kinetic energy densities requires the adding current terms to restore the Galilean covariance of the theory (see e.q. [61, 111–114].)

B. Coulomb Terms

The direct Coulomb energy and exchange contribution in the Slater approximation are:

$$\mathcal{E}_C(\boldsymbol{r}) = \frac{1}{2} V_C(\boldsymbol{r}) n_{\text{ch}}(\boldsymbol{r}) - \frac{e^2\pi}{4}\left(\frac{3n_p(\boldsymbol{r})}{\pi}\right)^{4/3}, \tag{12a}$$

$$V_C(\boldsymbol{r}) = e^2 \int \mathrm{d}^3\boldsymbol{r}' \, \frac{n_{\text{ch}}(\boldsymbol{r}')}{|\boldsymbol{r} - \boldsymbol{r}'|}, \tag{12b}$$

where e is the proton charge, and n_{ch} is the charge density, which is obtained from the proton and neutron densities by convolution (here noted as "$*$") with the appropriate charge form factors (see Sec. VI for details):

$$n_{\text{ch}} = G^n_E * n_n + G^p_E * n_p. \tag{12c}$$

Including the form factors does not significantly improve the mass fits, but improves somewhat the fit of the charge radii. In principle, one might allow the coefficient of the Coulomb exchange term to vary; this is done, for example, in atomic physics to obtain better estimates of the Coulomb exchange energy. We find, however, that fitting the nuclear binding energies leads with high accuracy to the same coefficient presented in Eq. (12a), so we leave it fixed and do not include this as a parameter in our model.

We require our energy density functional to be an isoscalar and include no isospin breaking terms other than those due to the neutron-proton mass difference (which we neglect here) and the Coulomb interaction. Additional isospin violation due to up and down quark mass differences and electromagnetic effects [115–119] beyond these two contributions are much smaller and are partly responsible for the Nolen-Schiffer anomaly [120], to which the screening of the Coulomb exchange also contributes at a comparable level [95, 121].

C. Homogeneous Terms: Infinite Nuclear and Neutron Matter

We parameterize the nuclear equation of state as:

$$\mathcal{E}_{\text{homo}} = \sum_{j=0}^{2} \mathcal{E}_j(n)\beta^{2j} \tag{13a}$$

$$\mathcal{E}_j(n) = \varepsilon_j(n) n = a_j n^{5/3} + b_j n^2 + c_j n^{7/3}, \tag{13b}$$

where n is the total density, and β is the asymmetry:

$$n = n_n + n_p, \qquad \beta = \frac{n_n - n_p}{n_n + n_p}. \tag{13c}$$

We have considered terms with powers of the density $n^{8/3} \sim n\tau$ and higher, but in all our fits of the nuclear masses, we found

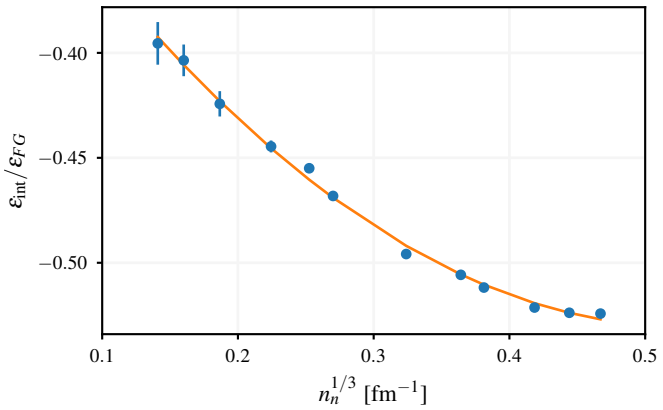

Figure 3. (Color online) The QMC results of Wlazłowski *et al.* [122] for the interaction energy per neutron displayed as the ratio $1/n_n\varepsilon_n/\varepsilon_{FG}$ defined in Eq. (15b) (with $\beta = 1$), where $\varepsilon_{FG} = 3\hbar^2(3\pi^2 n_n)^{2/3}/(10m_n)$. If $a_n = 0$ in Eq. (15b), the ratio $\varepsilon_{\rm int}/\varepsilon_{FG}$ would tend to 0 for $n_n \to 0$. For densities $n_n^{1/3}|a_{nn}| < 1$ (where $a_{nn} = 18.9$ fm is the s-wave neutron-neutron scattering length) the leading order correction to the kinetic energy density per particle contribution would be instead linear in density $4\pi\hbar^2 a_{nn} n_n/m_n$.

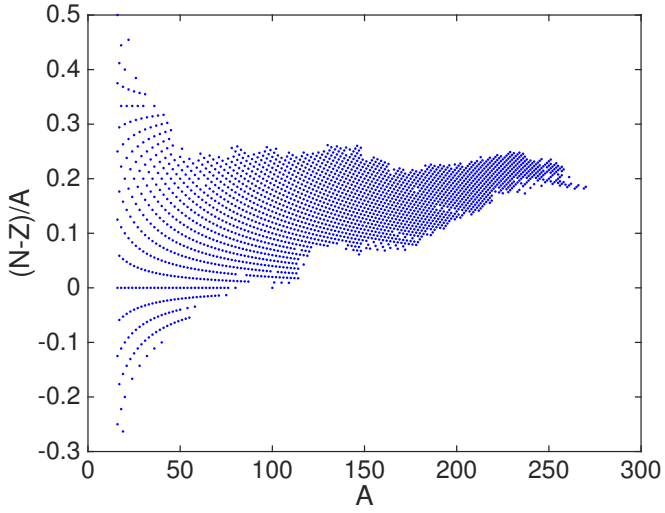

Figure 4. (Color online) The contribution to the ground state energies of the terms quartic in isospin density $\delta E_{I4} = \int \mathrm{d}^3\boldsymbol{r}\ \mathcal{E}_2(n)\beta^4$, evaluated perturbatively with NEDF-1, see Table IV. In the lower panel we display the ratio $(N-Z)/A$ for the nuclei we have considered. Among the 2375 nuclei we have considered, there are 33 nuclei with $N = Z$, 78 nuclei with $Z > N$, and 70 nuclei with $|N-Z|/A > 1/4$.

such terms to be unconstrained in magnitude, barely improving the quality of the fits.

In infinite homogeneous nuclear matter, as might be found in a neutron star for example, the gradient, spin-orbit, entrainment, and Coulomb terms vanish (charge neutrality is maintained by a background of electrons). The semiclassical expansion of the kinetic energy density $\mathcal{E}_{\rm kin}$ becomes exact in the leading Thomas Fermi term $\tau = \tau_{TF}$. Thus, neglecting the small neutron-proton mass difference $m_n \approx m_p \approx m$, the functional acquires the simple form:

$$\mathcal{E}(n_n, n_p) = \frac{3\hbar^2(3\pi^2)^{2/3}}{10m}(n_n^{5/3} + n_p^{5/3}) + \sum_{j=0}^{2}\left(a_j n^{5/3} + b_j n^2 + c_j n^{7/3}\right)\beta^{2j}, \quad (14)$$

This portion of the functional is essentially an expansion in powers of the Fermi momenta k_F: $k_{n,p} = (3\pi^2 n_{n,p})^{1/3}$ with only three terms k_F^5, k_F^6, and k_F^7. This type of expansion is ubiquitous in many-body perturbation theory, and also applies to fitting the neutron matter equation of state ($n_p = 0$, $\beta = 1$):

$$\mathcal{E}_n(n_n) = \frac{3\hbar^2}{10m_n}(3\pi^2 n_n)^{2/3} n_n + \mathcal{E}_{\rm int}(n_n), \quad (15a)$$

$$\mathcal{E}_{\rm int}(n_n) = a_n n_n^{5/3} + b_n n_n^2 + c_n n_n^{7/3}, \quad (15b)$$

The coefficients a_n, b_n, and c_n are fixed by fitting the neutron matter equation of state (EoS) as calculated with QMC including up to N^{3}LO two-body and up to N^{2}LO three-body interactions from chiral perturbation theory [122]:

$$\begin{aligned} a_n &= a_0 + a_1 + a_2 = -32.6\,\text{MeV fm}^2, \\ b_n &= b_0 + b_1 + b_2 = -115.4\,\text{MeV fm}^3, \\ c_n &= c_0 + c_1 + c_2 = 109.1\,\text{MeV fm}^4. \end{aligned} \quad (16)$$

As shown in Fig. 3, all three terms are needed in Eq. (15b) for an accurate reproduction of the neutron EoS (see Sec. V D). We include the $j = 2$ quartic terms in Eq. (14) by determining the values of a_2, b_2, and c_2 from the values of a_n, b_n, and c_n describing the QMC results (16), without adding additional free parameters to the NEDF.[1]

As we shall discuss in section II H, adding the quartic β^4 ($j = 2$) terms does not significantly impact the quality of the fits. However, the best fit functional with only quadratic β^2 ($j = 1$) terms, does not reproduce the neutron matter equation of state, especially near $n \approx 0.1$ fm^{-3} (see Fig. 23). The contribution of this term to nuclear masses is small (typically less than 1 MeV) since in most nuclei $\beta < 0.25$, see Fig. 4. These results demonstrate two important points: 1) quartic terms $\propto \beta^4$ ($j = 2$) appear to be needed to reproduce the neutron matter equation of state, 2) nuclear masses do not constrain these quartic terms. Thus, quartic terms provide a direct (and independent) way to incorporate the equation of state of neutron matter into the NEDF.

At this time we do not have an equally accurate QMC calculation of nuclear matter with varying isospin composition, so we must rely instead on a phenomenological approach. Our main assumption is that we can describe both the isoscalar ($j = 0$, β^0) and isovector ($j = 1$, β^2) parts of the nuclear

[1] We also performed a fully self-consistent mass fit for spherical even-even nuclei with additional powers of densities $\sum_{j=0,1}(a_j n^{5/3} + b_j n^2 + c_j n^{7/3} + d_j n^{8/3})\beta^{2j}$. While this leads to a lower energy rms $\chi_E \approx 1.2$ MeV, the charge radii rms increases to $\chi_r \approx 0.1$ fm and the value of the compressibility $K_0 \approx 170$ MeV is very low. Typically in these cases the parameter a_0 becomes significant and acquires relatively large negative values, similar to the behavior seen in Fig. 7. The terms $d_j n^{8/3}$ are not very significant. See also the discussion in section II H.

equation of state using the same three powers of Fermi momenta Eqs. (15b) and (16) as required to fit the equation of state of pure neutron matter. This approach differs from typical Skyrme-like parameterizations, which include terms with higher powers of densities, e.g. $n^{8/3}$ arising from τn type of terms, where τ is kinetic energy density.

One could in principle consider additional terms of the type $\tau n^{1/3} \propto n^2$, $\tau n^{2/3} \propto n^{7/3}$, and $\tau n \propto n^{8/3}$, but the contribution to the bulk energy of such terms would be practically indistinguishable from terms n^2, $n^{7/3}$, and $n^{8/3}$. Their contribution might become important only in the surface region, and since

$$\tau n^{1/3} - \frac{3}{5}(3\pi^2)^{2/3} n^2 \propto \frac{|\boldsymbol{\nabla} n|^2}{n^{2/3}}, \tag{17a}$$

$$\tau n^{2/3} - \frac{3}{5}(3\pi^2)^{2/3} n^{7/3} \propto \frac{|\boldsymbol{\nabla} n|^2}{n^{1/3}}, \tag{17b}$$

$$\tau n - \frac{3}{5}(3\pi^2)^{2/3} n^{8/3} \propto |\boldsymbol{\nabla} n|^2, \tag{17c}$$

most of these terms could be incorporated effectively in gradient corrections, see sections II D and II I.

The terms $a_j n^{5/3}$ are somewhat unexpected and are not included in Skyrme-like parameterizations. Tondeur [123] introduced only a term a_1 (without theoretical justification), but it makes sense to include the other a_j for several reasons. First, the QMC calculations of Wlazłowski *et al.* [122], Gezerlis and Carlson [124], and Gandolfi *et al.* [125] (see Fig. 3) are consistent with the existence of a non-vanishing parameter a_n in the neutron equation of state, which implies that $a_n = \sum_{j=0}^{2} a_j \neq 0$. Then, these terms also appear naturally in the case of the unitary Fermi gas [126], which has been confirmed to high precision in many experiments. The unitary Fermi gas is a system of two species of fermions, interacting with an s-wave interaction with zero range and infinite scattering length. In response to the Many-Body X challenge posed by Bertsch in 1999, Baker [127] showed that the system was stable. The energy density of the unitary Fermi gas scales exactly like the kinetic energy density of a free Fermi gas $\mathcal{E} \propto n^{5/3}$. Since both neutron and protons have similar s-wave interaction properties, one expects the nuclear energy density to behave somewhat like the unitary Fermi gas.

Although the energy density of the unitary Fermi gas scales as the kinetic energy, this is not necessarily due to a mass renormalization as one might naïvely suspect. QMC calculations of the single quasi-particle dispersion [128] and spectral weight function [129, 130] both find almost the effective mass in the unitary Fermi gas to be close to the bare mass $\approx m$. However, this does not preclude the interpretation that some part of the energy arises from the kinetic energy density τ as is the case in the unitary Fermi gas [108, 114, 131]. The QMC calculations are simply not yet of sufficient accuracy to confirm or exclude an effective mass different from unity.

D. Gradient terms

We include a gradient term of the following form, similar to terms considered in the past [123, 132] and in Skyrme NEDFs [133]:

$$\mathcal{E}_{\boldsymbol{\nabla} n} = \eta_s \sum_{q=n,p} \frac{\hbar^2}{2m} |\boldsymbol{\nabla} n_q|^2. \tag{18}$$

One might consider a more general term of the form

$$\mathcal{E}_{\boldsymbol{\nabla} n} = \eta_0 \frac{\hbar^2}{2m} |\boldsymbol{\nabla} n_n + \boldsymbol{\nabla} n_p|^2 + \eta_1 \frac{\hbar^2}{2m} |\boldsymbol{\nabla} n_n - \boldsymbol{\nabla} n_p|^2. \tag{19}$$

Note that this form of gradient term alone in an orbital-free theory leads to unphysical density profiles with a discontinuity in $\boldsymbol{\nabla} n$ at a finite radius, beyond which the density vanishes exactly. However, in the presence of $\mathcal{E}_{\text{kin}}$ in an orbital-based approach the density is well behaved. We have found that the nuclear mass fits are basically insensitive to the linear combination $\eta_m = \eta_0 - \eta_1$, and we use $\eta_s = (\eta_0 + \eta_1)/2$ and $\eta_m = (\eta_0 - \eta_1)/2 = 0$. The linear combination $\eta_m = (\eta_0 - \eta_1)/2$ can instead be used to independently fit the static isovector dipole polarizability of nuclei, as it favors a small separation between the neutron and proton surfaces if $\eta_1 > 0$.

Additionally, one could consider density-dependent terms of the type arising in Eqs. (17a),

$$\mathcal{E}_\tau \propto \tau n^\sigma - \boldsymbol{j}^2 n^{\sigma-1} - \frac{3}{5}(3\pi^2)^{2/3} n^{5/3+\sigma} \propto \frac{|\boldsymbol{\nabla} n|^2}{n^{1-\sigma}}. \tag{20}$$

The presence of the current density here is required in order to restore Galilean covariance [111]. Since the density gradients are peaked at the nuclear surface the dependence of these coupling constants on density are not expected to lead to any noticeable changes in the quality of nuclear mass fits and the corresponding coupling constants would play a subdominant role (see section II H).

E. Spin-Orbit Coupling

Related to the gradient term is the spin-orbit coupling, which we include in the same form as in the Skyrme NEDF [133]:

$$\mathcal{E}_{\text{SO}} = W_0 \boldsymbol{J} \cdot \boldsymbol{\nabla} n \tag{21}$$

where $\boldsymbol{J} = \boldsymbol{J}_n + \boldsymbol{J}_p$ is the total spin current. Alternatively, one can introduce a more general form of the spin-orbit coupling

$$\mathcal{E}_{\text{SO}} = W_0 \boldsymbol{J} \cdot \boldsymbol{\nabla} n + W_1 (\boldsymbol{J}_n - \boldsymbol{J}_p) \cdot (\boldsymbol{\nabla} n_n - \boldsymbol{\nabla} n_p) \tag{22}$$

but following Fayans [97], we only include the isoscalar portion here as the isovector contribution is small. The isovector dependence of the spin-orbit interaction could be used to independently fine-tune proton and neutron single particle spectra near the Fermi level however.

F. Pairing interaction

The pairing energy depends on the anomalous density:

$$\mathcal{E}_\Delta = \sum_{q=n,p} \int \mathrm{d}^3\boldsymbol{r}\; g_{\text{eff}}(\boldsymbol{r}) |\nu_q(\boldsymbol{r})|^2 \tag{23}$$

and the effective pairing coupling strength $g_{\rm eff}(\boldsymbol{r})$ is obtained via a renormalization [134–136] of the bare pairing strength, which may depend on neutron and proton densities.

In the case of pairing one can consider volume, surface, or mixed pairing coupling constants, but previous studies of large sets of nuclei have shown [135, 137] that there is little evidence preferring one form to another. Phenomenological studies [137] also show that the proton pairing coupling is stronger than the neutron pairing coupling, a result at odds with the naïve expectation that the proton pairing coupling should be weaker due to the Coulomb interaction [138–140].

It would also be peculiar to find that isospin invariance is broken by the pairing interaction in this manner as well, when no other more important terms of the NEDF break isospin symmetry. This likely points to the fact that the pairing coupling can have a more complex structure, which conserves the charge symmetry,

$$\mathcal{E}_{\Delta} = \int \mathrm{d}^3\boldsymbol{r}\; g_{\rm eff}(\boldsymbol{r}) \left(|\nu_n(\boldsymbol{r})|^2 + |\nu_p(\boldsymbol{r})|^2\right) + \int \mathrm{d}^3\boldsymbol{r}\; h_{\rm eff}(\boldsymbol{r}) \left(|\nu_n(\boldsymbol{r})|^2 - |\nu_p(\boldsymbol{r})|^2\right)\beta, \quad (24a)$$

where $\beta = (n_n - n_p)/(n_n + n_p)$. The dependence on neutron and proton densities of the bare coupling constants should satisfy isospin symmetry:

$$g\big(n_n(\boldsymbol{r}), n_p(\boldsymbol{r})\big) = g\big(n_p(\boldsymbol{r}), n_n(\boldsymbol{r})\big), \quad (24b)$$

$$h\big(n_n(\boldsymbol{r}), n_p(\boldsymbol{r})\big) = h\big(n_p(\boldsymbol{r}), n_n(\boldsymbol{r})\big). \quad (24c)$$

Since in measured nuclei one has predominantly $N \geq Z$, see Fig. 17, a phenomenological analysis that leads to an apparent coupling for protons larger than the one for neutrons can be reconciled with renormalized coupling constants $g_{\rm eff}(\boldsymbol{r}) < 0$ and $h_{\rm eff}(\boldsymbol{r}) > 0$. We will neglect for now this additional type of pairing coupling controlled by the coupling constant $h_{\rm eff}(\boldsymbol{r})$. For now, we will also not account for the role of the Coulomb interaction on the pairing of the protons.

In an orbital-free approach the role of pairing is revealed only by the presence of the odd-even staggering of the energy term. As shown in Table I, it has a small effect on the overall quality of global mass fits and it may be omitted as a variational parameter.

G. Entrainment

Entrainment (the Andreev-Bashkin effect) was predicted by Andreev and Bashkin [141] to occur in superfluid mixtures of ^{3}He and ^{4}He, and is rather surprising at first sight, since superfluids are expected to flow without resistance. In particular, one might have expected that if somehow one would bring into motion only one superfluid component, superfluidity will have the consequence that the other component remains at rest. The entrainment term (25) is indeed dissipationless, and thus it does not violate superfluidity, but allows the motion of one superfluid to influence (entrain) the other. It is natural to expect a similar phenomenon to arise in nuclei, where proton and neutron (super)fluids can coexist. Entrainment should also plays a role in neutron stars and has been studied intermittently since 1975 [142–150].

The formalism describing these systems is called three fluid hydrodynamics – two superfluids and one normal component – and is a generalization of Landau's two fluid hydrodynamic phenomenological model of superfluids at finite temperatures below the critical temperature. Since in nuclear systems both neutron and proton subsystems can have a superfluid and a normal component at finite temperatures, and since the normal components can move independently in isovector modes, a proper generalization of the superfluid dynamics to nuclear systems would be a four fluid hydrodynamics, with two superfluid and two normal components, thus a somewhat more complex system than the superfluid mixtures considered so far in literature.

When moving to a new frame, both protons and neutrons experience the same boost $\boldsymbol{v}_{n,p} \longrightarrow \boldsymbol{v}_{n,p} + \boldsymbol{v}$. We can thus introduce an additional Galilean invariant term in the two-component system proportional to $|\boldsymbol{v}_n - \boldsymbol{v}_p|^2$, which we parameterize as:

$$\mathcal{E}_{\rm entrain}(\psi_n, \psi_p) = g_{\rm ent}\left(\frac{n_n n_p}{n^2}\right)\frac{n}{2m}\left|\frac{\boldsymbol{j}_n}{n_n} - \frac{\boldsymbol{j}_p}{n_p}\right|^2, \quad (25)$$

where $\boldsymbol{j}_{n,p} = m n_{n,p} \boldsymbol{v}_{n,p}$ and the function $g_{\rm ent}(x)$ controls the entrainment of the neutron and proton fluids. The presence of such a term leads to a renormalization of the isovector reduced mass of the collective flow, since the collective flow energy has the form

$$\mathcal{E}_{\rm flow} = \frac{m n_n \boldsymbol{v}_n^2}{2} + \frac{m n_p \boldsymbol{v}_p^2}{2} + g_{\rm ent}\left(\frac{n_n n_p}{n^2}\right)\frac{mn|\boldsymbol{v}_n - \boldsymbol{v}_p|^2}{2} \quad (26)$$
$$= \frac{m(n_n \boldsymbol{v}_n + n_p \boldsymbol{v}_p)^2}{2n} + \left[\frac{n_n n_p}{n^2} + g_{\rm ent}\left(\frac{n_n n_p}{n^2}\right)\right]\frac{mn|\boldsymbol{v}_n - \boldsymbol{v}_p|^2}{2}.$$

Since this type of coupling between neutron and proton fluids is absent when either density vanishes we require that $g_{\rm ent}(0) = 0$. The requirement that the total kinetic energy is always positive leads to the condition $x + g_{\rm ent}(x) > 0$. The significant effect of this term is seen in the dynamics only, when the motion of one fluid will drag along the other, and therefore the presence of such an additional term will affect strongly the excitation energies of isovector modes such as the giant dipole resonances (GDRs) and the Thomas-Reiche-Kuhn sum rule. The simplest choice for this coupling is $g_{\rm ent}(x) = \alpha x$ with $1 + \alpha > 0$, however Borumand *et al.* [145] recommend $g_{\rm ent}(x) \propto x^{2/3}$.

H. SeaLL1 NEDF

We characterize the parameters of the theory according to their significance for mass fits and dynamics. We define a parameter as *dominant* if varying this parameter by less than 5% or so reduces the χ_E of the best fit by 0.1 MeV per nucleon. We define a parameter as *subdominant* if it can be varied by 10% or more with a similar decrease in the quality of the fit. We define a parameter as *unconstrained* if it can be set to zero at this level of accuracy.

Our analysis shows that a minimal orbital-free NEDF has 4 dominant parameters, and 2 subdominant parameters, consistent with the analysis presented above.

Kinetic (none): The kinetic energy density $\mathcal{E}_{\rm kin}$ Eq. (11) contains no free parameters - just $\hbar$ and the bare nucleon masses m_n and m_p and the kinetic densities $\tau_{n,p}$. However, since the orbital-free approach depends on densities alone, an approximation of the kinetic energy densities in terms of densities introduces a single parameter κ. This is discussed in section II A and II I

Coulomb (none): The Coulomb interactions $\mathcal{E}_C$ Eq. (12) also contains no free parameter in either formulation. In principle, the proton and neutron form-factors can be included, but these have only a small effect. This is discussed in section II B.

Homogeneous (3 dominant, 1 subdominant): The homogeneous portion of the functional $\mathcal{E}_{\rm homo}$ Eq. (13) adds only 3 significant parameters. In principle, up to 9 parameters a_j, b_j, and c_j for $j \in \{0,1,2\}$ describe the equation of state for homogeneous nuclear matter. However, three of these nine (for $j = 2$) are fixed by the equation of state of neutron matter as determined *in ab initio* calculations. Two of the remaining six parameters (a_0, and the combination of $a_1 - b_1 n_0^{1/3}$, where n_0 is symmetric matter saturation density) are found to be unconstrained at the level of changing the energy rms by $\delta\chi_E < 0.1\,$MeV and are thus set to 0. In our full SeaLL1, we keep c_1 as a fitting parameter, although it is significantly less dominant than the others. We fix c_1 sometimes in the orbital-free theory to provide a reasonable description of the neutron skins, see section V B. Either c_1 or the linear combination $a_1 - b_1 n^{1/3}$ can be used to tune the density dependence of the symmetry energy.

This counting echoes the dominant and subdominant roles of the various nuclear saturation and symmetry properties in fitting masses. In particular, the dominant parameters fix the saturation density n_0, saturation energy ε_0, and quadratic symmetry energy S_2. The slope of the quadratic symmetry energy L_2 is subdominant as far as mass fits are concerned, but important for properties such as the neutron skin thickness, which is why we keep an additional parameter in the SeaLL1 functional.

Gradients (1 dominant): The gradient corrections $\mathcal{E}_{\nabla n}$ Eq. (18) add a single new parameter η_s.

Spin-orbit (1 subdominant): The spin-orbit coupling term $\mathcal{E}_{\rm SO}$ Eq. (21) add a single new parameter W_0. This parameter is subdominant for the mass fits, but is crucial for producing the shell structure of nuclei. In the orbital-free approach this term is practically incorporated in the gradient contribution.

Pairing (1 parameter): The pairing interaction $\mathcal{E}_\Delta$ Eq. (23) adds an additional parameter g_0 in the orbital-based approach. Its contribution is practically incorporated in the homogeneous isoscalar terms in the orbital-free approach. A different parameter δ measuring the odd-even staggering is required for the orbital-free formulation. However, as is seen for the liquid drop models in Table I, this additional parameter is quite unconstrained.

Entrainment (1 for dynamics): The entrainment interaction $\mathcal{E}_{\rm entrain}$ Eq. (25) adds an additional parameter α important for isovector dynamics only, such as the GDR mode.

The orbital-based approach is specified by 7 parameters: b_0, c_0, characterizing isoscalar nuclear properties, a_1, b_1, defining the isovector nuclear properties, η_s defining the surface tension, W_0 the strength of the isoscalar spin-orbit interaction, and bare (unrenormalized) pairing coupling constant g. In the orbital-free approach, we are left with only 4 significant phenomenological parameters: η_s, b_0, c_0, and a linear combination $a_1 = b_1 n^{1/3}$, since c_1 is unconstrained. The orbital-free approach has the additional parameter κ controlling the Padé gradient approximation of the kinetic energy density.

The full form of the functional SeaLL1 is:

$$\mathcal{E}[n_n,n_p] = \overbrace{\frac{\hbar^2}{2m}(\tau_n+\tau_p)}^{\text{kinetic}} + \overbrace{\sum_{j=0}^{2}\left(a_j n^{5/3} + b_j n^2 + c_j n^{7/3}\right)\beta^{2j}}^{\text{homogeneous}} + \overbrace{\eta_s \sum_{q=n,p}\frac{\hbar^2}{2m}|\boldsymbol{\nabla} n_q|^2}^{\text{gradient}}$$
$$+ \underbrace{W_0 \boldsymbol{J}\cdot\boldsymbol{\nabla} n}_{\text{spin-orbit}} + \underbrace{\sum_{q=n,p} g_{\rm eff}(\boldsymbol{r})|\nu_q(\boldsymbol{r})|^2}_{\text{pairing}} + \underbrace{\frac{e^2}{2}\int \mathrm{d}^3\boldsymbol{r}'\frac{n_p(\boldsymbol{r})n_p(\boldsymbol{r}')}{|\boldsymbol{r}-\boldsymbol{r}'|} - \frac{3e^2}{4}\left(\frac{n_p(\boldsymbol{r})}{3\pi}\right)^{4/3}}_{\text{Coulomb}}. \quad (27)$$

The parameter values for the SeaLL1 functional are summarized in Table II. The 7 shaded parameters b_0, c_0, b_1, c_1, η_s, W_0 and g are significant for fitting nuclear masses and radii. The other parameters are either fixed independently (e.g. by the properties of neutron matter) or have been determined to be unconstrained for mass fits through a principle component

	SeaLL1	*hydro*	Comments
n_0	**0.154**	*0.154*	Adjusted (see Fig. 5)
a_0	**0**	*same*	Insignificant
b_0	**−684.5(10)**	*−685.6(2)*	
c_0	**827.26**	*828.76*	$2c_0 n_0^{\frac{2}{3}} = -\frac{3\hbar^2}{10m}\left(\frac{3\pi^2}{2}\right)^{\frac{2}{3}} - \frac{3}{2}b_0 n_0^{\frac{1}{3}}$
a_1	**64.3**	*50.9*	$a_1 = n_0^{1/3} b_1$
b_1	**119.9(61)**	*94.9(14)*	
c_1	**−256(25)**	*−160.0*	Fixed in orbital-free theory
a_2	**−96.8**	*−83.5*	$a_2 = a_n - a_0 - a_1$
b_2	**449.2**	*475.2*	$b_2 = b_n - b_0 - b_1$
c_2	**−461.7**	*−559.6*	$c_2 = c_n - c_0 - c_1$
a_n	**−32.6**	*same*	from neutron matter EoS (16)
b_n	**−115.4**	*same*	from neutron matter EoS (16)
c_n	**109.1**	*same*	from neutron matter EoS (16)
η_s	**3.93(15)**	*3.370(50)*	
W_0	**73.5(52)**	*0.0*	Fixed in orbital-free theory
g_0	**−200**	*N/A*	g_0 fit in Ref. [135]
κ	**N/A**	*0.2*	Semi-classical (see section II I)
$\frac{\hbar^2}{2m}$	**20.7355**	*same*	units (MeV = fm = 1)
e^2	**1.439 96**	*same*	cgs units ($4\pi\epsilon_0 = 1$)
χ_E	**1.74**	*3.04*	606 even-even nuclei
		2.86	2375 nuclei
χ_r	**0.034**	*0.038*	345 charge radii
		0.041	883 charge radii

Table II. Best fit parameters for the SeaLL1 functional (in bold) and the orbital-free approximation (next column in italic when different). The errors quoted for the fit parameters should be interpreted as estimating by how much this parameter can be independently changed while refitting the other and incurring a cost of at most $\delta\chi_E < 0.1$ MeV.

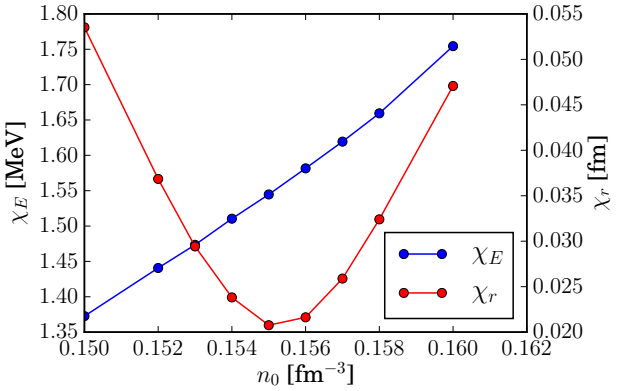

Figure 5. (Color online) Saturation density n_0 dependence of the energy residual χ_E and charge radii residual χ_r of the SeaLL1 functional. After holding n_0 fixed (through the parameter c_0), the remaining 5 shaded parameters in Table II were fit by minimizing only $\chi_E^2 = \sum|E_{N,Z} - E(N,Z)|^2/N_E$ over the $N_E = 196$ spherical even-even nuclei with $A \geq 16$ measured (not extrapolated) from Audi *et al.* [1] and Wang *et al.* [2]. The value $n_0 = 0.154\,\text{fm}^{-3}$ fixed in the SeaLL1 functional represents a compromise between these residuals here both χ_E and χ_r increase by about 10%.

analysis described in Appendix V B.

Our fitting strategy is described in details in Appendix V B and we only recall here its most important characteristics. First, we explored the parameter space with a simplified version of the orbital-free NEDF. This NEDF is characterized by seven parameters (a_0, a_1, b_0, b_1, c_0, c_1, and η_s) which we fitted on $N_E = 2375$ experimentally-measured atomic masses and $N_r = 883$ nuclear charge radii as listed in Audi *et al.* [1] and Wang *et al.* [2]. From this series of fits and its statistical analysis, we found that (i) the parameters a_0 and c_1 are unconstrained and can be set to zero; (ii) the mass and radii are sensitive only to a single linear combination of the parameters a_1 and b_1. The parameter c_1 can be used interchangeably with the linearly independent combination $a_1 - n_0^{1/3} b_1$ to control the slope L_2 of the symmetry energy, which also controls the neutron skin thickness of neutron rich nuclei, see below Eq. (36b) and the related discussion in section III D. We will fix here $a_1 = n_0^{1/3} b_1$, where $n_0 = 0.154\,\text{fm}^{-3}$ is the saturation density (see discussion below).

The next step consists in minimizing the residuals $\chi_E^2 = \sum|E_{N,Z} - E(N,Z)|^2/N_E$ over the $N_E = 196$ spherical even-even nuclei with $A \geq 16$ measured (not extrapolated) from Audi *et al.* [1] and Wang *et al.* [2] with the full orbital-based functional. This involves adjusting the 5 dominant parameters shaded in Table II – the saturation density having been fixed from the study of charge radii. Note that the pairing parameter g_0 is fixed at the value suggested in Ref. [135]: Although this is in principle a fitting parameter, it plays only a minor role in global mass fits as discussed in the introduction. The SeaLL1 parameters of the orbital-based NEDF (in bold) yield $\chi_E = 1.51$ MeV over the $N_E = 196$ spherical even-even nuclei, while the orbital-free NEDF yield $\chi_E = 2.86$ MeV over $N_E = 2375$ nuclei.[2] The pairing fields were treated using the renormalization procedure described in Refs. [134, 135] with a cut-off energy of 100 MeV.

As discussed in Appendix V B, we find that fitting the binding energies alone in the orbital-free approach results in quite a low saturation density $n_0 \approx 0.14\,\text{fm}^{-3}$, and a poorer fit to both charge radii and density profiles. To explore the influence of saturation density n_0 on the quality of the fit, we performed mass-only fits for the remaining 5 parameters with various saturation densities n_0 ranging from $0.15\,\text{fm}^{-3}$ to $0.16\,\text{fm}^{-3}$. For each fit, we also calculate the rms radii residuals $\chi_r^2 = \sum|\delta r|^2/N_r$ for the $N_r = 123$ corresponding nuclei in [3]. These results are shown in Fig. 5, which demonstrates that the charge radii strongly prefer $n_0 \approx 0.155\,\text{fm}^{-3}$ in contrast to the rather weak lower bias from the mass fits. To incorporate this preference

[2] At first sight it is surprising that the value of χ_E in the orbital-free approach over 606 even-even nuclei is larger than the value obtained for 2375 nuclei. The reason is simple and related to the compensation of the shell-correction energies with the deformation energies discussed in Introduction and Ref. [44].

in our fits, we fix the saturation density $n_0 = 0.154\,\mathrm{fm}^{-3}$ by adjusting c_0 using the Eq. (54). This represents a compromise between the two biases where both χ_E and χ_r increase by about 10%. With this fixed value of n_0, we fit the remaining 5 parameters of the SeaLL1 functional by minimizing only χ_E over the $N_E = 196$ spherical even-even nuclei as summarized in Table II.

I. Orbital-Free Functional

Although we advocate working with the full orbital-based SeaLL1 functional presented above, for tasks such as globally fitting mass parameters, one can work with a much simpler orbital-free formulation. The main challenge in formulating an orbital-free theory is to express terms with the auxiliary densities $\tau_{n,p}$, $\boldsymbol{J}_{n,p}$, and $\boldsymbol{j}_{n,p}$ by an appropriate functional of the number densities $n_{n,p}$. Although formally possible, it is still an open research question as to how best reduce an orbital-based DFT to an orbital-free version. We discuss in more detail our approach based on a semiclassical approximation in Appendix V A. To summarize here, we suggest using the following combination for the kinetic and spin-orbit contributions in an orbital-free theory:

$$\mathcal{E}_{\mathrm{kin}}[n_n, n_p] + \mathcal{E}_{\mathrm{SO}}[n_n, n_p] = \qquad \text{(orbital-free)}$$
$$= \frac{\hbar^2}{2m} \sum_{q=n,p} \tau_{TF}[n_q] F(X_q) - \frac{W_0^2}{2} \frac{2m}{\hbar^2} n (\boldsymbol{\nabla} n)^2. \quad (28a)$$

where

$$F(X) = \frac{1 + (1+\kappa)X + 9\kappa X^2}{1 + \kappa X}, \qquad X = \frac{\tau_2[n]}{\tau_{TF}[n]}, \quad (28b)$$

$$\tau_{TF}[n] = \tfrac{3}{5}(3\pi^2)^{2/3} n^{5/3}, \qquad \tau_2[n] = \frac{1}{9} |\boldsymbol{\nabla}\sqrt{n}|^2. \quad (28c)$$

The ratio X characterizes the size of the gradients in the system in terms of the leading τ_{TF} and subleading τ_2 terms of the semiclassical expansion [11, 24, 151] of the kinetic density τ. The Padé approximant $F(X)$ suggested by DePristo and Kress [152] and advocated in [11] interpolates between the semiclassical limit $X \ll 1$ valid in the core of large nuclei, and the approximation $\tau \approx \tau_{TF} + |\boldsymbol{\nabla}\sqrt{n}|^2$ introduced by Weizsäcker [8] which correctly reproduces the asymptotic fall off of the density when $X \gg 1$. When spin-orbit is missing, $\tau_{TF}[n_q]F(X_q)$ gives a semi-classical approximation of the kinetic density τ. This approximation requires a single additional parameter κ. The value of κ can be chosen approximately by comparisons between τ and $\tau_{TF}[n_q]F(X_q)$, and between their resulting kinetic energies E_{kin}, for the same set of single-particle wavefunctions. We found $\kappa \approx 0.2$ will give a reasonable semi-classical approximation for τ and E_{kin}.

The semi-classical spin-orbit contribution is suggested by Brack *et al.* [49], which brings a parameter W_0 corresponding to the one in Eq. (21). Like the full self-consistent theory, this parameter is also subdominant for the mass fits and its contribution can be incorporated in the gradient term. Furthermore, due to the missing of shell structure in the orbital-free theory, this parameter is even more unconstrained.

The orbital-free formulation of the NEDF requires the additional parameter κ to approximate the gradient corrections. As discussed above we choose $\kappa = 0.2$. Following SeaLL1, we fix the saturation density $n_0 = 0.154\,\mathrm{fm}^{-3}$, and fit the 3 parameters b_0, b_1 and η_s shaded in Table II. The spin-orbit contribution was absorbed in the gradient term and if desired the unconstrained parameter c_1 can be used to fix the neutron skin thickness. The parameter values are determined by performing the same least squares minimization of the binding energy residuals as SeaLL1, but over all $N_E = 2375$ nuclei (including the deformed and odd-even, odd-odd ones) with $A \geq 16$ measured from Audi *et al.* [1] and Wang *et al.* [2].

The parameter values and rms residuals of orbital-free theory are also summarized in Table II. As expected, the rms residuals $\chi_E = 2.67\,\mathrm{MeV}$ is larger than the χ_E of SeaLL1 due to the lack of shell corrections in the orbital-free theory, but are comparable with results from the liquid-drop formula in Table I.

J. Principal Component Analysis

The parameters listed in Table IV are highly correlated. To analyze these, we consider as significant changes $\delta\chi_E \approx 0.1\,\mathrm{MeV}$ since this is the typical level of sensitivity of the mass fits. We keep the changes relatively small because otherwise the model is not well approximated by a quadratic error model if $\delta\chi_E > 0.1\,\mathrm{MeV}$. Numerically we find that even 0.1 MeV is too large, but yields qualitatively correct information after a full refitting. Note that $\delta(\chi_E^2) = (\chi_E + \delta\chi_E)^2 - \chi_E^2 = 2\,\chi_E\,\delta\chi_E + (\delta\chi_E)^2$, so we must normalize $\delta(\chi_E^2)$ by $2\,\chi_E \cdot 0.1\,\mathrm{MeV}$ in order to consider changes $\delta\chi_E \approx 0.1\,\mathrm{MeV}$.

To compare the parameters in a meaningful way, we must make them dimensionless and of order unity. We do this by scaling them with appropriate powers of $n_0 = 0.154\,\mathrm{fm}^{-3}$ and $\varepsilon_F = \frac{\hbar^2}{2m}(3\pi^2 n_0/2)^{2/3} = 35.294\,20\,\mathrm{MeV}$, which we take as fixed parameters close to the saturation values:

$$\tilde{a}_j = \frac{a_j n_0^{2/3}}{\varepsilon_F}, \qquad \tilde{b}_j = \frac{b_j n_0}{\varepsilon_F}, \qquad \tilde{c}_j = \frac{a_j n_0^{4/3}}{\varepsilon_F}. \quad (29)$$

(It is important to retain a significant number of digits for isoscalar quantities, as it will be come clearer below.) In particular, we consider the covariance matrix $\boldsymbol{C}$ such that the residual deviation is

$$\frac{\delta(\chi_E^2)}{2\chi_E \cdot 0.1\,\mathrm{MeV}} \approx \boldsymbol{\delta}^T \cdot \boldsymbol{C}^{-1} \cdot \boldsymbol{\delta} = \sum_n \frac{(\delta p_n)^2}{\lambda_n^2}. \quad (30a)$$

where $\boldsymbol{\delta}$ is the deviations vector of the dimensionless parameters Eq. (29) from their best fit values as listed in Table IV, and we have diagonalized $\boldsymbol{C}\mathbf{v}_n = \lambda_n^2 \mathbf{v}_n$ to obtain the principal components p_n

$$p_n = \boldsymbol{v}_n \cdot \begin{pmatrix} \tilde{a}_0 & \tilde{b}_0 & \cdots & \tilde{\eta}_s & \tilde{W}_0 \end{pmatrix}. \quad (30b)$$

Since the parameters are of order unity, we may directly consider the λ_n as a measure of the errors: changing p_n by λ_n

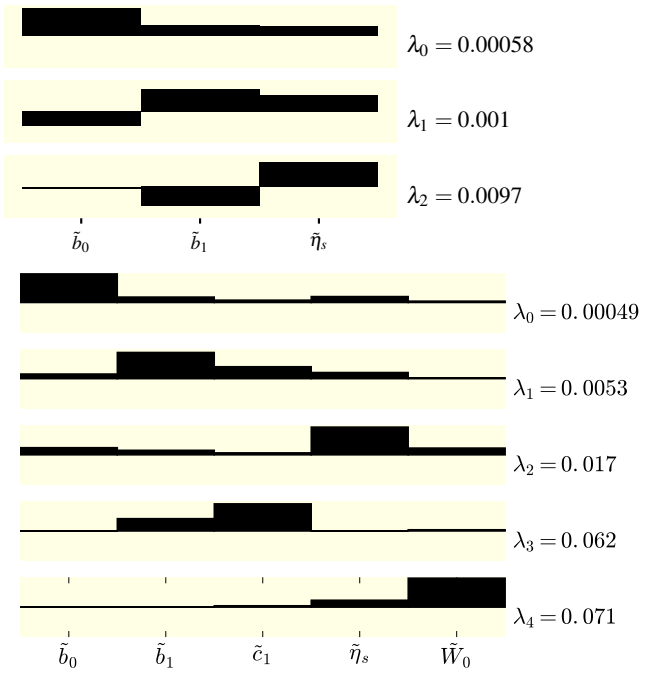

Figure 6. The principal component analysis of the SeaLL1 NEDF in the case of the orbital-free (upper) and orbital-based (bottom) approach.

will affect the fit on the scale of $\delta\chi_E \approx 0.1$ MeV. Therefore, the smaller the value of the parameter λ_n, the more precisely the fit to nuclear masses constrains the value of the corresponding linear combination of NEDF parameters. A similar approach was used by Bertsch *et al.* [153] in the analysis of Skyrme-type NEDFs.

In Fig. 6 we show a principal component analysis of the SeaLL1 functional. The orbital-based analysis includes only 196 spherical even-even nuclei used the fine-tune the parameters of the functional, while the analysis of the orbital-free functional includes all 2375 nuclei as described in Table I. Their features can be understood in terms of the saturation and symmetry parameters, see Eqs (35).

$$S = \frac{\mathcal{E}(n_0,0) - \mathcal{E}(n_0/2,n_0/2)}{n_0}, \tag{31}$$

$$L = 3n\frac{\mathrm{d}}{\mathrm{d}n}\left(\frac{\mathcal{E}(n,0)}{n}\right)\Big|_{n_0} = 3n_0\varepsilon_n'(n_0) \tag{32}$$
$$= \frac{6}{5}\frac{\hbar^2}{2m}(3\pi^2 n_0)^{2/3} + 2a_n n_0^{2/3} + 3b_n n_0 + 4c_n n_0^{4/3}.$$

where $\varepsilon_n(n)$ is the energy per particle of the neutron equation of state (15a). Since the saturation density n_0 minimizes the energy of symmetric matter, the slope of the full symmetry energy L at n_0 depends only on the equation of state of pure neutron matter. Thus, the QMC neutron equation of state alone fixes the global density dependence of the symmetry energy

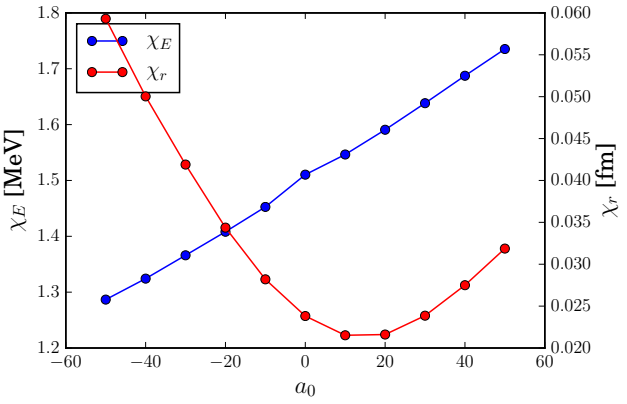

Figure 7. (Color online) The changes in χ_E and χ_r for the $N_E = 196$ even-even spherical nuclei with $A \geq 16$, similarly to Fig. 5 as a function of the fixed parameter a_0, while the rest of the 7 parameters of SeaLL1 specified in Table II are optimized.

$L = 3n_0\varepsilon_n'(n_0) \approx 30$ MeV. We may express these as follows:

$$\frac{\varepsilon_0}{\varepsilon_F} = \frac{3}{5} + \tilde{a}_0 + \quad \tilde{b}_0 + \tilde{c}_0, \tag{33a}$$

$$0 = \frac{3}{5} + \tilde{a}_0 + \frac{3}{2}\tilde{b}_0 + 2\tilde{c}_0, \tag{33b}$$

$$\frac{K_0}{\varepsilon_F} = -\frac{6}{5} - 2\tilde{a}_0 \quad + \quad 4\tilde{c}_0, \tag{33c}$$

$$\frac{S}{\varepsilon_F} = \frac{3}{5}(2^{2/3}-1) + (\tilde{a}_1 + \tilde{b}_1 + \tilde{c}_1) + (\tilde{a}_2 + \tilde{b}_2 + \tilde{c}_2), \tag{33d}$$

$$\frac{L}{\varepsilon_F} = \frac{6}{5}2^{2/3} + 2\tilde{a}_n + 3\tilde{b}_n + 4\tilde{c}_n, \tag{33e}$$

where K_0 is the isoscalar compressibility, see Eq. (35). The most significant component p_0 in both fits is the sum of the $j = 0$ coefficients $\tilde{a}_0 + \tilde{b}_0 + \tilde{c}_0$ which fixes the saturation energy ε_0 Eq. (33a), see also Fig. 22. (Remember that we have chosen $a_0 = 0$ and that c_0 is determined from Eq. (33b).) Next are mixtures of η_s and the symmetry energy S, Eq. (33d), which are correlated by the finite size of the nuclei; the latter is the sum of the $j = 1$ coefficients $\tilde{a}_1 + \tilde{b}_1 + \tilde{c}_1$. While we have chosen to keep the value of the parameter $a_0 = 0$, its value can be varied without affecting significantly the quality of the overall mass and charge radii fit, see Fig. 7. By changing adopted the value $a_0 = \pm 20\,\mathrm{fm}^{-3}$ and keeping ε_0 and the saturation density fixed one can change the compressibility by $\delta K_0 = \pm 2\delta\tilde{a}_0\varepsilon_F = \pm 2\delta a_0 n_0^{2/3} \approx \pm 23$ MeV. The power of this kind of analysis resides in formulating a "power-counting" scheme, which organizes the various linear combinations of parameters in the order of relevance in the mass fit.

III. PHYSICAL PROPERTIES

A. Global mass table

Since our orbital-based NEDF was fit on spherical even-even nuclei only, we validate its predictive power by performing a fully microscopic calculation of the nuclear binding energies of 606 even-even nuclei with $A \geq 16$ in [1, 2]. We used an extension of the axial DFT solver HFBTHO code [154–156] that includes the SeaLL1 and the regularization of the pairing channel [134]. Calculations were performed in a deformed basis of 20 harmonic oscillator shells. In the pairing channel, a cut-off of 100 MeV was adopted in accordance with [135].

Fig. 8 shows the residuals of the nuclear masses calculated with SeaLL1 with respect to the experimental values of these even-even nuclei, which yields a rms residual of $\chi_E = 1.74$ MeV. Besides the larger residuals in the light nuclei region, the residuals show the typical arc-like features common to many NEDF calculations, for both isotonic and isotopic chains. The poor performance of SeaLL1 for light nuclei is likely related to the center-of-mass corrections (not accounted for here) and is also observed in the UNEDF functionals [66, 157]. Since the unaccounted for center-of-mass corrections are larger for light nuclei, our parameter fit limited to spherical nuclei leads to an underestimate of the masses of heavier spherical nuclei, see Fig. 8. In the case of the heavier deformed nuclei our neglect of the angular momentum projection corrections leads to an overestimate of their masses. Overall the masses have a bias $\epsilon_E = \langle \delta E \rangle = 0.97$ MeV and a standard deviation $\sigma_E = 1.46$ MeV, see Fig. 9. This bias enters the rms error $\chi_E^2 = \sigma_E^2 + \epsilon_E^2$ which leads to a value of $\chi_E = 1.46$ MeV. This σ_E is an upper estimate of the rms energy χ_E we expect if the SeaLL1 parameters would have been instead fitted to all even-even nuclei.

The residuals for the two-nucleon separation energies for the same set of even-even nuclei are shown in Fig. 10 and they are naturally less affected by the errors induced by the neglect of the center-of-mass corrections and angular momentum projection corrections in deformed nuclei.

B. Charge radii and density distribution

The residuals of radii for 345 matching even-even nuclei in [3] is also calculated, which gives a rms residual of $\chi_r = 0.034$ fm, as shown in Fig. 11.

Using the parameters determined from the mass fits, SeaLL1 also models the neutron and proton densities in the nuclei, allowing us to extract the charge densities for these nuclei using Eq. (12c). As a good benchmark, in Fig. 12 we compare the proton and charge densities of ^{48}Ca and ^{208}Pb calculated with SeaLL1 with the charge densities extracted from electron scattering experiments [158]. The calculated ^{208}Pb has a slightly larger radius and slightly smaller diffuseness compared to those extracted from data, which is consistent with the charge radii comparison between SeaLL1 and experiment in Fig. 11.

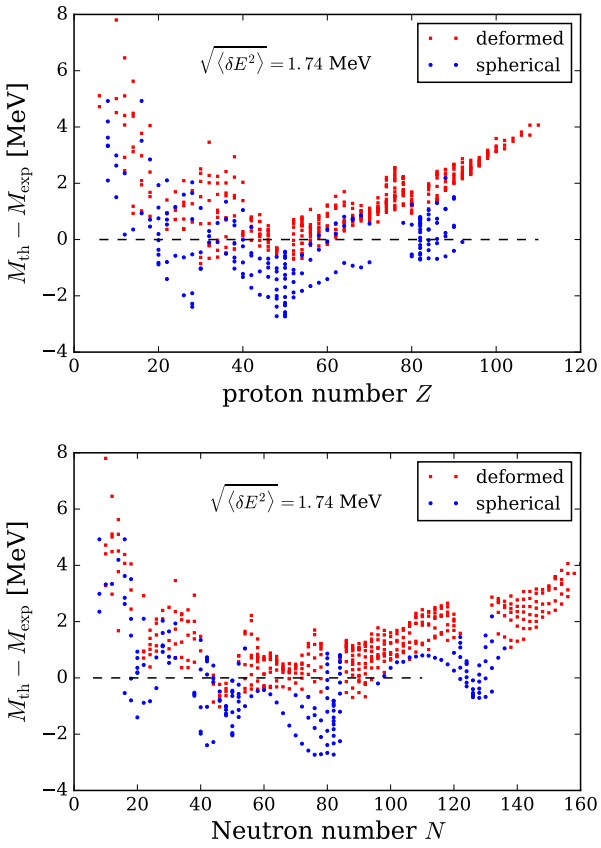

Figure 8. Mass residuals between SeaLL1 and measured masses for 606 even-even nuclei, of these 410 deformed nuclei and 196 spherical nuclei, plotted with red squares and blue bullets respectively.

C. Spherical shell structure

Shell structure is a fundamental property of atomic nuclei. In an independent-particle picture, the shell structure can be associated with the single-particle spectra of the mean-field potential. Reproducing the correct ordering and distribution of single-particle levels is essential for nuclear structure theories, and also important for the application of the NEDF in nuclear dynamics, such as nuclear fission and collision. Fig. 13 and 14 display the single-particle levels for neutrons and protons in ^{48}Ca and ^{208}Pb, respectively. Compared with the empirical values, the $N = 28$ and $Z = 20$ gaps in ^{48}Ca are clearly too small with SeaLL1. The single particle proton levels in ^{208}Pb show that the $Z = 82$ gap is also smaller in SeaLL1. Such patterns are also observed in UNEDF2 functional which, however, included single-particle spin-orbit splittings in their fit [159]. This might point to the need to consider the contribution from the isovector spin-orbit contribution in Eq. (22) proportional to W_1.

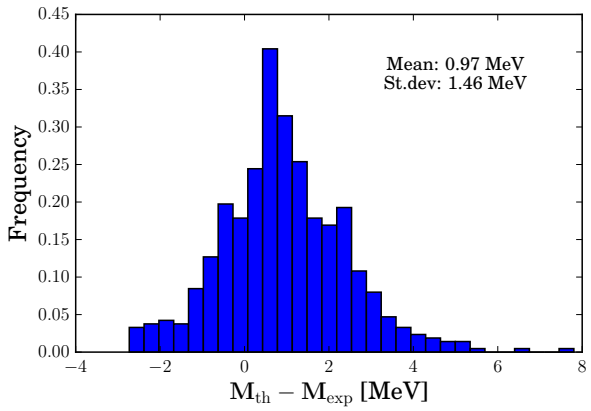

Figure 9. The histogram of the mass residuals between SeaLL1 and experiment for 606 even-even nuclei.

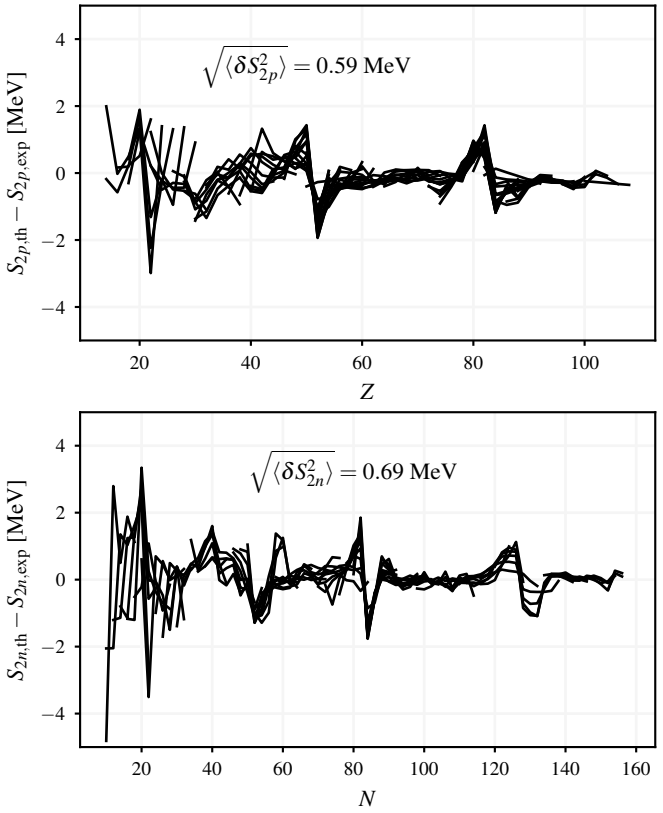

Figure 10. The residual of the two-nucleon separation energies between SeaLL1 and experiment for 606 even-even nuclei: $S_{2p}(Z)$ for constant N (upper) and $S_{2n}(N)$ for constant Z (lower) chains connected by lines.

D. Symmetry Energy and Neutron Skin Thickness

The isoscalar parameters $j = 0$ and quadratic isovector parameters $j = 1$ (β^2) may be directly related to the saturation and symmetry properties respectively by expanding the energy per nucleon of homogeneous nuclear matter Eq. (14) about the

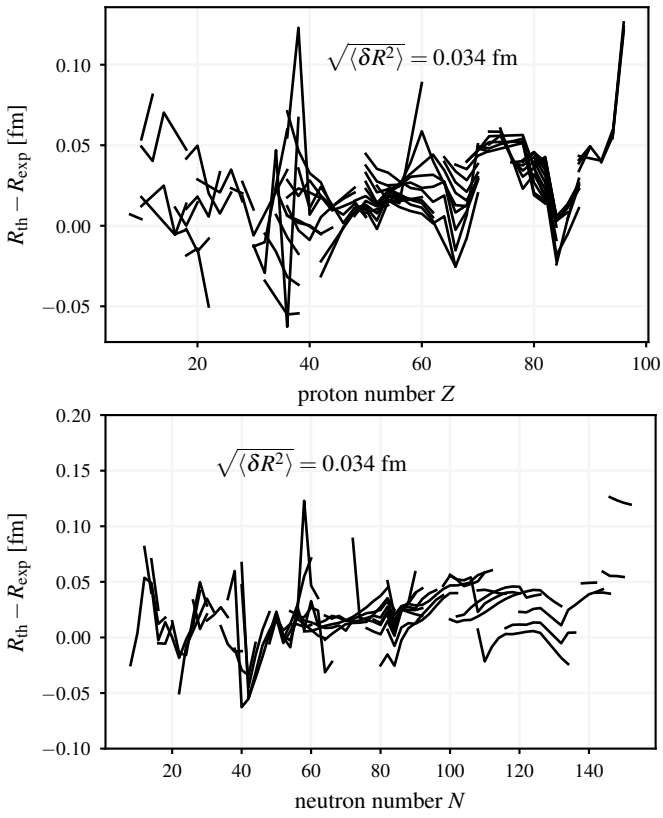

Figure 11. Radii residuals between SeaLL1 and experiment for 345 even-even nuclei. Isotonic (upper) and isotopic (lower) chains are connected by lines.

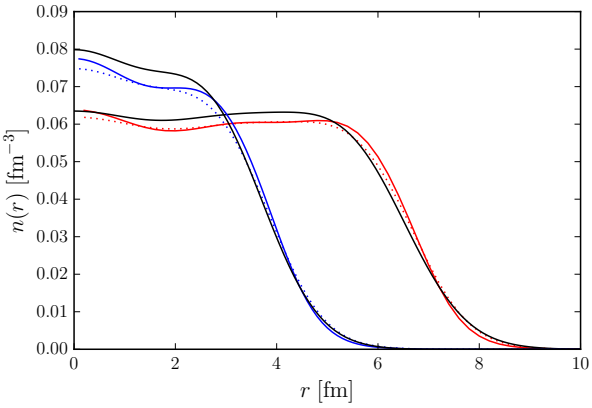

Figure 12. (Color online) The calculated proton $n_p(r)$ (solid) and charge $n_{\mathrm{ch}}(r)$ (dotted) densities for ^{48}Ca (red) and ^{208}Pb (blue), calculated with SeaLL1 compared to charge densities (black) extracted from electron scattering experiments [158].

symmetric saturation point $n_n = n_p = n_0/2$:

$$\frac{\mathcal{E}(n_n, n_p)}{n} = \epsilon_0(n) + \epsilon_2(n)\beta^2 + \epsilon_4(n)\beta^4 + O(\beta^6). \qquad (34)$$

The saturation density n_0, energy per nucleon ε_0, and incompressibility K_0 are then defined by the minimum $\varepsilon_0'(n_0) = 0$,

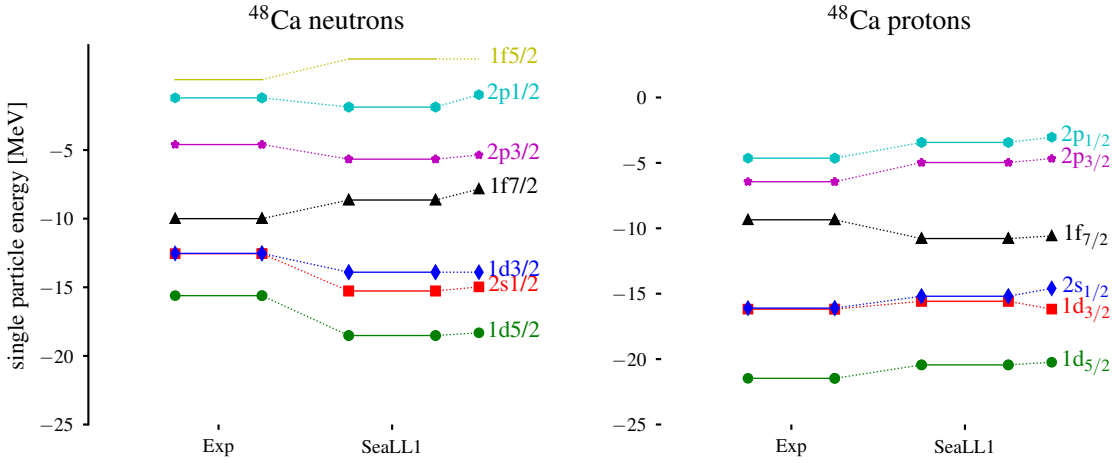

Figure 13. (Color online) Single particle energies in ^{48}Ca calculated with SeaLL1. These are compared with the empirical values (Exp) of Ref. [160].

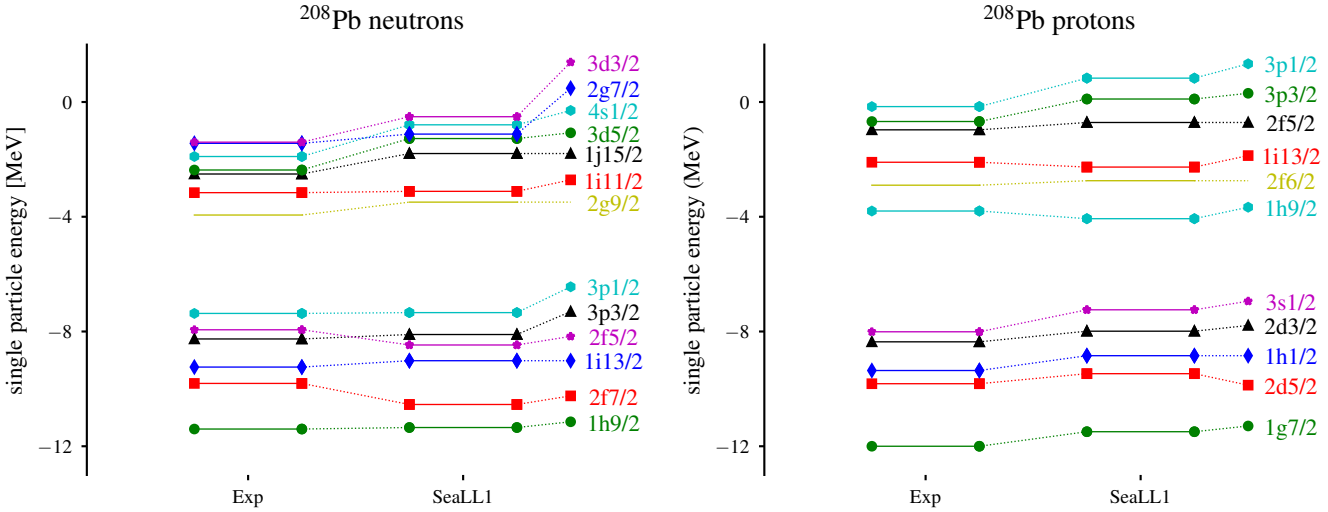

Figure 14. (Color online) Same as Fig. 13 but for ^{208}Pb.

and depend only on the $j = 0$ isoscalar parameters a_0, b_0, and c_0. Expanding about n_0 in $\delta = (n - n_0)/3n_0$ and in powers of $\beta = (n_n - n_p)/n$, one can define various "local" contributions to the symmetry energy $S_{2,4}$, its density dependent slope $L_{2,4}$, etc.:

$$\begin{aligned}
\epsilon_0(n) &= \tfrac{6}{5}\varepsilon_F + a_0 n^{2/3} + b_0 n + c_0 n^{4/3} \\
&= \varepsilon_0 + \tfrac{1}{2}K_0\delta^2 + O(\delta^3), \\
\epsilon_2(n) &= -\tfrac{4}{15}\varepsilon_F + a_1 n^{2/3} + b_1 n + c_1 n^{4/3} \\
&= S_2 - L_2\delta + \tfrac{1}{2}K_2\delta^2 + O(\delta^3), \\
\epsilon_4(n) &= S_4 - L_4\delta + \tfrac{1}{2}K_4\delta^2 + O(\delta^3)
\end{aligned} \tag{35}$$

Since we include also quartic terms β^4, we must differentiate between these local symmetry parameters S_2, L_2, etc. and the full symmetry parameters defined as the difference between symmetric matter and pure neutron matter (see also the discussion of Lattimer [161]). Using $a_1 = b_1 n_0^{/3}$, see Table II, we obtain the values for S_2 and L_2 given by relations:

$$S_2 = \frac{1}{3}\varepsilon_F + 2a_1 n_0^{2/3} + c_1 n_0^{4/3}, \tag{36a}$$

$$L_2 = \frac{2}{3}\varepsilon_F + 5a_1 n_0^{2/3} + 4c_1 n_0^{4/3}. \tag{36b}$$

As shown in Table III, the binding energy of nuclear matter and the symmetry energy predicted by SeaLL1 fit agrees well with the value obtained with the mass formula (2), see also the discussion in the Appendix section V B and Table V. Our fits generally estimate the slope of the symmetry energy L_2 from 29 MeV to 36 MeV. However, our fits with orbital-free functionals (NEDF-E, NEDF-En, NEDF-Er, and NEDF-Enr, see section V B) demonstrate that this quantity is not well constrained by the masses and can be adjusted independently with the combination $a_1 - b_1 n_0^{1/3}$ and/or coefficient c_1.

We also compute the neutron skin thickness of ^{48}Ca and

NEDF	ρ_0 [fm^{-3}]	$-\epsilon_0$	K_0	S	L	L_2	Neutron skin ^{208}Pb [fm]	^{48}Ca [fm]
SeaLL1	0.154	15.58	230.0	31.7	32.4	31.6	0.131	0.155

Table III. Saturation, symmetry, and neutron skin properties for *SeaLL1*. All values in MeV unless otherwise specified.

^{208}Pb, for which precision measurements CREX and PREX[3] are underway, see [162] for details. For NEDF-1 through NEDF-3rn, the neutron skin of ^{208}Pb ranges from 0.07 fm to 0.09 fm while the ^{48}Ca skin ranges from 0.106 fm to 0.125 fm. The ^{208}Pb neutron skin appears quite a bit thinner than the value $0.156^{+0.025}_{-0.021}$ fm of Tamii *et al.* [163] extracted from measurements of the dipole polarizability using the method suggested by Reinhard and Nazarewicz [164] based on observed correlations between these two quantities in Skyrme models, and with the recent measurement of 0.15(3) fm [165], but the results of NEDF-E, NEDF-Er, NEDF-En, and NEDF-Enr demonstrate that this is also controlled by the same combination $a_1 - b_1 n_0^{1/3}$ as L_2, and hence unconstrained by the masses.

Since the slope of the symmetry energy $L = L_2 + L_4 + \cdots \approx 30$ MeV is fixed by the neutron matter equation of state, see Appendix, requiring a larger value of $L_2 \approx 60$ MeV to explain the neutron skin thickness of ^{208}Pb also suggests that at least quartic terms are required in the functional.

E. Fission pathway of ^{240}Pu

One of the long term goals of developing a NEDF is to predict and describe fission observables in heavy nuclei. In this context, fission pathways are often used as a benchmark for NEDFs. To this end, we computed the potential energy surface of ^{240}Pu with SeaLL1 by performing a constrained HFB calculation with constraints of mass quadrupole moment Q_{20} and octuple moment Q_{30} on the plane $0 \le Q_{20} \le 200\,\mathrm{b}, 0 \le Q_{30} \le 40\,\mathrm{b}^{3/2}$, as shown in Fig. 15. The definitions and units of Q_{20} and Q_{30} are consistent with Ref. [166]. Fig. 16 displays the potential energy curve of ^{240}Pu as a function of Q_{20} on the (asymmetric) fission pathway with SeaLL1, SkM* [167], and UNEDF1-HFB [168]. The characteristics of the HO basis used in the calculation are the same as in [169].

Since all these calculations were done with the HFBTHO DFT solver, triaxiality is not included and the height of the first fission barrier is typically overestimated for all 3 functionals by about 2 MeV [169]. Compared with SkM* and UNEDF1-HFB, SeaLL1 gives a lower excitation energy of the fission isomer ($E_I = 0.54$ MeV) and lower heights of both fission barriers ($E_A = 6.84$ MeV, and $E_B = 4.20$ MeV respectively for inner and outer barriers). This discrepancy is not too surprising since we do not include the deformation properties of heavy nuclei into the optimization of SeaLL1, unlike SkM* and UNEDF1-HFB [157].

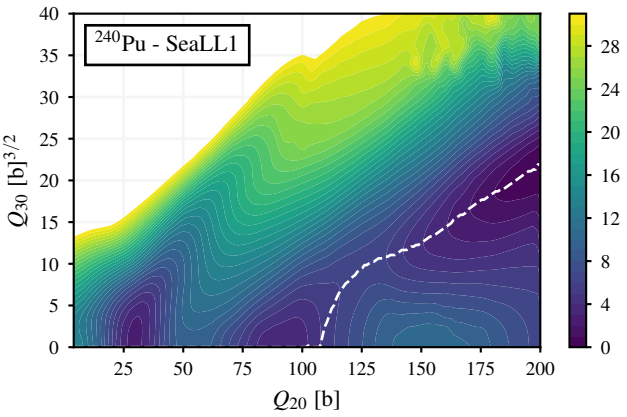

Figure 15. (Color online) Potential energy surface of ^{240}Pu with SeaLL1 on the plane $0 \le Q_{20} \le 200\,\mathrm{b}, 0 \le Q_{30} \le 40\,\mathrm{b}^{3/2}$. The most likely, asymmetric, fission path is denoted as white dashed line.

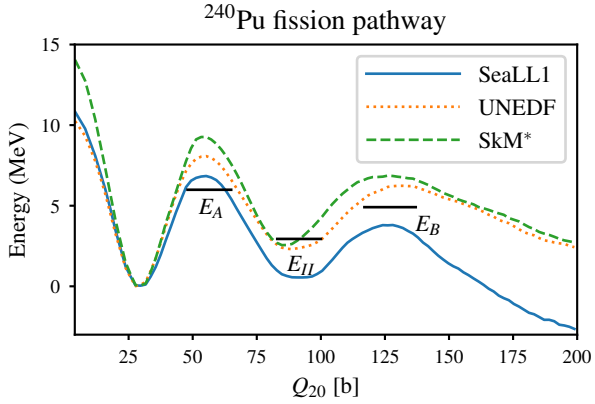

Figure 16. (Color online) Fission pathway for ^{240}Pu along the mass quadrupole moment Q_{20} calculated using HFBTHO with SeaLL1, SkM*, and UNEDF1.

F. Neutron and Proton Drip Lines

In Fig. 17 we compare the proton and neutron drip lines obtained with SeaLL1 against the predictions of UNEDF1, as well as those obtained with other Skyrme parametrizations extracted from the supplemental data of Erler *et al.* [170] and using FRLDM [58]. SeaLL1 predicts that there are 7716 stable nuclei with $Z \le 120$, as compared with 8450 in case of UNEDF1, 7212 for SLy4. The position of the neutron drip line may dramatically impact the astrophysical r-process, which is predicted to follow lines of constant separation energy in close proximity to the neutron dripline [174, 175]. Meyer [174] considered neutron star ejecta as the site of r-process nucleosynthesis, and determined that the reaction flow is very

[3] Proposals and related information available at http://hallaweb.jlab.org/parity/prex

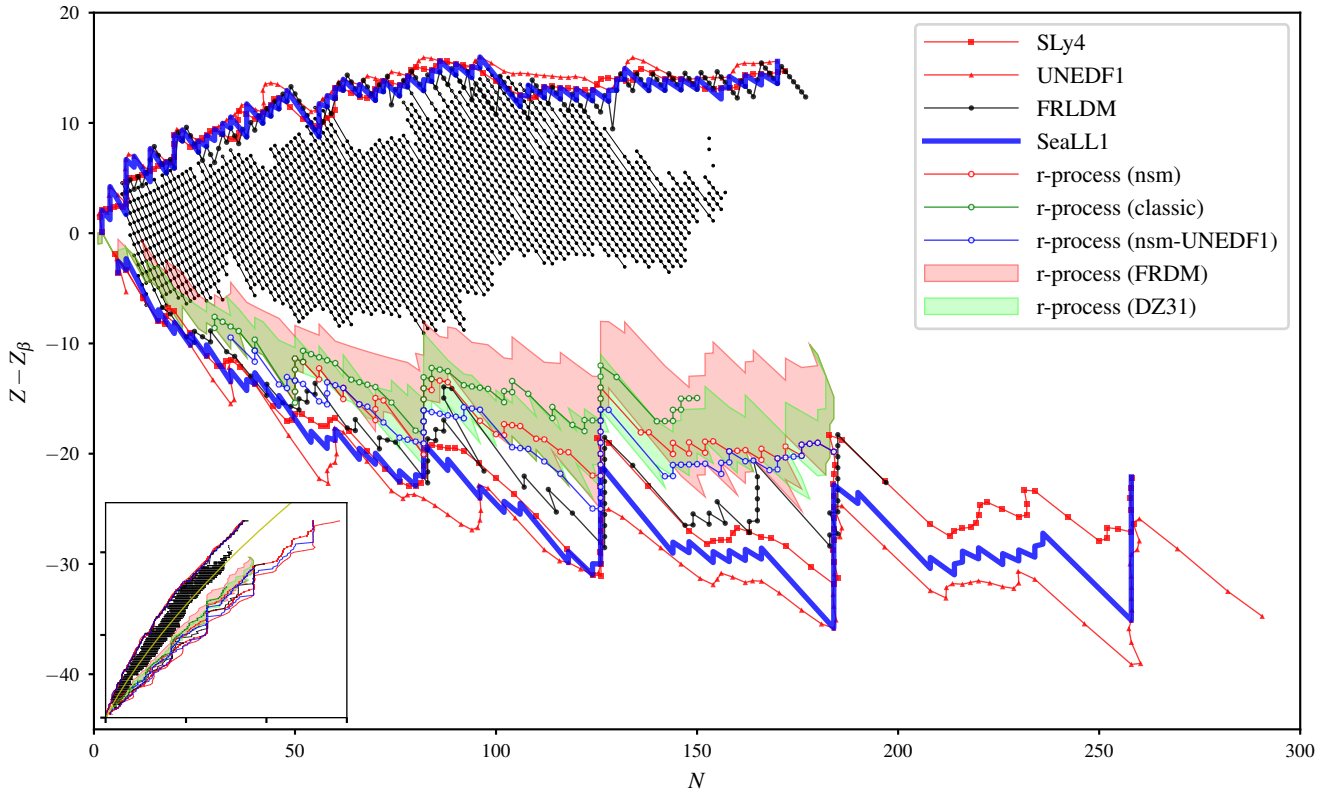

Figure 17. (Color online) Fully self-consistent calculations of the proton and neutron driplines for the SeaLL1 NEDF (thick blue line) compared with predictions of the functionals SLy4 and UNEDF1 extracted from Ref. [170], and FRLDM [58]. The vertical axis is shifted by the approximate β-stability line $Z_\beta(N)$ which minimizes Eq. (1) at constant A with parameters from Table I: $\partial_Z E(A-Z,Z)|_{Z=Z_\beta} = 0$, $Z_\beta = A/(2 + a_C A^{2/3}/2a_I)$. The inset shows the usual Z vs. N plot, with the $Z = Z_\beta(N)$ curve as a solid (yellow) line. The 2375 nuclear masses from [1, 2] are displayed as dots. We have plotted possible r-process trajectories predicted to be realized in the case of two neutron star mergers [6, 7] (red circles), in a classical hot $(n,\gamma) \leftrightarrow (\gamma,n)$ in equilibrium r-process [171] (green circles) with the FRDM model [58] and neutron star merger with the UNEDF1 functional [66] (blue circles). With pink and green bands we display the r-process paths obtained by Mendoza-Temis *et al.* [172] under various conditions using the FRDM model [58] and the Duflo-Zuker model [173].

close to the dripline. One should keep in mind also that the precise position of the drip lines is difficult to pinpoint, since the fluctuations, comparable to the theoretical errors, in the separation energies have large fluctuations in their vicinity. Even though his simulations were performed for relatively cold matter (recent simulations seem to indicate that the star material is somewhat heated [176, 177]), it will be interesting to simulate the r-process using SeaLL1. The predicted position of the neutron dripline will likely affect the structure of the neutron star crust inferred from older studies [82–84, 178–183]. The corresponding increase in the neutron skin thickness will also affect the profile and the pinning energy of quantized vortices in the neutron star crust [184–190].

Fusion cross sections [191, 192] will also be significantly altered, particularly in stellar environments where neutron rich nuclei fuse via pycnonuclear reactions [193, 194], and where the neutron gas surrounding nuclei leads to their swelling [195]. A thicker neutron skin with further enhance this effect.

G. Neutron star crust

The baryon matter in the Universe organizes itself based on the short-range nuclear attraction and the long-range Couloumb repulsion. At densities much lower than the nuclear saturation density, $n \approx 0.16\,\mathrm{fm}^{-3}$, the nuclear and atomic length scales are well separated, nuclei in matter are expected to form the Coulomb lattice embedded in the neutron-electron seas that minimizes the Coulomb interaction energy. At subsaturation baryon densities, $0.1n_0 < n < 0.8n_0$, conditions expected in the bottom layers of the inner crust of neutron star, there is a strong competition between the Coulomb and strong interactions, which leads to the emergence of various complex structures with similar energies that are collectively referred to as "nuclear pasta" [181, 196, 197]. Pasta nuclei are eventually dissolved into uniform matter at a certain nucleon density below n_0. Existence of pasta phases would modify some important processes by changing the hydrodynamic properties and the neutrino opacity in core-collapse supernovae [198, 199] and proto-neutron stars [200, 201]. Also, the pasta phases may

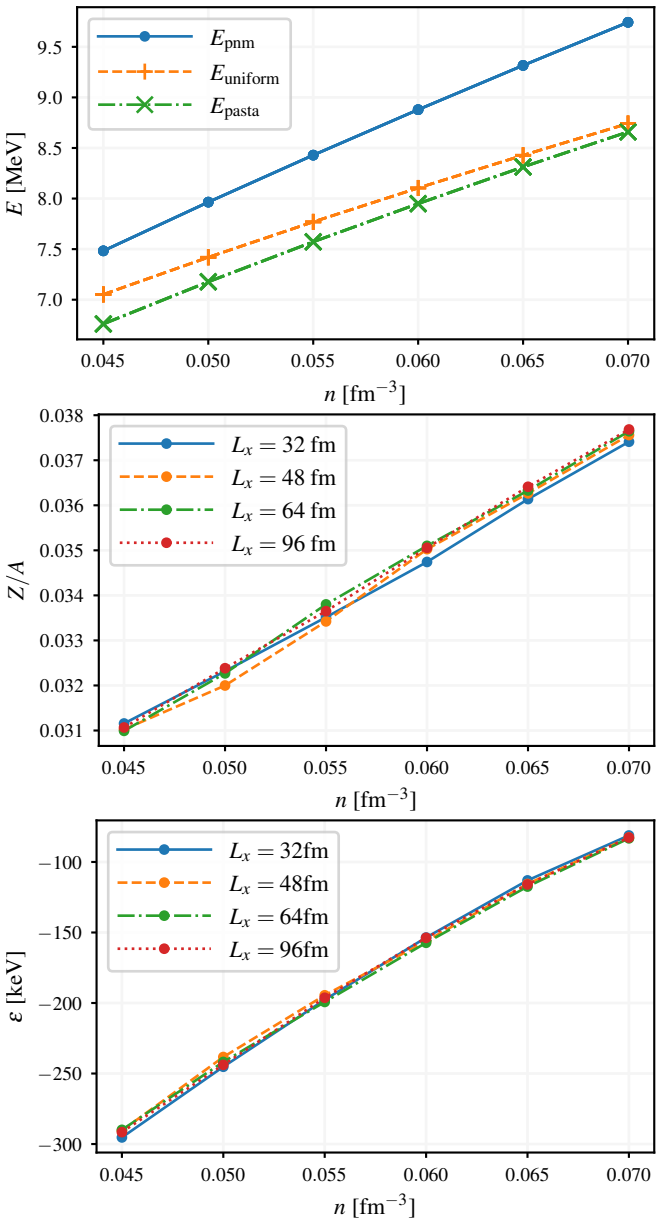

Figure 18. (Color online) Top panel: energy per baryon in the pasta phase ($E_{\rm past}$), energy per neutron in pure neutron matter ($E_{\rm pnm}$), and energy per baryon in uniform nuclear matter ($E_{\rm uni}$) as a function of average baryon density. Middle panel: Charge ratio of the nuclear pasta as a function of average baryon density. Bottom panel: the energy per nucleon difference between the uniform and the inhomogeneous matter configurations in β-equilibrium as a function of the average baryon density.

influence neutron star quakes and pulsar glitches via the change of mechanical properties of the crust matter [202–204].

Since its prediction, significant progress has been made in simulating the pasta phases [205–207]. In this section, we use the hydrodynamics model to simulate the pasta phases at average baryon densities $0.045 \le n \le 0.07\,\mathrm{fm}^{-3}$. In the nuclear-pasta system, the chemical potentials of baryons and electrons satisfy the β-equilibrium condition

$$\mu_n = \mu_p + \mu_e \tag{37}$$

where μ_q is the chemical potential of species $q = n, p, e$ for neutrons, protons, and electrons, respectively, and $\Delta m = m_n - m_p$ is the neutron-proton mass difference. The total energy is the sum of the baryon energy $E_{\rm baryon}$, the electron density $E_{\rm elec}$, and the proton-neutron mass difference

$$E_{\rm pasta} = E_{\rm baryon} + E_{\rm elec} - \Delta m c^2 Z. \tag{38}$$

For the baryon energy, we use the hydrodynamics model defined in Sec. V B with the SeaLL1 parametrization. The electron energy is the Thomas-Fermi energy for relativistic electrons

$$E_{\rm elec} = \int \mathrm{d}^3\boldsymbol{r}\ (3\pi^2 n_e)^{4/3}\frac{\hbar c}{4\pi^2} \tag{39}$$

where the electron density is determined from Eq. (38) as

$$n_e(\boldsymbol{r}) = \Theta(\mu_n - \mu_p + V_c(\boldsymbol{r}) + \Delta m c^2) \times \frac{1}{3\pi^2}\left(\frac{\mu_n - \mu_p + V_c(\boldsymbol{r}) + \Delta m c^2}{\hbar c}\right)^3. \tag{40}$$

where $V_c(\boldsymbol{r})$ is the Coulomb potential experienced by electrons, which includes both the direct and the relativistic exchange parts [11] (notice the positive sign, opposite from the non-relativistic Slater approximation)

$$V_c(\boldsymbol{r}) = e^2\int \mathrm{d}^3\boldsymbol{r}'\ \frac{n_c(\boldsymbol{r}')}{|\boldsymbol{r}-\boldsymbol{r}'|} + \frac{1}{2}e^2\left(\frac{3}{\pi}n_e(\boldsymbol{r})\right)^{1/3} \tag{41}$$

where $n_c(\boldsymbol{r}) = n_p(\boldsymbol{r}) - n_e(\boldsymbol{r})$ is the charge density. Through solving the hydrodynamics equation similar to Eq. (50a) for baryons and Eq. (40) for electrons, the charge number $Z = \int \mathrm{d}^3\boldsymbol{r}\ n_e(\boldsymbol{r})$ is determined self-consistently for a given baryon number $A = N_n + N_p$ where $N_p = Z$ is satisfied for charge neutrality. Numerically, we perform this calculation in a 3D cubic lattice with periodic boundary conditions at average baryon densities $n = 0.045$, 0.05, 0.055, 0.06, 0.065 and $0.07\,\mathrm{fm}^{-3}$. To explore the role of finite size effect, the size of cubic lattice is chosen as $L_x = 32$, 48, 64 and 96 fm respectively for all ns. The lattice constant is fixed as $dx = 1.00$ fm. In Fig. 18 we compare the energy of uniform pure neutron matter, with uniform matter in β-equilibrium, and allowing for the formation of inhomogeneities. Even though for various size cubic boxes the spatial distribution of the matter at a given average density is not identical, the gain in energy and the proton/neutron ratios are practically the same and at an average density slightly above $0.07\,\mathrm{fm}^{-3}$ the matter distribution becomes homogeneous.

IV. COMPARISON WITH OTHER NEDFs

The accuracy of the ground state binding energies obtained using SeaLL1 NEDF compares extremely well with other approaches.

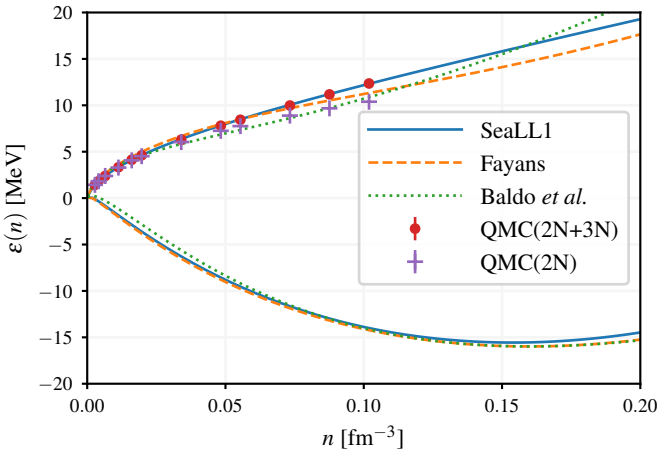

Figure 19. (Color online) The energy per nucleon for pure neutron matter and symmetric neutron matter used in SeaLL1, compared to the corresponding energies used by Fayans [97] and Baldo *et al.* [99, 100, 208]. For comparison we have shown with a dashed line the results of the QMC calculation of Wlazłowski *et al.* [122], with 2N and 3N interactions as well the result with the 2N interactions alone.

The UNEDF1 nuclear energy functional introduced by Kortelainen *et al.* [66] has a residual of $\chi_E = 1.91$ MeV per nucleus for 555 even-even nuclei from AME2013 [209] and an rms of 0.75 MeV and 0.79 MeV for the S_{2n} and S_{2p} compared to $\chi_E = 1.74$ MeV, 0.69 MeV and 0.59 MeV for S_{2n} and S_{2p} respectively fin case of SeaLL1. The UNEDF2 functional of Kortelainen *et al.* [159] depends on 14 parameters. It is also characterized by a larger pairing coupling constant for protons than for neutrons. As mentioned in section II F, this result is in agreement with large-scale surveys of the odd-even mass differences [137], but stands in contrast with isospin invariance and the expectation that Coulomb effects should reduce proton pairing as discussed Lesinski *et al.* [138], Hebeler *et al.* [139], and Yamagami *et al.* [140]. A natural solution might be to include in the NEDF a pairing contribution of the form specified in Eq. (24a).

Baldo *et al.* [99, 100] introduced an energy density functional based on information extracted from Brueckner-Hartree-Fock calculations of neutron and symmetric nuclear matter [208], and a few additional parameters to describe pairing and spin-orbit interaction and finite range effects. This approach is similar to the one suggested by Fayans [97, 98], in the spirit of the Kohn-Sham DFT [10]. They assume that no quartic terms in isospin β^4 are present in the NEDF, as their equation of state for neutron matter is softer than the equation of state determined in QMC calculations of Wlazłowski *et al.* [122], see discussion in section V D. These authors find a $\chi_E = 1.58$ MeV for 579 even-even nuclei in AME2003 [209] and a $\chi_r = 0.027$ fm for 313 nuclei.

Goriely *et al.* [62, 64] have produced over the years a series of high-accuracy mass models based on Skyrme NEDFs. Their best model gives an average rms slightly lower than 0.5 MeV for the entire mass table. However, in contrast with the UNEDF and BPCM family, and our own work, this result was obtained by adding a number of phenomenological corrections, a procedure which so far has not been adopted by the other practitioners using microscopic approaches.

Finally, we also mention work with the relativistic mean-field theory (RMFT) of nuclei. State-of-the-art parametrizations of the relativistic NEDF yields a χ_E between from 2 MeV to 3 MeV for even nuclei using the AME2012 data set [210, 211].

V. CONCLUSIONS

The nuclear energy density functional (NEDF) developed in this work, which we call SeaLL1, contains 7 significant parameters, each clearly related to specific properties of nuclei. Even in its present form, which has not yet been fully optimized, the SeaLL1 NEDF describes the nuclear masses of 606 even-nuclei from the AME2012 evaluation [1, 2] with a mean energy error of 0.97 MeV and a standard deviation 1.46 MeV, two-neutron and two-proton separation energies with rms errors of 0.69 MeV and 0.59 MeV respectively, and the charge radii of 345 even-even nuclei [3] with an rms error of 0.034 fm. SeaLL1 also incorporates the equation of state of pure neutron matter from quantum Monte Carlo calculations with chiral effective field theory NN interactions at N3LO level and NNN interactions at the N2LO level.

The NEDF presented here is physically intuitive, and provides a clear strategy for improving the quality of mass fits by separating contributions of various energy scales in the χ_E of nuclear masses. In this respect, the approach outlined here and used before by Bertsch *et al.* [153], is similar in spirit to an effective field theory. Here we have identified the bulk properties, and shown that they can be properly accounted for with a minimal number of 7 parameters.

As in the mass formulas Eqs. (1) and (2), one needs two parameters b_0 and c_0 to reproduce the symmetric nuclear binding energy and saturation density. With these parameters, the isoscalar nuclear compressibility also acquires a reasonable value, although the saturation density is a little low. The saturation density is not well constrained by the mass fits alone, but can be constrained by also considering the charge radii as discussed in Fig. 5.

Two other parameters, a_1 and b_1, control the symmetry properties of nuclear matter. This is similar to the parameters a_I and a_I' in nuclear mass formula Eq. (2), but we find that the linear combination $a_1 - b_1 n_0^{1/3}$ is poorly constrained by the masses. This gives one an essentially independent control of the "local" symmetry energy slope L_2 (not the full L, which is fully determined by the neutron equation of state), along with neutron skin thicknesses.

Correlated with these two parameters (see Fig. 6) is a gradient term with parameter η_s that controls the diffuseness of the nuclear surface. This defines the strength of the gradient correction term needed in the NEDF that characterizes the nuclear surface tension and surface properties.

The addition of quartic isovector terms $\propto \beta^4$ permit the NEDF to match the neutron matter equation of state without significantly affecting the global mass fit. We thus find that nuclear masses and the neutron matter equation of state are essentially uncoupled.

Two additional parameters are required, W_0 and g, to describe the spin-orbit interaction and the pairing correlations.

In its orbital-based formulation, the SeaLL1 NEDF contains several new elements with respect to commonly used Skyrme-like density functional theories:

- Terms proportional to $n^{5/3}$, similar to those found in the study of the unitary Fermi gas.
- There is a need to consider quartic terms in isospin density $(n_n - n_p)^4$ in the NEDF if one aims to describe correctly both nuclei and neutron matter within the same unified framework, and in particular the neutron star crust. The binding energies, charge radii, and neutron skin thickness appear to be insensitive to the properties of the neutron equation of state, which can essentially be fit independently. The position of the neutron dripline appears to be controlled by the full symmetry energy S and its density dependence L, unlike the neutron skin thickness, which is controlled by the "local" density dependence of the symmetry energy L_2. The properties of nuclear matter in stellar environments (when $N \gg Z$) will therefore be controlled by S and L, influencing for example the reaction flow in the r-process, the structure of the neutron star crust, and the vortex pinning mechanism in neutron star crust.
- Entrainment terms

$$\mathcal{E}_{\text{entrain}} = g_{\text{ent}} \left(\frac{n_n n_p}{n^2}\right) \frac{n}{2m} \left|\frac{\boldsymbol{j}_n}{n_n} - \frac{\boldsymbol{j}_p}{n_p}\right|^2, \qquad \text{(Eq. 25)}$$

  where $\boldsymbol{j}_{n,p}$ are the density currents (10f), do not appear in any standard theory of large amplitude collective motion in nuclear physics [56, 212, 213], despite being allowed by symmetry. They have direct analogues in superfluid mixtures – the Andreev-Bashkin effect – and are as natural to consider in the presence of mixed proton and neutron superfluids in neutron stars as they are in mixtures of ^{3}He and ^{4}He superfluids [141–143]. These terms have little influence on ground state properties, but a strong effect on excited isovector modes. Such terms have been discussed in the physics of neutron stars where they are relevant for describing glitches, the damping of gravitational instabilities, and other collective modes [144–150]. The parameter α can be determined by fixing the excitation energy of the giant dipole resonance and the correct value of the Thomas-Reiche-Kuhn sum rule.
- A second type of entrainment contribution can be introduced as well, with which one can control the Gamow-Teller transitions and β-transition matrix elements.

$$\tilde{\mathcal{E}}_{\text{spin entrain}} = \tilde{g}_{\text{ent}} \left(\frac{n_n n_p}{n^2}\right) \frac{n}{2m} \left|\frac{\boldsymbol{J}_n}{n_n} - \frac{\boldsymbol{J}_p}{n_p}\right|^2, \qquad (42)$$

  where $\boldsymbol{J}_{n,p}$ are the spin-density currents (10g).

By using a principal component analysis, we establish that a number of parameters play an insignificant role in the mass fit, and their values can be varied significantly without affecting the quality of the χ_E. We refer to these as insignificant or subdominant parameters, and identify how they can be used to fine-tune the values of other observables.

For example, although not included in our fit, we obtain a reasonable value of the nuclear compressibility $K_0 = 230$ MeV, see Table III. However, its value could be even further fine-tuned by changing the value of the insignificant parameter a_0, which vanishes in our SeaLL1 fit, while keeping saturation density and binding energy of symmetric nuclear matter fixed:

$$K_0 = \frac{6}{5}\varepsilon_F - 12\varepsilon_0 + 2a_0 n_0^{2/3}, \qquad (43)$$

see also Eq. (33c) and Table II.

Although the full symmetry energy S and its density dependence L at saturation are fixed by the properties of pure neutron matter, the values of the local symmetry energy S_2, and its density dependence L_2 can be independently controlled by the insignificant parameters $a_1 - b_1 n_0^{1/3}$ and c_1,

$$S_2 = \frac{1}{3}\varepsilon_F + \left(a_1 + b_1 n_0^{1/3}\right) n_0^{2/3} + c_1 n_0^{4/3}, \qquad \text{(Eq. 36a)}$$

$$L_2 = \frac{2}{3}\varepsilon_F + \frac{5}{2}\left(a_1 + b_1 n_0^{1/3}\right) n_0^{2/3} - \frac{1}{2}\left(a_1 - b_1 n_0^{1/3}\right) n_0^{2/3} + 4c_1 n_0^{4/3}. \qquad \text{(Eq. 36b)}$$

This allows one the freedom to control the neutron skin thickness without affecting the quality of the mass fits.

Additional control may be obtained by introducing generalizations of the terms included in SeaLL1. These may be used to refine other nuclear properties, including the static electric dipole polarizability, nucleon effective masses, single-particle spectra, proton and neutron pairing gaps, fission barriers and the second fission isomer energies.

For example,

$$\mathcal{E}_{\boldsymbol{\nabla} n} = \eta_0 \frac{\hbar^2}{2m}|\boldsymbol{\nabla} n_n + \boldsymbol{\nabla} n_p|^2 + \eta_1 \frac{\hbar^2}{2m}|\boldsymbol{\nabla} n_n - \boldsymbol{\nabla} n_p|^2 \quad \text{(Eq. 19)}$$

with $\eta_0 \neq \eta_1$ would allow one to adjust the neutron skin thickness somewhat independently from the symmetry properties of the functional. The single-particle spectra for ^{48}Ca and ^{208}Pb obtained with SealLL1 have a larger neutron gaps and smaller proton gaps than measured experimentally (see Figs. 13 and 14). This could be remedied by tuning independently tuning the parameters $W_0 \neq W_1$ in the spin-orbit term:

$$\mathcal{E}_{\text{SO}} = W_0 \boldsymbol{J} \cdot \boldsymbol{\nabla} n + W_1 (\boldsymbol{J}_n - \boldsymbol{J}_p) \cdot (\boldsymbol{\nabla} n_n - \boldsymbol{\nabla} n_p). \quad \text{(Eq. (22))}$$

One could further tune the single-particle spectra by judiciously introducing terms of the type

$$\mathcal{E}_\tau \propto \tau n^\sigma - \boldsymbol{j}^2 n^{\sigma-1} - \frac{3}{5}(3\pi^2)^{2/3} n^{5/3+\sigma} \propto \frac{|\boldsymbol{\nabla} n|^2}{n^{1-\sigma}}, \quad \text{(Eq. (20))}$$

with obvious isospin structure not explicitly illustrated, which affect the nucleon effective masses. For example, until now it was not realized that a standard term in Skyrme-like functionals

terms τn^σ can be used in the combination (20) and would play a subdominant role in mass fits.

Similarly, a long standing feature of standard NEDFs requires breaking the isospin symmetry of the pairing contribution, even needing stronger proton pairing than neutron pairing [137, 157] despite the Coulomb repulsion. This can easily remedied instead by using a modified pairing form of the type:

$$\mathcal{E}_{\Delta} = \sum_{q=n,p} \int \mathrm{d}^3\boldsymbol{r}\; g_{\mathrm{eff}}(\boldsymbol{r})|\nu_q(\boldsymbol{r})|^2 + \int \mathrm{d}^3\boldsymbol{r}\; h_{\mathrm{eff}}(\boldsymbol{r})\left[|\nu_n(\boldsymbol{r})|^2 - |\nu_p(\boldsymbol{r})|^2\right]\beta, \quad \text{(Eq. (24a))}$$

with $h_{\mathrm{eff}}(\boldsymbol{r}) \neq 0$.

An additional subdominant term of the type

$$\tilde{\mathcal{E}}_{\mathrm{spin}} = \alpha_1\left(\boldsymbol{s}_n^2 + \boldsymbol{s}_p^2\right) + \alpha_2 \boldsymbol{s}_n \cdot \boldsymbol{s}_p, \tag{44a}$$

should be considered as well. The contribution of spin densities is typically much smaller than the contributions of the densities in nuclei, $\int \mathrm{d}^3\boldsymbol{r}\; n_{n,p}(\boldsymbol{r}) \gg \left|\int \mathrm{d}^3\boldsymbol{r}\; \boldsymbol{s}_{n,p}(\boldsymbol{r})\right|$, as in even-even nuclei $\boldsymbol{s}_{n,p}(\boldsymbol{r}) \equiv 0$, and thus these terms will play a noticeable role in odd A and odd N-odd Z nuclei mainly [214]. The term proportional to α_2 will be important mostly in odd-odd nuclei. These type of contributions will affect in particular β-decay matrix elements.

The structure of the double-humped fission barriers also depends critically on the character of shell-corrections (see Fig. 16, and is thus sensitive to the single-particle spectrum structure. Hence, fission properties may be tuned by adjusting all of the subdominant terms discussed above without degrading the ability of the functional to fit masses and charge radii. Thus, while the fission properties of the simple SeaLL1 functional as presented are quite reasonable without any fine tuning, there is room for substantial improvement through these 10 or so subdominant parameters: the more complicated spin-orbit terms (22) with $W_0 \neq W_1$, gradient terms (19) with $\eta_0 \neq \eta_1$, gradient terms modifying the nucleon effective masses (20), density dependent pairing terms (24a) with both couplings g_{eff} and h_{eff} non-vanishing, subdominant corrections to the symmetry energy (36a) and (36b) with $a_1 - b_1 n_0^{1/3} \neq 0$ and $c_1 \neq 0$ and even the compressibility K_0 (43) for non-vanishing values of the parameter a_0, and spin-density terms (44a) in particular for odd A nuclei and odd Z-odd N nuclei.

We now have a clear path to refine the structure of the NEDF, systematically adding physically motivated parameters in order to better describe nuclear physics observables, such as the static dipole polarizability, the energies of the giant dipole and of the Gamow-Teller resonances, the Thomas-Reiche-Kuhn sum rule, the neutron skin thickness, finer details of the shell structure, nucleon effective mass, pairing gaps, fission, etc. The next step is to account for correlation energies; the center-of-mass corrections, which, in the case of self-bound systems, present some challenges [215–222]; the particle number; and angular momentum projections [223]. Previous results indicate that accounting for these should reduce the rms energy from about 1.7 MeV to about 0.5 MeV [28, 45–60]. Further improvement will likely require a proper accounting for quantum chaos [69–77].

ACKNOWLEDGMENTS

We are grateful to George F. Bertsch for numerous discussions and suggestions, to Rebecca Surman, Gabriel Martinez-Pinedo and Meng-Ru Wu for providing the data for the r-process trajectories, to Jeremy W. Holt, David B. Kaplan, Jérôme Margueron, Piotr Magierski, and Sanjay Reddy for comments. This work was supported in part by US DOE Grant No. DE-FG02-97ER-41014 and a WSU Seed Grant. Some calculations reported here have been performed at the University of Washington Hyak cluster funded by the NSF MRI Grant No. PHY-0922770.

APPENDIX

A. Orbital-Free Functional

Here we discuss some details of the orbital-free theory described in section III.

As mentioned there, the main challenge in formulating an orbital-free theory is to express terms with the auxiliary densities $\tau_{n,p}$, ν, $\boldsymbol{J}_{n,p}$, and $\boldsymbol{j}_{n,p}$ by an appropriate functional of the number densities $n_{n,p}$. One approach is to start with a semiclassical expansion. Neglecting the spin-orbit interaction (21), the kinetic density τ admits the following semiclassical expansion [11, 24, 151]:

$$\tau \approx \overbrace{\tfrac{3}{5}(3\pi^2)^{2/3}n^{5/3}}^{\tau_{TF}[n]} + \overbrace{\frac{1}{9}\left|\boldsymbol{\nabla}\sqrt{n}\right|^2}^{\tau_2[n]} + \tau_4[n] + \cdots \tag{45}$$

The factor of $1/9$ can be derived rigorously for smoothly varying densities, along with higher order terms discussed in Eq. (48) below. This should be compared with the factor of unity originally suggested by Weizsäcker [8], later shown to be valid only if the density has small amplitude rapid oscillations [11, 24, 151]. For nuclei, the semiclassical result is relevant for the bulk, but gives incorrect asymptotic behavior, while Weizsäcker's result reproduces the correct asymptotic behavior, but is a poor approximation in the bulk, see [49] for a discussion. Resolving this tension is an active area of research in DFT, and many suggestions have been compared [224].

The simplest option is to treat the coefficient $1/9 = \eta$ as a phenomenological parameter, since gradient terms can also be generated by interactions [225–227]. Fitting the nuclear masses yields values of η close to 0.5, roughly half-way between the semiclassical and Weizsäcker values (see the discussion in the supplement refsec:suppl-mater). Stocker *et al.* [228] used a similar approach in order to discuss the anomaly in the nuclear curvature energy – the term in the nuclear mass formula $\propto A^{1/3}$.

Another appealing approach suggested by DePristo and Kress [152] and advocated in [11] is to use a Padé approximant $F(X)$ to interpolate between the semiclassical and asymptotic results:

$$\tau \approx \tau_{TF}[n]F(X), \qquad X = \frac{\tau_2[n]}{\tau_{TF}[n]}. \tag{46}$$

DePristo and Kress [152] motivate a rather complicated form $F(X)$, but for nuclei, we find little improvement over the

following single-parameter form:

$$F(X) = \frac{1 + (1+\kappa) + 9\kappa X^2}{1 + \kappa X} = \begin{cases} 1 + X & X \ll 1 \\ 9X & X \gg 1. \end{cases} \tag{47}$$

Note: the approximation $\eta \approx 1/9$ mentioned above is implemented with $F(X) = 1 + 9\eta X$.

The next order in the semiclassical expansion of non-interacting fermions [11, 24] is:

$$\tau_4[n] = \frac{1}{810(3\pi^2)^{2/3}} f(n), \tag{48}$$
$$f(n) = n^{1/3}\left[\left(\frac{\boldsymbol{\nabla} n}{n}\right)^4 - \frac{27}{8}\left(\frac{\boldsymbol{\nabla} n}{n}\right)^2 \frac{\boldsymbol{\nabla}^2 n}{n} + 3\left(\frac{\boldsymbol{\nabla}^2 n}{n}\right)^2\right].$$

This type of correction has been studied in nuclear physics and shown to lead to quite accurate estimates of the kinetic energy density within the extended Thomas-Fermi approximation [24, 49, 229]. Within a DFT, such terms can also arise due to the finite range of the interactions in a matter similar to some Skyrme interactions [225–227]. However, these terms – even with adjustable parameters – do not significantly change the quality of the mass fits, so we do not consider them in our main analysis. Including them perturbatively in the fit, however, does improve the fit of the charge radii. For example, fitting the overall coefficient reduce the charge radii residual χ_r (see details in Section V B) from $\chi_r \approx 0.14\,\text{fm}$ to $\chi_r \approx 0.09\,\text{fm}$. Fitting each of the three terms independently further reduces the residuals to $\chi_r \approx 0.06\,\text{fm}$. Fourth-order terms are neglected as they can lead to a complex behavior of the emerging equation for the densities, which can be difficult to rationalize. (See, for example, the analysis of fourth order differential equations arising in case of non-local potentials by Bulgac [230].) Higher order gradient corrections than Eq. (48) lead to an unphysical behavior of the densities in the classically forbidden regions. Furthermore, the semiclassical expansion has an asymptotic character [151], and corrections beyond second order do not always improve the functional. Finally, when using a properly fit Padé approximant Eq. (28b), we find that $\int \tau_{TF}[n]F(X) - \tau_{TF}[n] - \tau_2[n]\mathrm{d}^3\boldsymbol{x} \approx \int \tau_4[n]\mathrm{d}^3\boldsymbol{x}$ for many nuclei. Thus, the Padé approximant Eq. (28b) seems to incorporate the qualitative effects of the $\tau_4[n]$ term. For these reasons, we do not include fourth-order corrections $\tau_4[n]$ in our orbital-free theory.

When spin-orbit interactions are included, they modify the semiclassical expansion. Thus, to properly express the orbital-free theory, we must consider both terms together. The correct semiclassical expansion of this combined energy density to second order is [49, 229]:

$$\begin{aligned}\mathcal{E}_{\text{kin}} + \mathcal{E}_{\text{SO}} &= \frac{\hbar^2}{2m}(\tau_n + \tau_p) + W_0 \boldsymbol{J} \cdot \boldsymbol{\nabla} n \\ &\approx \frac{\hbar^2}{2m}\left(\tau_{TF}[n_n] + \tau_{TF}[n_p] + \tau_2[n_n] + \tau_2[n_p]\right) \\ &\quad - \frac{W_0^2}{2}\frac{2m}{\hbar^2} n(\boldsymbol{\nabla} n)^2. \end{aligned} \tag{49}$$

Note that the sign of the last term differs from the expression (7) in [229] which contains only the kinetic component. The result here combines both the kinetic and spin-orbit contributions, altering the sign. (The remaining terms in the functional only alter the mean-field potential, and so they do not affect this result.)

This expansion suffers the same problems as the pure semiclassical expansion of the kinetic energy Eq. (45). Thus, for the reasons discussed above, we replace $\tau_{TF} + \tau_2$ with the Padé approximant Eq. (28b). In principle, a similar correction could be used with the spin-orbit term, however, this term has the form $n(\boldsymbol{\nabla} n)^2$ instead of $\tau_2 \propto (\boldsymbol{\nabla} n)^2/n$. It is therefore suppressed in the tails and does not effect the asymptotic behavior of the nuclear density profile. Note that the scaling is similar to the gradient correction. For this reason we keep the semiclassical form, but refit the coefficient η_s to compensate for any inaccuracies.

The equations that determine the equilibrium densities of a nucleus in the orbital-free theory are obtained by minimizing the energy of a given nucleus $E(N,Z) = \int \mathrm{d}^3\boldsymbol{r}\ \mathcal{E}[n_n, n_p]$ with respect to the densities, while constraining the total numbers of neutrons N and protons Z with two chemical potentials $\mu_{n,p}$:

$$-\frac{\hbar^2}{2m}\boldsymbol{\nabla} \cdot \left(\frac{F'(X_q)}{9}\boldsymbol{\nabla} n_q^{1/2}\right) + U_q n_q^{1/2} = \mu_q n_q^{1/2}, \tag{50a}$$
$$U_q = \frac{\partial \mathcal{E}[n_n, n_p]}{\partial n_q}, \text{ for } q \in \{n, p\}. \tag{50b}$$

We present these here as the inclusion of $F(X)$ acts as a density-dependent effective mass. No such complication appears in the HFB formulation, which proceeds as described in [110].

B. Orbital-Free NEDF parameters

We start by considering the functional with the simplified kinetic energy

$$\mathcal{E}_{\text{kin}}[n_n, n_p] = \frac{\hbar^2}{2m}\sum_{q=n,p} \tau_{TF}[n_q]F(X_q), \tag{51}$$

where τ_{TF}, X_q, and $F(X)$ are given in Eqs. (46) and (47).

As discussed above, when using the simplified form $F(X) = 1 + 9\eta X$, the best fit value of $\eta \approx 0.5$. One might naïvely think that this corresponds to a dynamical theory of superfluid neutron and proton pairs with an effective nucleon pair mass $m_{\text{eff}} \approx 2m$ (see i.e. [231] and references therein). Such a theory with $\eta = 0.5$, however, leaves the potentials U_q wrong by a factor of 2. To correctly describe a dynamical theory of superfluid neutron and proton pairs, one would need a value of $\eta = 1/4$. Thus, in this approximation, the parameter η must simply be interpreted as an approximate way to control the falloff of the densities in the surface region where the interaction effects are still strong.

We now consider our NEDF as an hydrodynamic model for nuclei and fit the parameters to the same $N_E = 2375$ measured nuclear masses with $A \geq 16$ from [1, 2] used to fit the liquid drop models in Table I. However, unlike the liquid drop model, our hydrodynamic model allows us also to consider properties of the density distribution. Thus, we also fit the $N_r = 883$ nuclear

NEDF	η	η_s [fm^3]	W_0 [MeV fm^5]	a_0 [MeV fm^2]	a_1 [MeV fm^2]	a_2 [MeV fm^2]	b_0 [MeV fm^3]	b_1 [MeV fm^3]	b_2 [MeV fm^3]	c_0 [MeV fm^4]	c_1 [MeV fm^4]	c_2 [MeV fm^4]	δ [MeV]	χ_E [MeV]	χ_r [fm]
0	0.4719	0	0	0	131.1	0	−741.570	−143	0	940.50	0	0	11.46	2.59	0.14
1	0.4742	0	0	0	122.6	0	−738.302	−128	0	934.38	0	0	11.47	2.58	0.13
2	0.4743	0	0	0	120.1	0	−740.226	−123	0	938.26	0	0	0	2.71	0.14
1r	0.4807	0	0	0	135.9	0	−702.003	−157	0	861.33	0	0	11.75	2.71	0.05
3	0.4800	0	0	−10	125.0	0	−695.08	−130	0	892.1	−0.0	0	11.41	2.58	0.14
3n	0.4739	0	0	−7.59	195.7	−220.7	−707.006	−322	913.194	902.50	100	−873.8	11.57	2.57	0.13
3nr	0.4815	0	0	−7.63	195.4	−220.4	−674.608	−317	876.220	837.29	75	−803.21	12.45	2.67	0.05
E	0.4885	0	0	0	34.60	0	−740.950	65.1	0	938.63	0	0	11.21	2.64	0.13
Er	0.4957	0	0	0	32.98	0	−707.394	62.1	0	870.91	0	0	12.71	2.74	0.05
En	0.4866	0	0	0	34.01	−66.60	−741.546	64.0	562.093	940.02	0	−830.90	11.26	2.62	0.13
Enr	0.4970	0	0	0	32.54	−65.13	−707.031	61.2	530.344	870.15	0	−761.03	12.51	2.74	0.05
En-rho	1/9	4.9731	0	0	29.71	−62.29	−672.625	55.9	501.277	934.85	0	−825.73	11.78	2.64	0.05
Enr-rho	1/9	5.0397	0	0	29.52	−62.11	−672.986	55.6	501.986	934.85	0	−825.73	13.72	2.68	0.05
En-so	1/9	5.4751	76.20	0	136.8	−169.4	−669.776	51.5	502.814	934.85	0	−825.73	11.73	3.18	0.05
	κ														
En-pade-1	0.07	5.0941	0	0	30.14	−62.73	−672.785	56.7	500.620	802.20	0	−693.08	10.40	2.82	0.07
En-pade-2	0.15	4.6365	0	0	30.37	−62.96	−672.213	57.2	499.610	801.41	0	−692.29	11.49	2.89	0.07
En-pade-3	0.20	4.4318	0	0	30.33	−62.91	−671.889	57.1	499.374	800.97	0	−691.85	11.94	2.93	0.07
En-pade-4	0.30	4.2098	0	0	31.50	−64.09	−672.625	59.3	497.894	801.98	0	−692.86	12.07	3.11	0.07
Hydro	0.20	3.3696	0	0	50.88	−83.47	−685.597	94.9	475.237	828.76	−160	−559.64	0	2.86	0.04
														g_0 [MeV fm^3]	
SeaLL1	N/A	3.93	73.50	0	64.30	−96.80	−684.50	119.90	449.20	827.26	−256	−461.70	−200	1.74	0.03

Table IV. Fit parameters and residuals for the various NEDFs. The top set of functionals down use the simplified form $F(X) = 1 + 9\eta X$ while the second set use the form in Eq. (47) with the parameter κ instead. The SeaLL1 parameters are shown in the last row for comparison.

NEDF	n_0 [fm^{-3}]	$-\varepsilon_0$	K	S	L	L_2	Neutron skin ^{208}Pb [fm]	Neutron skin ^{48}Ca [fm]
0	0.136	15.24	222.5	26.8	34.1	32.8	0.082	0.118
1	0.136	15.22	222.4	26.7	35.9	34.7	0.087	0.123
2	0.136	15.21	222.2	26.7	36.8	35.6	0.089	0.125
1r	0.148	15.48	227.7	27.1	30.9	29.6	0.078	0.116
3	0.136	15.21	216.5	26.7	34.7	33.4	0.088	0.124
3n	0.137	15.20	218.2	30.0	29.3	16.7	0.068	0.107
3nr	0.147	15.44	222.9	31.0	31.2	15.5	0.068	0.107
E	0.136	15.28	223.1	29.7	68.2	66.9	0.159	0.174
Er	0.147	15.53	228.1	30.6	70.2	68.9	0.161	0.176
En	0.136	15.27	222.9	30.1	29.1	66.1	0.152	0.172
Enr	0.147	15.53	228.2	31.1	31.1	68.3	0.156	0.174
En-rho	0.160	15.85	234.4	32.3	33.5	68.9	0.138	0.149
Enr-rho	0.160	15.87	234.6	32.4	33.5	68.6	0.138	0.149
En-so	0.160	15.74	233.1	32.2	33.5	65.4	0.120	0.139
En-pade-1	0.160	15.86	234.5	32.4	33.5	69.6	0.157	0.176
En-pade-2	0.160	15.83	234.2	32.3	33.5	69.9	0.166	0.189
En-pade-3	0.160	15.82	234.1	32.3	33.5	69.8	0.170	0.194
En-pade-4	0.160	15.85	234.4	32.3	33.5	71.6	0.181	0.206

Table V. Saturation, symmetry, and neutron skin properties for the various NEDFs. All values in MeV unless otherwise specified.

charge radii from [3] with $\chi_r^2 = \sum|\delta r|^2/N_r$. When we include the charge radii in the fit, we minimize the following quantity $\chi_E^2/(3\,\text{MeV})^2 + \chi_r^2/(0.05\,\text{fm})^2$ which roughly equalizes the weight of the mass and radii contributions in the fit.

At this point, we have 7 parameters in our NEDF: η, $a_{0,1}$, $b_{0,1}$, and $c_{0,1}$ (the $j = 2$ parameters are fixed by the neutron matter equation of state). In addition, we include by hand the conventional even-odd staggering Eq. (2b) with a coefficient δ to describe pairing correlations, even though this has very little significance in the fits. The results of various fits scenarios we have considered are summarized below in table IV where we present sets of parameters for various fit strategies, and in Table V where we present the saturation, symmetry, and neutron skin properties.

We have considered the following type of fits:

NEDF-0: A six parameter least-squares fit of the $N_E = 2375$ nuclear masses [1, 2] including η, b_0, c_0, a_1, b_1, and δ but setting the nucleon charge form factors Eq. (12c) $G_E^p \equiv 1$ and $G_E^n \equiv 0$.

NEDF-1: The same as NEDF-0, but including the measured charge form factors. Comparing with NEDF-0 we see that the electric form factors are not significant for the overall mass fits, but slightly impact the charge radii at the 0.01 fm level (for the reduced χ_r).

NEDF-2: The same as NEDF-1, but without the pairing parameter $\delta = 0$. Comparing with NEDF-1 we see that odd-event staggering is also relatively unconstrained at the level of 0.1 MeV per nucleus. This is consistent with the results from the mass formulas in Table I.

NEDF-1r: The same as NEDF-1, but including the $N_r = 883$ charge radii into the fit. We see that there is significant room to improve the description of the charge radii without significantly degrading the mass fits.

NEDF-3: The same as NEDF-1, but with all 8 parameters, including a_0 and c_1 that we omitted from the previous fits. In conjunction with the principal component analysis shown in Fig. 21, this fit demonstrates that the terms with parameters a_0 and c_1 are unconstrained.

NEDF-3n: The same as NEDF-1, but with all 8 parameters, including a_0 and c_1 that we omitted from the previous fits, and the β^4 parameters for the terms quartic in isospin,

constrained by the QMC neutron matter equation of state [122] using Eqs. (15b). That the quality of the fit, isoscalar, and isovector parameters change very little, demonstrates that the neutron matter equation of state is essentially independent of the nuclear masses.

NEDF-3nr: The same as NEDF-3n but including the charge radii as in fit NEDF-1r. That the a_0 and c_1 terms are unconstrained for both masses and radii is also emphasized by this fit.

NEDF-E: Following the principal component analysis of NEDF-3n (discussed below) we find the combination $a_1 - b_1 n_0^{1/3}$ to be only weakly constrained by the mass fit. To test this, we set $a_1 = b_1 n_0^{1/3}$ where $n_0 = 0.154\,\mathrm{fm}^{-3}$ is a constant. The combination $a_1 - b_1 n_0^{1/3}$, to which the masses are insensitive, allows independent control the slope L_2 of the symmetry energy (see Eq. (33e)). From the fits we see that this same combination also controls the neutron skin thicknesses.

NEDF-Er: The same as NEDF-E but including the charge radii as in fit NEDF-1r.

NEDF-En: This is our main fit. It is the same as NEDF-E but includes the β^4 parameters adjusted to reproduce the neutron matter equation of state as in fit NEDF-3n.

NEDF-Enr: The same as NEDF-En but including the charge radii as in fit NEDF-1r.

In all fits above, the parameter η is around $1/2$, which deviates from the Weiszäcker value $1/9$. In our latest fits, we fix $\eta = 1/9$ and introduce a new gradient term η_s.

From the equilibrium condition of symmetric nuclear matter we get a relationship between $\tilde{a}_0$, $\tilde{b}_0$, and $\tilde{c}_0$

$$0 = \frac{3}{5} + \tilde{a}_0 + \frac{3}{2}\tilde{b}_0 + 2\tilde{c}_0 \tag{52}$$

or using the original parameters:

$$a_0 = -\frac{3\varepsilon_F}{5k_0^2} - \frac{3}{2}b_0 k_0 - 2c_0 k_0^2 \tag{53}$$

here $k_0 = n_0^{1/3}$, $n_0 = 0.16$. If a_0 is set to be 0, there is a relationship between b_0 and c_0:

$$c_0 = -\frac{3\varepsilon_F}{10k_0^4} - \frac{3b_0}{4k_0} \tag{54}$$

Using this relationship, the saturation density derived from the NEDF will be fixed to be $n_0 = 0.16$.

NEDF-En-rho: We fix $\eta = 1/9$ and add $\mathcal{E}_{\nabla n}$ into the NEDF. The saturation density n_0 is fixed to be 0.16 by adding a constraint between b_0 and c_0. Then the number of significant parameters in this NEDF is reduced to 3.

NEDF-Enr-rho: The same as NEDF-En-rho but including the charge radii as in fit NEDF-1r.

In our earlier fits, we do not include the contribution of spin-orbit interaction, which is crucial for the proper description of nuclear static properties.

NEDF-En-so: Following NEDF-En-rho, we add $\mathcal{E}_{\mathrm{SO}}$ into the NEDF. The spin-orbit strength W_0 is fixed to be the value suggested in [97]. The significant fitting parameters are the same with NEDF-En-rho.

When we fix $\eta = 1/9$ and neglect higher order extended Thomas-Fermi (ETF) expansion in the kinetic energy, the asymptotic form of density can be proved to be

$$n(r) \underset{r\to\infty}{\longrightarrow} \frac{1}{r^2} e^{-r/a}, \quad a = \sqrt{-\frac{1}{36}\frac{\hbar^2}{2m}\frac{1}{\mu}}. \tag{55}$$

where μ is the chemical potential (which is negative). Unfortunately, the diffuseness a is too small by a factor of 3 compared with the realistic nuclear surfaces, which corresponds to $\eta = 1$ in the asymptotic region. In order to obtain a nucleus density with correct asymptotic behavior, we suggest using the following Padé approximation in the representation of extended Thomas-Fermi approximation for the kinetic density, see Eqs. (46) and (47):

$$\tau_q = \tau_{TF,q} F(X) \tag{56}$$

where the function $F(x)$ has the asymptotic behavior:

$$F(X) = \begin{cases} 1 + X, & X \ll 1 \\ 9X, & X \gg 1 \end{cases} \tag{57}$$

In this approximation, we can get both correct behavior for the nucleus density in the near and asymptotic region. Through varying the parameter κ we obtain the following fits.

NEDF-En-pade-1: Following NEDF-En-so, we use the Padé approximation for the kinetic energy, and the parameter $b = 0.065$

NEDF-En-pade-2: Same with NEDF-En-pade-1, but $\kappa = 0.15$

NEDF-En-pade-3: Same with NEDF-En-pade-1, but $\kappa = 0.2$

NEDF-En-pade-4: Same with NEDF-En-pade-1, but $\kappa = 0.3$

These fits are summarized in Table IV, with the saturation and symmetry properties in Table V. The residuals for fit NEDF-1 are shown in Fig. 20 and compared with a fit to the nuclear with mass formula Eq. (2).

The reduced χ_E for these fits is comparable to that obtained using the nuclear mass formulas Eq. (1) with 4 parameters (plus δ) and Eq. (2) with 5 parameters (plus δ). This is consistent with our hypothesis that a NEDF for masses should contain no more than 5 significant parameters. Note, however, that unlike the mass formulas, the NEDF also gives a good description of charge radii – for which the mass formula says nothing – and provides access to nuclear dynamics.

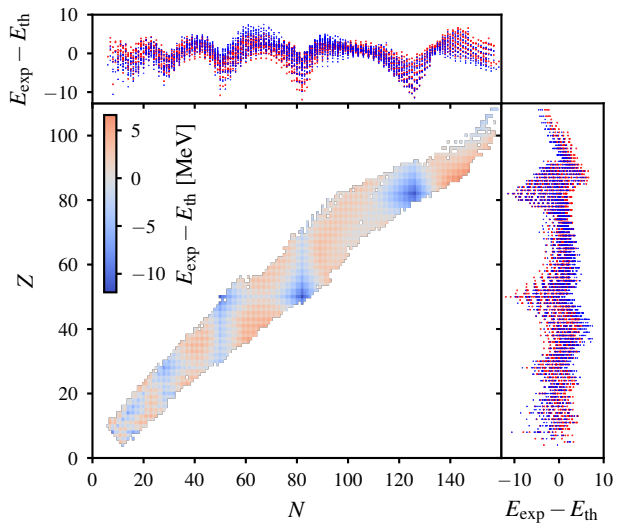

Figure 20. (Color online) The blue pluses show the results obtained using the orbital-free approximation with $\chi_E = 2.86\,\text{MeV}$, while the red crosses are the results of the fits using nuclear mass formula Eq. (2), with $\chi_E = 2.64\,\text{MeV}$. When compared against each other, the rms energy deviation between the two fits is $\Delta\chi_E = 1.10\,\text{MeV}$. Thus, the orbital-free theory essentially reproduces the nuclear mass formula Eq. (2). The main plot is the same as in Fig. 1 in which one can see clearly the magic numbers separately for neutrons and protons.

C. Principal Component Analysis

The principal components for fits NEDF-1 and NEDF-3 are shown in Fig. 21.

In the case of NEDF-3, we see that two parameters are completely unconstrained. These include $\tilde{a}_0 \approx -0.088$ and $\tilde{c}_1 = -0.017$. These values are an order of magnitude smaller than the other coefficients: hence, the unconstrained components can be easily removed by setting $a_0 = c_1 = 0$ which we do in most of our fits.

Finally, both plots indicate that a combination of the $j = 1$ parameters is highly unconstrained. Thus, in NEDF-1, the combination $\tilde{b}_1 - \tilde{a}_1$ can be given almost any value of order unity without changing χ_E more than 0.1 MeV. This is directly tested in the changes from NEDF1 to NEDF-E, NEDF-Er, NEDF-En, and NEDF-Enr, where we change the sign of b_1 and set $a_1 = b_1 n_0^{2/3}$. Indeed, we see that χ_E changed by about 0.1 MeV. Notice from Table V that the slope of the symmetry energy L_2 changes from about 30 MeV to 70 MeV while the other parameters remain about the same. This also significantly changes the neutron skin thickness, demonstrating a correlation between L_2 and the skin thickness, similar to that seen in other mean-field models [232]. This is consistent with Eq. (33e) where we see that $\tilde{b}_1$ gives us a direct handle on L_2. Finally, we have some unconstrained parameters, including $\tilde{\delta}$.

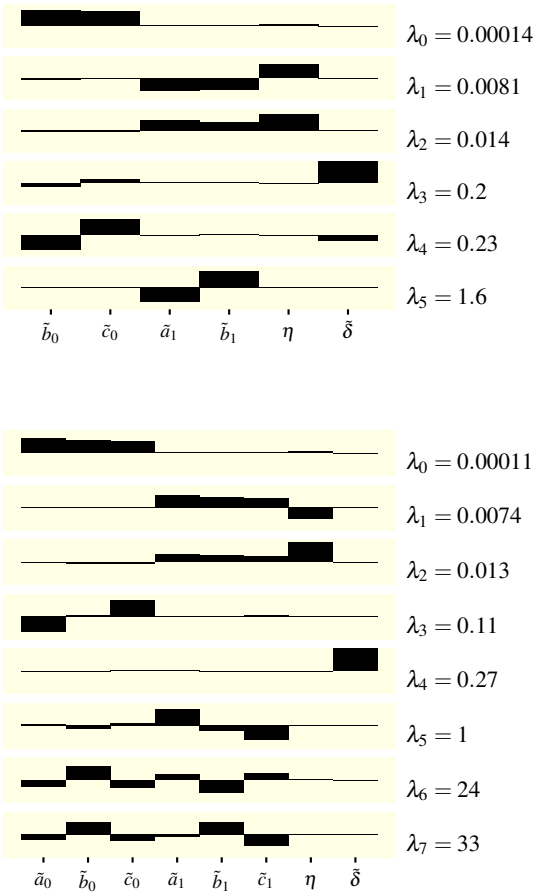

Figure 21. Principal component analysis for the NEDF-1 fit (top) and the NEDF-3 fit (bottom). Plotted are the components of the eigenvectors $\boldsymbol{v}_n$ defining the principal component Eq. (30b) as linear combinations of the various dimensionless parameters. From this we see that for NEDF1 the most-significant component $p_0 \approx \tilde{b}_0 + \tilde{c}_0$ which fixes the saturation energy to high precision. At the same time the component $p_4 \approx \tilde{b}_0 - \tilde{c}_0$ in NEDF-1 (and similarly in NEDF-3n) is not well constrained. We also see that the least-significant component $p_5 \approx \tilde{a}_1 - \tilde{b}_1$ is essentially unconstrained. For NEDF-3, we find three insensitive components, two of which can be used to set the smallest parameters $a_0 = c_1 = 0$. After removing these, one obtains a similar analysis as for NEDF-1 above.

D. Saturation, Symmetry Properties, and Neutron Matter

When only β^2 isospin contributions are included in the functional, our fits to the nuclear binding energies display a feature reported in other NEDFs discussed in literature: the energy per neutron in pure neutron matter appears to be well constrained at a density of $n_n \approx 0.1\,\text{fm}^{-3}$ where all functionals cross, see Fig. 23. The symmetry energy S is indicated for the functionals NEDF-En and Enr. The slope $L \approx 30\,\text{MeV}$ is fixed by the neutron matter equation of state alone (if used as a constraint, see Eq. (32)). In this case the slope $L_2/3n_0$ may be tuned without significantly affecting the mass fit by adjusting the insensitive

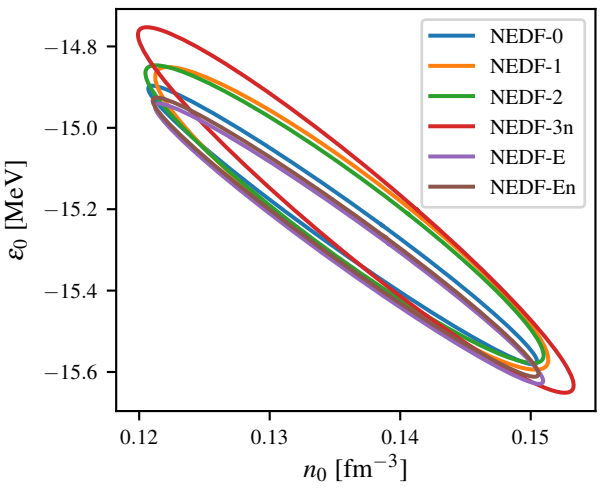

Figure 22. (Color online) The various ellipses show the region in the (ε_0, n_0) plane, in which the NEDF parameters can be changed and to lead to changes in the residual $\delta\chi_E < 0.2$ MeV. While the equilibrium energy ε_0 and density n_0 are controlled mainly by the combination $\tilde{b}_0 + \tilde{c}_0$, which is constrained with very high precision, the combination $\tilde{b}_0 - \tilde{c}_0$ remains significantly less constraint, see Section II J. This aspect allows us to manipulate to a certain degree the saturation properties, while affecting the overall fit only slightly.

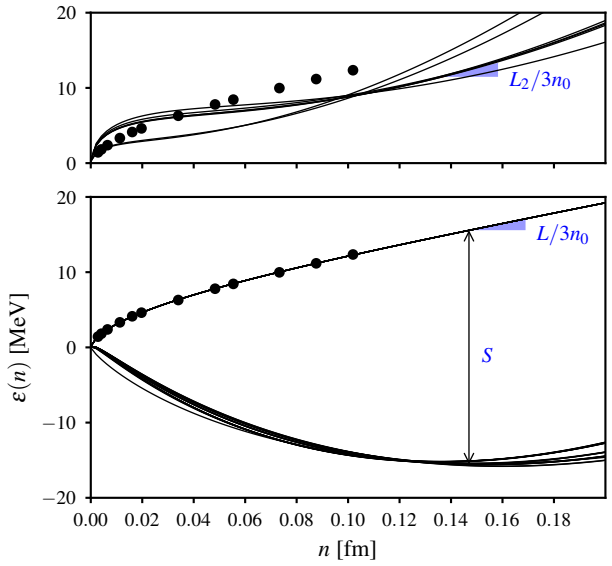

Figure 23. (Color online) The energy density per nucleon for symmetric nuclear matter (all orbital-free functionals) and neutron matter (for NEDF-3n, 3nr, En, Enr only) in the lower panel and pure neutron matter (upper panel) for NEDF-0, 1, 1r, 2, 3, E, and Er (which do not constrain the neutron equation of state and have only β^2 contributions). The black dots shows the QMC results [122].

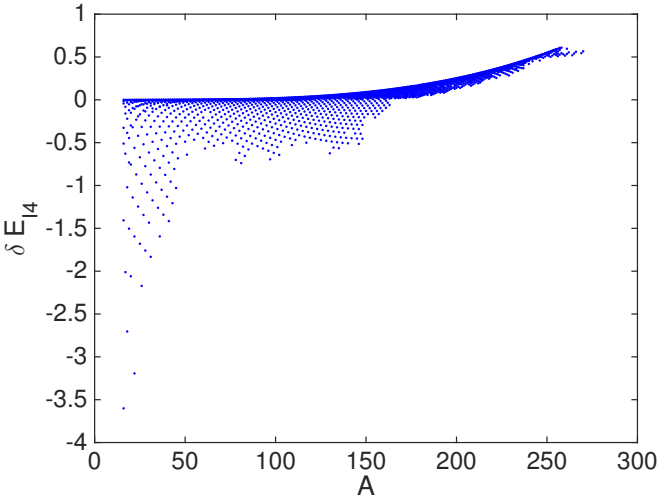

Figure 24. (Color online) The contribution to the ground state energies of the terms quartic in isospin density $\delta E_{I4} = \int d^3\boldsymbol{r}\ \mathcal{E}_2(n)\beta^4$, evaluated perturbatively with NEDF-1, see Table IV.

combination $a_1 - b_1 n_0^{1/3}$ or c_1, see Section II J. Functionals with only quadratic isospin contributions (β^2) appear to cross near $n \approx 0.1$ fm^{-3}, see also Ref. [233] and references therein. However, the value for the energy per neutron ≈ 9 MeV at this point in our fits is significantly smaller than the value ≈ 12.19 MeV obtained in QMC calculations of Wlazłowski *et al.* [122] or the equations of state for neutron matter used by Fayans [97] and Baldo *et al.* [99, 100, 208], see Fig. 19. This feature is not present when the β^4 terms are included (NEDF-3n, NEDF-3nr, NEDF-En and NEDF-Enr) and the QMC results are thus automatically reproduced.

The inclusion of the $j = 2$ terms quartic in β^4 have very little significance on mass fits. This demonstrates an important point: the equation of state of pure neutron matter has very little impact on the form of the NEDF, if only nuclei are considered. In measured nuclei, the ratio $\beta = (n_n - n_p)/n \approx (N - Z)/A$ is $|\beta| < 1/4$ (with a very small number of exceptions), hence nuclear masses are essentially insensitive to the presence of the β^4 terms, as $|\beta|^4 < 1/256$. To assess the magnitude of these effects, we have evaluated the β^4 contributions to the nuclear binding energies perturbatively, see Fig. 24. This contribution is quite small and can be easily overlooked when discussing known nuclei, but is crucial in order to correctly reproduce the energy of neutron matter. Evaluating Eq. (34) at $n = 0.1$ fm^{-3} one obtains

$$\left.\frac{\mathcal{E}}{n}\right|_{n=0.1} = [-4.399 + 13.961\beta^2 + 2.635\beta^4]\ \text{MeV}. \qquad (58)$$

When one averages β^2 and β^4 over all nuclei one obtains the values 0.028 and 0.001 respectively, which are noticeably lower than the "maximum" values of $1/16 \approx 0.062$ and $1/256 \approx 0.004$ and thus the contribution of the terms in β^4 to χ_E and nuclear masses is further reduced. The contributions of these terms to the averaged energy density per nucleon over β at $n = 0.1$ fm^{-3} are

$$\left.\frac{\mathcal{E}}{n}\right|_{n=0.1} = [-4.399 + 0.391 + 0.0026]\ \text{MeV}, \qquad (59)$$

and the contribution of the quartic term in β to the total energy

is practically invisible in nuclei.

Thus, using properties of the neutron matter to constrain the form of the NEDF and/or arguing against the inclusion of higher powers of $(n_n - n_p)$ [64, 97, 99, 100, 164, 234–237] is an ill-advised procedure, and the applications of functionals constructed in this manner, in particular to star environments, should be regarded with suspicion. The statement often made in the literature (see e.g. Horowitz *et al.* [233] and references therein) that the value of the symmetry energy at $n \approx 0.1\,\mathrm{fm}^{-3}$ is well constrained by nuclear masses must only be applied to the local expansion S_2 at this density, but not to the symmetry energy difference S between symmetric and pure neutron matter.

VI. CHARGE FORM FACTORS

The charge form factors are determined experimentally, and we approximate the Fourier transforms of the form factors with the dipole term for the proton, $G_E^p(Q) \approx (1 + Q^2/0.71\,\mathrm{GeV}^2)^{-2}$ [238], and $G_E^n(Q) \approx a(1+Q^2 r_+^2/12)^{-2} - a(1+Q^2 r_-^2/12)^{-2}$ with $r_\pm^2 = r_{\mathrm{avg}}^2 \pm \langle r_n^2\rangle/2a$, $\langle r_n^2\rangle = -0.1147(35)\,\mathrm{fm}^2$, $r_{\mathrm{avg}} = 0.856(32)\,\mathrm{fm}$, and $a = 0.115(20)$ [239].

[1] G. Audi, M. Wang, A.H. Wapstra, F.G. Kondev, M. MacCormick, X. Xu, and B. Pfeiffer, "The AME2012 atomic mass evaluation," Chin. Phys. C **36**, 1287 (2012).

[2] M. Wang, G. Audi, A.H. Wapstra, F.G. Kondev, M. MacCormick, X. Xu, and B. Pfeiffer, "The AME2012 atomic mass evaluation," Chin. Phys. C **36**, 1603 (2012).

[3] I. Angeli and K.P. Marinova, "Table of experimental nuclear ground state charge radii: An update," At. Data. Nucl. Data Tables **99**, 69 – 95 (2013).

[4] F. W. Aston, "Isotopes and atomic weights," Nature **105**, 605 – 636 (1920).

[5] A. S. Eddington, "The internal constitution of the stars," Nature **106**, 14–20 (1920).

[6] M.R. Mumpower, R. Surman, G.C. McLaughlin, and A. Aprahamian, "The impact of individual nuclear properties on -process nucleosynthesis," Progress in Particle and Nuclear Physics **86**, 86 – 126 (2016).

[7] M.R. Mumpower, R. Surman, G.C. McLaughlin, and A. Aprahamian, "Corrigendum to "the impact of individual nuclear properties on r-process nucleosynthesis" [j. prog. part. nucl. phys. 86c (2015) 86–126]," Progress in Particle and Nuclear Physics **87**, 116 (2016).

[8] C. F. v. Weizsäcker, "Zur theorie der kernmassen," Z. Phys. A **96**, 431–458 (1935).

[9] P. Hohenberg and W. Kohn, "Inhomogeneous electron gas," Phys. Rev. **136**, B864–B871 (1964).

[10] W. Kohn and L. J. Sham, "Self-consistent equations including exchange and correlation effects," Phys. Rev. **140**, A1133–A1138 (1965).

[11] Reiner M. Dreizler and Eberhard K. U. Gross, *Density Functional Theory: An Approach to the Quantum Many–Body Problem* (Springer-Verlag, Berlin, 1990).

[12] H. A. Bethe and R. F. Bacher, "Nuclear Physics A. Stationary states of nuclei," Rev. Mod. Phys. **8**, 82–229 (1936).

[13] P.-G. Reinhard, M. Bender, W. Nazarewicz, and T. Vertse, "From finite nuclei to the nuclear liquid drop: Leptodermous expansion based on self-consistent mean-field theory," Phys. Rev. C **73**, 014309 (2006).

[14] H. Weyl, "Über die asymptotische verteilung der eigenwerte," Nachr. Königl. Ges. Wiss. Göttingen , 110–117 (1911).

[15] Hermann Weyl, "Das asymptotische verteilungsgesetz der eigenwerte linearer partieller differentialgleichungen (mit einer anwendung auf die theorie der hohlraumstrahlung)," Math. Ann. **71**, 441–479 (1912).

[16] Hermann Weyl, "Über die abhängigkeit der eigenschwingungen einer membran und deren begrenzung," J. f. d. reine u. angew. Math. **141**, 1 (1912).

[17] Hermann Weyl, "Über das spektrum der hohlraumstrahlung," J. f. d. reine u. angew. Math. **141**, 163 (1912).

[18] Hermann Weyl, "Über die randwertaufgabe der strahlungstheorie und asymptotische spektralgesetze," J. f. d. reine u. angew. Math. **143**, 177 (1913).

[19] Hermann Weyl, "Das asymptotische verteilungsgesetz der eigenschwingungen eines beliebig gestalteten elastischen körpers," Rend. Circ. Mat. Palermo **39**, 1–49 (1915).

[20] Hermann Weyl, "Ramifications, old and new, of the eigenvalue problem," Bull. Amer. Math. Soc. **56**, 115–139 (1950).

[21] Mark Kac, "Can one hear the shape of a drum?" Am. Math. Monthly **73**, 1–23 (1966).

[22] R. T. Waechter, "On hearing the shape of a drum: an extension to higher dimensions," Math. Proc. Cambridge Philos. Soc. **72**, 439–447 (1972).

[23] Heinrich P. Baltes and Eberhard R. Hilf, *Spectra of finite systems* (Bibliographisches Institut, Mannheim, 1976).

[24] Matthias Brack and Rajat K Bhaduri, *Semiclassical physics*, Frontiers in physics, Vol. 96 (Addison-Wesley, Advanced Book Program, Reading, Mass., 1997).

[25] R Balian and C Bloch, "Distribution of eigenfrequencies for the wave equation in a finite domain: I. Three-dimensional problem with smooth boundary surface," Ann. Phys. (NY) **60**, 401–447 (1970).

[26] R. Balian and C. Bloch, "Distribution of eigenfrequencies for the wave equation in a finite domain. II. Electromagnetic field. Riemannian spaces," Ann. Phys. (NY) **64**, 271–307 (1971).

[27] R. Balian and C. Bloch, "Distribution of eigenfrequencies for the wave equation in a finite domain: III. Eigenfrequency density oscillations," Ann. Phys. (NY) **69**, 76–160 (1972).

[28] V. M. Strutinsky and A. G. Magner, "Semi-classical theory for nuclear shell structure," Fiz. Elem. Chastits At. Yadra **7**, 356–478 (1976), [Sov. J. Part. Nucl. **7**, 138 (1976)].

[29] O. Bohigas, S. Tomsovic, and D. Ullmo, "Manifestations of classical phase space structures in quantum mechanics," Phys. Rep. **223**, 43 – 133 (1993).

[30] Martin C. Gutzwiller, "Periodic orbits and classical quantization conditions," Journal of Mathematical Physics **12**, 343–358 (1971).

[31] M. V. Berry and M. Tabor, "Closed orbits and the regular bound spectrum," Proceedings of the Royal Society of London A: Mathematical, Physical and Engineering Sciences **349**, 101–123 (1976).

[32] M V Berry and M Tabor, "Calculating the bound spectrum by path summation in action-angle variables," Journal of Physics

A: Mathematical and General **10**, 371 (1977).
[33] Otto Haxel, J. Hans D. Jensen, and Hans E. Suess, "On the "magic numbers" in nuclear structure," Phys. Rev. **75**, 1766–1766 (1949).
[34] Maria Goeppert Mayer, "On closed shells in nuclei. II," Phys. Rev. **75**, 1969–1970 (1949).
[35] Maria Goeppert Mayer, "Nuclear configurations in the spin-orbit coupling model. i. empirical evidence," Phys. Rev. **78**, 16–21 (1950).
[36] Maria Goeppert Mayer, "Nuclear configurations in the spin-orbit coupling model. II. theoretical considerations," Phys. Rev. **78**, 22–23 (1950).
[37] L.D. Landau, "Theory of Fermi liquids," Zh. Eksp. Teor. Fiz. **30**, 1058–1064 (1956).
[38] L.D. Landau, "Oscillations of a Fermi liquid," Zh. Eksp. Teor. Fiz. **32**, 59–66 (1957).
[39] A. B. Migdal, *Theory of Finite Fermi Systems and Applications to Atomic Nuclei* (Wiley, New York, 1967).
[40] H. Nishioka, Klavs Hansen, and B. R. Mottelson, "Supershells in metal clusters," Phys. Rev. B **42**, 9377–9386 (1990).
[41] Walt A. de Heer, "The physics of simple metal clusters: experimental aspects and simple models," Rev. Mod. Phys. **65**, 611–676 (1993).
[42] Matthias Brack, "The physics of simple metal clusters: self-consistent jellium model and semiclassical approaches," Rev. Mod. Phys. **65**, 677–732 (1993).
[43] J. Pedersen, S. Bjornholm, J. Borggreen, K. Hansen, T. P. Martin, and H. D. Rasmussen, "Observation of quantum supershells in clusters of sodium atoms," Nature **353**, 733–735 (1991).
[44] Aurel Bulgac and Caio Lewenkopf, "Stable deformations in large metallic clusters," Phys. Rev. Lett. **71**, 4130–4133 (1993).
[45] V. M. Strutinsky, "Influence of nucleon shells on energy of a nucleus," Yad. Fiz. **3**, 614–625 (1966), [Sov. J. Nucl. Phys. **3**, 449 (1966)].
[46] V. M. Strutinsky, "Shell effects in nuclear masses and deformation energies," Nucl. Phys. A **95**, 420 – 442 (1967).
[47] V. M. Strutinsky, "'Shells' in deformed nuclei," Nucl. Phys. A **122**, 1 – 33 (1968).
[48] M. Brack, Jens Damgaard, A. S. Jensen, H. C. Pauli, V. M. Strutinsky, and C. Y. Wong, "Funny hills: The shell-correction approach to nuclear shell effects and its applications to the fission process," Rev. Mod. Phys. **44**, 320–405 (1972).
[49] M Brack, C Guet, and H. B Håkansson, "Selfconsistent semi-classical description of average nuclear properties—a link between microscopic and macroscopic models," Phys. Rep. **123**, 275–364 (1985).
[50] William D. Myers and Wladyslaw J. Swiatecki, "Nuclear masses and deformations," Nucl. Phys. **81**, 1–60 (1966).
[51] William D. Myers and W. J. Swiatecki, "Average nuclear properties," Ann. Phys. (NY) **55**, 395–505 (1969).
[52] W. D. Myers and W. J. Swiatecki, "The nuclear droplet model for arbitrary shapes," Ann. Phys. (NY) **84**, 186–210 (1974).
[53] W. D. Myers and W. J. Swiatecki, "A Thomas-Fermi model of nuclei. part i. formulation and first results," Ann. Phys. (NY) **204**, 401–431 (1990).
[54] W. D. Myers and W. J. Swiatecki, "A Thomas-Fermi model of nuclei. II. fission barriers and charge distributions," Ann. Phys. (NY) **211**, 292–315 (1991).
[55] W. D. Myers and W. J. Swiatecki, "Nuclear properties according to the Thomas-Fermi model," Nucl. Phys. A **601**, 141–167 (1996).
[56] Peter Ring and Peter Schuck, *The nuclear many-body problem*, 1st ed., Theoretical and Mathematical Physics Series No. 17 (Springer-Verlag, Berlin Heidelberg New York, 2004).
[57] Aage Bohr and Ben R. Mottelson, *Nuclear Structure* (World Scientific, Singapore, 1998).
[58] P. Moller, J. R. Nix, W. D. Myers, and W. J. Swiatecki, "Nuclear ground-state masses and deformations," At. Data. Nucl. Data Tables **59**, 185–381 (1995).
[59] Peter Möller, William D. Myers, Hiroyuki Sagawa, and Satoshi Yoshida, "New finite-range droplet mass model and equation-of-state parameters," Phys. Rev. Lett. **108**, 052501 (2012).
[60] P. Möller, A.J. Sierk, T. Ichikawa, and H. Sagawa, "Nuclear ground-state masses and deformations: Frdm(2012)," Atomic Data and Nuclear Data Tables **109**, 1 – 204 (2016).
[61] Michael Bender, Paul-Henri Heenen, and Paul-Gerhard Reinhard, "Self-consistent mean-field models for nuclear structure," Rev. Mod. Phys. **75**, 121–180 (2003).
[62] S. Goriely, N. Chamel, and J. M. Pearson, "Skyrme-Hartree-Fock-Bogoliubov nuclear mass formulas: Crossing the 0.6 mev accuracy threshold with microscopically deduced pairing," Phys. Rev. Lett. **102**, 152503 (2009).
[63] J. P. Delaroche, M. Girod, J. Libert, H. Goutte, S. Hilaire, S. Péru, N. Pillet, and G. F. Bertsch, "Structure of even-even nuclei using a mapped collective hamiltonian and the d1s gogny interaction," Phys. Rev. C **81**, 014303 (2010).
[64] S. Goriely, N. Chamel, and J. M. Pearson, "Hartree-Fock-Bogoliubov nuclear mass model with 0.50 MeV accuracy based on standard forms of Skyrme and pairing functionals," Phys. Rev. C **88**, 061302 (2013).
[65] S. Goriely and R. Capote, "Uncertainties of mass extrapolations in Hartree-Fock-Bogoliubov mass models," Phys. Rev. C **89**, 054318 (2014).
[66] M. Kortelainen, J. McDonnell, W. Nazarewicz, E. Olsen, P. G. Reinhard, J. Sarich, N. Schunck, S. M. Wild, D. Davesne, J. Erler, and A. Pastore, "Nuclear Energy Density Optimization: UNEDF2," (2014).
[67] D. Lunney, J. M. Pearson, and C. Thibault, "Recent trends in the determination of nuclear masses," Rev. Mod. Phys. **75**, 1021–1082 (2003).
[68] Aage Bohr and Ben R. Mottelson, *Nuclear Structure*, Vol. I (Benjamin Inc., New York, 1969).
[69] O. Bohigas and P. Leboeuf, "Nuclear masses: Evidence of order-chaos coexistence," Phys. Rev. Lett. **88**, 092502 (2002); "Erratum: Nuclear masses: Evidence of order-chaos coexistence [Phys. Rev. Lett. 88, 092502 (2002)]," Phys. Rev. Lett. **88**, 129903(E) (2002).
[70] Sven Åberg, "Nuclear physics: Weighing up nuclear masses," Nature **417**, 499–501 (2002).
[71] H. Olofsson, S. Åberg, O. Bohigas, and P. Leboeuf, "Correlations in nuclear masses," Phys. Rev. Lett. **96**, 042502 (2006).
[72] H. Olofsson, S. Åberg, and P. Leboeuf, "Semiclassical theory of bardeen-cooper-schrieffer pairing-gap fluctuations," Phys. Rev. Lett. **100**, 037005 (2008).
[73] A. Molinari and H.A. Weidenmüller, "Statistical fluctuations of ground-state energies and binding energies in nuclei," Phys. Lett. B **601**, 119–124 (2004).
[74] A. Molinari and H. A. Weidenmüller, "Nuclear masses, chaos, and the residual interaction," Phys. Lett. B **637**, 48–52 (2006).
[75] Jorge G. Hirsch, Víctor Velázquez, and Alejandro Frank, "Quantum chaos and nuclear mass systematics," Phys. Lett. B **595**, 231–236 (2004).
[76] Jorge G. Hirsch, A. Frank, J. Barea, P. Van Isacker, and V. Velázquez, "Bounds on the presence of quantum chaos in nuclear masses," Eur. J. Phys. A **25**, 75–78 (2005).
[77] José Barea, Alejandro Frank, Jorge G. Hirsch., and Piet Van Isacker, "Nuclear masses set bounds on quantum chaos," Phys. Rev. Lett. **94**, 102501 (2005).

[78] H. B. G. Casimir, "On the attraction between two perfectly conducting plates," Proc. K. Ned. Akad. Wet. **51**, 793 (1948).

[79] G. L. Klimchitskaya, U. Mohideen, and V. M. Mostepanenko, "The Casimir force between real materials: Experiment and theory," Rev. Mod. Phys. **81**, 1827–1885 (2009).

[80] M. E. Fisher and P. G. de Gennes, "Phénomènes aux parois dans un mélange binaire critique," C. R. Acad. Sci. Ser. B **287**, 207 (1978).

[81] A. Hanke, F. Schlesener, E. Eisenriegler, and S. Dietrich, "Critical Casimir Forces between Spherical Particles in Fluids," Phys. Rev. Lett. **81**, 1885–1888 (1998).

[82] Aurel Bulgac and Piotr Magierski, "Quantum corrections to the ground state energy of inhomogeneous neutron matter," Nucl. Phys. A **683**, 695 – 712 (2001); "Erratum to: "Quantum corrections to the ground state energy of inhomogeneous neutron matter"," Nucl. Phys. A **703**, 892 – (2002).

[83] P. Magierski, A. Bulgac, and P.-H. Heenen, "Exotic nuclear phases in the inner crust of neutron stars in the light of Skyrme-Hartree-Fock theory," Nucl. Phys. A **719**, C217 – C220 (2003).

[84] Piotr Magierski and Aurel Bulgac, "Nuclear structure and dynamics in the inner crust of neutron stars," Nucl. Phys. A **738**, 143 – 149 (2004), proceedings of the 8th International Conference on Clustering Aspects of Nuclear Structure and Dynamics.

[85] Piotr Magierski and P.-H. Heenen, "Structure of the inner crust of neutron stars: Crystal lattice or disordered phase?" Phys. Rev. C **65**, 045804 (2002).

[86] Aurel Bulgac, Piotr Magierski, and A. Wirzba, "Fermionic Casimir effect in case of Andreev reflection," Europhys. Lett. **72**, 327–333 (2005).

[87] Yongle Yu, Aurel Bulgac, and Piotr Magierski, "Shell Correction Energy for Bubble Nuclei," Phys. Rev. Lett. **84**, 412–415 (2000).

[88] Aurel Bulgac, Piotr Magierski, and Andreas Wirzba, "Scalar Casimir effect between Dirichlet spheres or a plate and a sphere," Phys. Rev. D **73**, 025007 (2006).

[89] M. Bordag and I. Pirozhenko, "Vacuum energy between a sphere and a plane at finite temperature," Phys. Rev. D **81**, 085023 (2010).

[90] Sahand Jamal Rahi, Thorsten Emig, Noah Graham, Robert L. Jaffe, and Mehran Kardar, "Scattering theory approach to electrodynamic Casimir forces," Phys. Rev. D **80**, 085021 (2009).

[91] Noah Graham, "Casimir energies of periodic dielectric gratings," Phys. Rev. A **90**, 032507 (2014).

[92] Antoine Canaguier-Durand, Paulo A. Maia Neto, Astrid Lambrecht, and Serge Reynaud, "Thermal Casimir effect for Drude metals in the plane-sphere geometry," Phys. Rev. A **82**, 012511 (2010).

[93] Martin Schaden, "Semiclassical estimates of electromagnetic Casimir self-energies of spherical and cylindrical metallic shells," Phys. Rev. A **82**, 022113 (2010).

[94] H. A. Jahn and E. Teller, "Stability of polyatomic molecules in degenerate electronic states. I. orbital degeneracy," Proc. Roy. Soc. London **161**, 220–236 (1937).

[95] Aurel Bulgac and Vasily R. Shaginyan, "A systematic surface contribution to the ground-state binding energies," Nucl. Phys. A **601**, 103–116 (1996).

[96] P. Möller, J.R. Nix, and K.L. Kratz, "Nuclear Properties for Astrophysical and Radioactive Ion Beam Applications," Atom. Data Nuc. Data Tab. **66**, 131 (1997).

[97] S. A. Fayans, "Towards a universal nuclear density functional," JETP Lett. **68**, 169–174 (1998).

[98] S. A. Fayans, S. V. Tolokonnikov, E. L. Trykov, and D. Zawischa, "Nuclear isotope shifts within the local energy-density functional approach," Nucl. Phys. A **676**, 49 – 119 (2000).

[99] M. Baldo, P. Schuck, and X. Viñas, "Kohn–Sham density functional inspired approach to nuclear binding," Phys. Lett. B **663**, 390–394 (2008).

[100] M. Baldo, L. M. Robledo, P. Schuck, and X. Viñas, "New Kohn-Sham density functional based on microscopic nuclear and neutron matter equations of state," Phys. Rev. C **87**, 064305 (2013).

[101] J. Carlson, S. Gandolfi, F. Pederiva, Steven C. Pieper, R. Schiavilla, K. E. Schmidt, and R. B. Wiringa, "Quantum monte carlo methods for nuclear physics," Rev. Mod. Phys. **87**, 1067–1118 (2015).

[102] Francesco Pederiva, Alessandro Roggero, and Kevin E. Schmidt, "Variational and diffusion monte carlo approaches to the nuclear few- and many-body problem," in *An Advanced Course in Computational Nuclear Physics: Bridging the Scales from Quarks to Neutron Stars*, edited by Morten Hjorth-Jensen, Maria Paola Lombardo, and Ubirajara van Kolck (Springer International Publishing, Cham, 2017) pp. 401–476.

[103] Carlo Barbieri and Arianna Carbone, "Self-consistent green's function approaches," in *An Advanced Course in Computational Nuclear Physics: Bridging the Scales from Quarks to Neutron Stars*, edited by Morten Hjorth-Jensen, Maria Paola Lombardo, and Ubirajara van Kolck (Springer International Publishing, Cham, 2017) pp. 571–644.

[104] Justin G. Lietz, Samuel Novario, Gustav R. Jansen, Gaute Hagen, and Morten Hjorth-Jensen, "Computational nuclear physics and post hartree-fock methods," in *An Advanced Course in Computational Nuclear Physics: Bridging the Scales from Quarks to Neutron Stars*, edited by Morten Hjorth-Jensen, Maria Paola Lombardo, and Ubirajara van Kolck (Springer International Publishing, Cham, 2017) pp. 293–399.

[105] Eskendr Gebrerufael, Klaus Vobig, Heiko Hergert, and Robert Roth, "Ab initio," Phys. Rev. Lett. **118**, 152503 (2017).

[106] Evgeny Epelbaum, Hermann Krebs, Dean Lee, and Ulf-G. Meißner, "Ab initio calculation of the Hoyle state," (2011).

[107] R. Machleidt and D. R. Entem, "Chiral effective field theory and nuclear forces," Phys. Rep. **503**, 1–75 (2011).

[108] Aurel Bulgac, "Time-dependent density functional theory and the real-time dynamics of Fermi superfluids," Annu. Rev. Nucl. Part. Sci. **63**, 97–121 (2013).

[109] Aurel Bulgac, Michael McNeil Forbes, and Gabriel Wlazłowski, "Towards quantum turbulence in cold atomic fermionic superfluids," J. Phys. B **50**, 014001 (2017).

[110] Shi Jin, Aurel Bulgac, Kenneth Roche, and Gabriel Wlazłowski, "Coordinate-space solver for superfluid many-fermion systems with the shifted conjugate-orthogonal conjugate-gradient method," Phys. Rev. C **95**, 044302 (2017).

[111] Y. M. Engel, D. M. Brink, K. Goeke, S. J. Krieger, and D. Vautherin, "Time-dependent Hartree-Fock theory with Skyrme's interaction," Nucl. Phys. A **249**, 215 – 238 (1975).

[112] J. Dobaczewski and J. Dudek, "Time-odd components in the mean field of rotating superdeformed nuclei," Phys. Rev. C **52**, 1827–1839 (1995).

[113] V. O. Nesterenko, W. Kleinig, J. Kvasil, P. Vesely, and Paul-Gerhard Reinhard, "TDDFT with Skyrme forces: Effect of time-odd densities on electric giant resonances," Int. J. Mod. Phys. E **17**, 89–99 (2008).

[114] Aurel Bulgac, Michael McNeil Forbes, and Piotr Magierski, "The unitary Fermi gas: From Monte Carlo to density functionals," Chap. 9, pp. 305 – 373, vol. 836 of [126] (2012).

[115] G.A. Miller, B.M.K. Nefkens, and I. Slaus, "Charge symmetry, quarks and mesons," Phys. Rep. **194**, 1–116 (1990).

[116] Gerald A. Miller, Allena K. Opper, and Edward J. Stephenson, "Charge symmetry breaking and QCD," Annu. Rev. Nucl. Part. Sci. **56**, 253–292 (2006).

[117] H Müther, A Polls, and R Machleidt, "Isospin symmetry breaking nucleon-nucleon potentials and nuclear structure," Physics Letters B **445**, 259 – 264 (1999).

[118] R. Machleidt and H. Müther, "Charge symmetry breaking of the nucleon-nucleon interaction: ρ-ω mixing versus nucleon mass splitting," Phys. Rev. C **63**, 034005 (2001).

[119] U. G. Meißner, A. M. Rakhimov, A. Wirzba, and U. T. Yakhshiev, "Neutron-proton mass difference in finite nuclei and the Nolen-Schiffer anomaly," The European Physical Journal A **36**, 37–48 (2008).

[120] J A Nolen and J P Schiffer, "Coulomb Energies," Annu. Rev. Nucl. Sci. **19**, 471–526 (1969).

[121] A. Bulgac and V. R. Shaginyan, "Proton single-particle energy shifts due to Coulomb correlations," Phys. Lett. B **469**, 1–6 (1999).

[122] G. Wlazłowski, J. W. Holt, S. Moroz, A. Bulgac, and K. J. Roche, "Auxiliary-field quantum Monte Carlo simulations of neutron matter in chiral effective field theory," Phys. Rev. Lett. **113**, 182503 (2014).

[123] F. Tondeur, "An energy density nuclear mass formula: (i). self-consistent calculation for spherical nuclei," Nucl. Phys. A **303**, 185 – 198 (1978).

[124] Alexandros Gezerlis and J. Carlson, "Low-density neutron matter," Phys. Rev. C **81**, 025803 (2010).

[125] S. Gandolfi, A. Gezerlis, and J. Carlson, "Neutron matter from low to high density," arXiv:1501.0567 (2015).

[126] Wilhelm Zwerger, ed., *The BCS–BEC Crossover and the Unitary Fermi Gas*, Lecture Notes in Physics, Vol. 836 (Springer-Verlag, Berlin Heidelberg, 2012).

[127] George A. Baker, Jr., "Neutron matter model," Phys. Rev. C **60**, 054311 (1999).

[128] J. Carlson and Sanjay Reddy, "Asymmetric two-component fermion systems in strong coupling," Phys. Rev. Lett. **95**, 060401 (2005).

[129] Piotr Magierski, Gabriel Wlazłowski, Aurel Bulgac, and Joaquín E. Drut, "Finite-temperature pairing gap of a unitary Fermi gas by quantum Monte Carlo calculations," Phys. Rev. Lett. **103**, 210403 (2009).

[130] Piotr Magierski, Gabriel Wlazłowski, and Aurel Bulgac, "Onset of a pseudogap regime in ultracold Fermi gases," Phys. Rev. Lett. **107**, 145304 (2011).

[131] Aurel Bulgac, "Local density functional theory for superfluid fermionic systems: The unitary gas," Phys. Rev. A **76**, 040502 (2007).

[132] J. P. Blocki, A. G. Magner, and P. Ring, "The slope-dependent nuclear-symmetry energy within the effective surface approximation," (2015).

[133] E. Chabanat, P. Bonche, P. Haensel, J. Meyer, and R. Schaeffer, "A Skyrme parametrization from subnuclear to neutron star densities part II. Nuclei far from stabilities," Nucl. Phys. A **635**, 231 – 256 (1998).

[134] Aurel Bulgac and Yongle Yu, "Renormalization of the Hartree-Fock-Bogoliubov equations in the case of a zero range pairing interaction," Phys. Rev. Lett. **88**, 042504 (2002).

[135] Yongle Yu and Aurel Bulgac, "Energy density functional approach to superfluid nuclei," Phys. Rev. Lett. **90**, 222501 (2003).

[136] P. J. Borycki, J. Dobaczewski, W. Nazarewicz, and M. V. Stoitsov, "Pairing renormalization and regularization within the local density approximation," Phys. Rev. C **73**, 044319 (2006).

[137] G. F. Bertsch, C. A. Bertulani, W. Nazarewicz, N. Schunck, and M. V. Stoitsov, "Odd-even mass differences from self-consistent mean field theory," Phys. Rev. C **79**, 034306 (2009).

[138] T. Lesinski, T. Duguet, K. Bennaceur, and J. Meyer, "Non-empirical pairing energy density functional," Eur. Phys. J. A **40**, 121–126 (2009).

[139] K. Hebeler, T. Duguet, T. Lesinski, and A. Schwenk, "Non-empirical pairing energy functional in nuclear matter and finite nuclei," Phys. Rev. C **80**, 044321 (2009).

[140] M. Yamagami, J. Margueron, H. Sagawa, and K. Hagino, "Isoscalar and isovector density dependence of the pairing functional determined from global fitting," Phys. Rev. C **86**, 034333 (2012).

[141] A. F. Andreev and E. P. Bashkin, "3-velocity hydrodynamics of superfluid solutions," Sov. Phys.–JETP **42**, 164 (1975), zh. Éksp. Teor. Fiz. **69**, 319 (1975).

[142] G. E. Volovik, V. P. Mineev, and I. M. Khalatnikov, "Theory of solutions of a superfluid Fermi liquid in a superfluid Bose liquid," Zh. Eksp. Teor. Fiz. **42**, 342–347 (1975).

[143] G.A. Vardanyan and D. M. Sedrakyan, "Magnetohydrodynamics od superfluid solutions," Sov. Phys.–JETP **81**, 1731–1737 (1981).

[144] M. A. Alpar, S. A. Langer, and J. A. Sauls, "Rapid postglitch spin-up of the superfluid core in pulsars," Astrophys. J. **282**, 533 (1984).

[145] M. Borumand, R. Joynt, and W. Kluźniak, "Superfluid densities in neutron-star matter," Phys. Rev. C **54**, 2745–2750 (1996).

[146] Egor Babaev, "Andreev-Bashkin effect and knot solitons in an interacting mixture of a charged and a neutral superfluid with possible relevance for neutron stars," Phys. Rev. D **70**, 043001 (2004).

[147] M.E. Gusakov and P. Haensel, "The entrainment matrix of a superfluid neutron–proton mixture at a finite temperature," Nucl. Phys. A **761**, 333 – 348 (2005).

[148] Nicolas Chamel and Pawel Haensel, "Entrainment parameters in a cold superfluid neutron star core," Phys. Rev. C **73**, 045802 (2006).

[149] N. Chamel, "Crustal entrainment and pulsar glitches," Phys. Rev. Lett. **110**, 011101 (2013).

[150] D. N. Kobyakov, C. J. Pethick, S. Reddy, and A. Schwenk, "Dispersion and decay of collective modes in neutron star cores,".

[151] R. O. Jones and O. Gunnarsson, "The density functional formalism, its applications and prospects," Rev. Mod. Phys. **61**, 689–746 (1989).

[152] Andrew E. DePristo and Joel D. Kress, "Kinetic-energy functionals via padé approximations," Phys. Rev. A **35**, 438–441 (1987).

[153] G. F. Bertsch, B. Sabbey, and M. Uusnäkki, "Fitting theories of nuclear binding energies," Phys. Rev. C **71**, 054311 (2005).

[154] R. Navarro Perez, N. Schunck, R.-D. Lasseri, C. Zhang, and J. Sarich, "Axially deformed solution of the Skyrme–Hartree–Fock–Bogolyubov equations using the transformed harmonic oscillator basis (III) HFBTHO (v3.00): A new version of the program," Computer Physics Communications (2017), 10.1016/j.cpc.2017.06.022.

[155] M.V. Stoitsov, N. Schunck, M. Kortelainen, N. Michel, H. Nam, E. Olsen, J. Sarich, and S. Wild, "Axially deformed solution of the Skyrme-Hartree–Fock–Bogoliubov equations using the transformed harmonic oscillator basis (II) HFBTHO v2.00d: A new version of the program," Computer Physics Communications **184**, 1592 – 1604 (2013).

[156] M.V. Stoitsov, J. Dobaczewski, W. Nazarewicz, and P. Ring, "Axially deformed solution of the Skyrme–Hartree–Fock–

Bogolyubov equations using the transformed harmonic oscillator basis. The program {HFBTHO} (v1.66p)," Computer Physics Communications **167**, 43 – 63 (2005).

[157] M. Kortelainen, J. McDonnell, W. Nazarewicz, P.-G. Reinhard, J. Sarich, N. Schunck, M. V. Stoitsov, and S. M. Wild, "Nuclear energy density optimization: Large deformations," Phys. Rev. C **85**, 024304 (2012).

[158] H. De Vries, C. W. De Jager, and C. De Vries, "Nuclear charge-density-distribution parameters from elastic electron scattering," At. Data. Nucl. Data Tables **36**, 495 – 536 (1987).

[159] M. Kortelainen, J. McDonnell, W. Nazarewicz, E. Olsen, P.-G. Reinhard, J. Sarich, N. Schunck, S. M. Wild, D. Davesne, J. Erler, and A. Pastore, "Nuclear energy density optimization: Shell structure," Phys. Rev. C **89**, 054314 (2014).

[160] N. Schwierz, I. Wiedenhover, and A. Volya, "Parameterization of the Woods-Saxon Potential for Shell-Model Calculations," arXiv:0709.3525 (2007).

[161] James M. Lattimer, "Symmetry energy in nuclei and neutron stars," Nucl. Phys. **A928**, 276 – 295 (2014).

[162] C.J. Horowitz, K.S. Kumar, and R. Michaels, "Electroweak measurements of neutron densities in CREX and PREX at JLab, USA," Eur. Phys. J. A **50**, 48 (2014), 10.1140/epja/i2014-14048-3.

[163] A. Tamii, I. Poltoratska, P. von Neumann-Cosel, Y. Fujita, T. Adachi, C. A. Bertulani, J. Carter, M. Dozono, H. Fujita, K. Fujita, K. Hatanaka, D. Ishikawa, M. Itoh, T. Kawabata, Y. Kalmykov, A. M. Krumbholz, E. Litvinova, H. Matsubara, K. Nakanishi, R. Neveling, H. Okamura, H. J. Ong, B. Özel-Tashenov, V. Yu. Ponomarev, A. Richter, B. Rubio, H. Sakaguchi, Y. Sakemi, Y. Sasamoto, Y. Shimbara, Y. Shimizu, F. D. Smit, T. Suzuki, Y. Tameshige, J. Wambach, R. Yamada, M. Yosoi, and J. Zenihiro, "Complete electric dipole response and the neutron skin in ^{208}Pb," Phys. Rev. Lett. **107**, 062502 (2011).

[164] P.-G. Reinhard and W. Nazarewicz, "Information content of a new observable: The case of the nuclear neutron skin," Phys. Rev. C **81**, 051303 (2010).

[165] C. M. Tarbert, D. P. Watts, D. I. Glazier, P. Aguar, J. Ahrens, J. R. M. Annand, H. J. Arends, R. Beck, V. Bekrenev, B. Boillat, A. Braghieri, D. Branford, W. J. Briscoe, J. Brudvik, S. Cherepnya, R. Codling, E. J. Downie, K. Foehl, P. Grabmayr, R. Gregor, E. Heid, D. Hornidge, O. Jahn, V. L. Kashevarov, A. Knezevic, R. Kondratiev, M. Korolija, M. Kotulla, D. Krambrich, B. Krusche, M. Lang, V. Lisin, K. Livingston, S. Lugert, I. J. D. MacGregor, D. M. Manley, M. Martinez, J. C. McGeorge, D. Mekterovic, V. Metag, B. M. K. Nefkens, A. Nikolaev, R. Novotny, R. O. Owens, P. Pedroni, A. Polonski, S. N. Prakhov, J. W. Price, G. Rosner, M. Rost, T. Rostomyan, S. Schadmand, S. Schumann, D. Sober, A. Starostin, I. Supek, A. Thomas, M. Unverzagt, Th. Walcher, L. Zana, and F. Zehr, "Neutron Skin of 208Pb from Coherent Pion Photoproduction," Phys. Rev. Lett. **112**, 242502 (2014).

[166] J. Dobaczewski and P. Olbratowski, "Solution of the Skyrme–Hartree–Fock–Bogolyubov equations in the Cartesian deformed harmonic-oscillator basis. (IV) {HFODD} (v2.08i): a new version of the program," Computer Physics Communications **158**, 158 – 191 (2004).

[167] J. Bartel, P. Quentin, M. Brack, C. Guet, and H.-B. Håkansson, "Towards a better parametrisation of Skyrme-like effective forces: A critical study of the SkM force," Nuclear Physics A **386**, 79 – 100 (1982).

[168] Nicolas Schunck, Jordan D McDonnell, Jason Sarich, Stefan M Wild, and Dave Higdon, "Error analysis in nuclear density functional theory," Journal of Physics G: Nuclear and Particle Physics **42**, 034024 (2015).

[169] N. Schunck, D. Duke, H. Carr, and A. Knoll, "Description of induced nuclear fission with Skyrme energy functionals: Static potential energy surfaces and fission fragment properties," Phys. Rev. C **90**, 054305 (2014).

[170] J. Erler, N. Birge, M. Kortelainen, W. Nazarewicz, E. Olsen, A. M. Perhac, and M. Stoitsov, "The limits of the nuclear landscape," Nature **486**, 509–512 (2012).

[171] R. Surman, M. Mumpower, and G. McLaughlin, "Systematic and Statistical Uncertainties in Simulated r-Process Abundances due to Uncertain Nuclear Masses," in *14th International Symposium on Nuclei in the Cosmos (NIC2016)*, edited by S. Kubono, T. Kajino, S. Nishimura, T. Isobe, S. Nagataki, T. Shima, and Y. Takeda (2017) p. 010612.

[172] Joel de Jesús Mendoza-Temis, Meng-Ru Wu, Karlheinz Langanke, Gabriel Martínez-Pinedo, Andreas Bauswein, and Hans-Thomas Janka, "Nuclear robustness of the *r* process in neutron-star mergers," Phys. Rev. C **92**, 055805 (2015).

[173] J. Duflo and A.P. Zuker, "Microscopic mass formulas," Phys. Rev. C **52**, R23–R27 (1995).

[174] B. S. Meyer, "Decompression of initially cold neutron star matter - A mechanism for the r-process?" Astrophys. J. **343**, 254–276 (1989).

[175] K. Langake and M. Wiescher, "Nuclear reactions and stellar processes," Rep. Prog. Phys. **64**, 1657–1701 (2001).

[176] S. Goriely, A. Bauswein, and H.-T. Janka, H.-T., "r-process nucleosynthesis in dynamically ejected matter of neutron star mergers," Astrophys. J. Lett. **738**, L32 (2011).

[177] S. Rosswog, O. Korobkin, A. Arcones, F.-K. Thielemann, and T. Piran, "The long-term evolution of neutron star merger remnants - I. The impact of r-process nucleosynthesis," MNRAS **439**, 744–756 (2014).

[178] Gordon Baym, Hans A. Bethe, and Christopher J Pethick, "Neutron star matter," Nucl. Phys. A **175**, 225 – 271 (1971).

[179] J. W. Negele and D. Vautherin, "Neutron star matter at sub-nuclear densities," Nucl. Phys. A **207**, 298–320 (1973).

[180] D. G. Ravenhall, C. J. Pethick, and J. R. Wilson, "Structure of matter below nuclear saturation density," Phys. Rev. Lett. **50**, 2066–2069 (1983).

[181] C. P. Lorenz, D. G. Ravenhall, and C. J. Pethick, "Neutron star crusts," Phys. Rev. Lett. **70**, 379–382 (1993).

[182] P. Magierski and A. Bulgac, "Nuclear hydrodynamics in the inner crust of neutron stars," Acta Phys. Pol. B **35**, 1203–1214 (2004).

[183] P. Magierski and P.-H. Heenen, "Structure of the inner crust of neutron stars: Crystal lattice or disordered phase?" Phys. Rev. C **65**, 045804 (2002).

[184] P. Avogadro, F. Barranco, R. A. Broglia, and E. Vigezzi, "Quantum calculation of vortices in the inner crust of neutron stars," Phys. Rev. C **75**, 012805 (2007).

[185] P. Avogadro, F. Barranco, R. A. Broglia, and E. Vigezzi, "Vortex-nucleus interaction in the inner crust of neutron stars," Nucl. Phys. A **811**, 378 – 412 (2008).

[186] P. M. Pizzochero, L. Viverit, and R. A. Broglia, "Vortex-nucleus interaction and pinning forces in neutron stars," Phys. Rev. Lett. **79**, 3347 – 3350 (1997).

[187] Pierre M. Pizzochero, "Pinning and Binding Energies for Vortices in Neutron Stars: Comments on Recent Results," (2007).

[188] Pierre M. Pizzochero, "Angular momentum transfer in Vela-like pulsar glitches," Astrophys. J. Lett. **743**, L20 (2011).

[189] Aurel Bulgac, Michael McNeil Forbes, and Rishi Sharma, "Strength of the vortex-pinning interaction from real-time dynamics," Phys. Rev. Lett. **110**, 241102 (2013).

[190] Yongle Yu and Aurel Bulgac, "Spatial structure of a vortex in low density neutron matter," Phys. Rev. Lett. **90**, 161101

(2003).
[191] L. R. Gasques, A. V. Afanasjev, E. F. Aguilera, M. Beard, L. C. Chamon, P. Ring, M. Wiescher, and D. G. Yakovlev, "Nuclear fusion in dense matter: Reaction rate and carbon burning," Phys. Rev. C **72**, 025806 (2005).
[192] E. G. Adelberger, A. García, R. G. Hamish Robertson, K. A. Snover, A. B. Balantekin, K. Heeger, M. J. Ramsey-Musolf, D. Bemmerer, A. Junghans, C. A. Bertulani, J.-W. Chen, H. Costantini, P. Prati, M. Couder, E. Uberseder, M. Wiescher, R. Cyburt, B. Davids, S. J. Freedman, M. Gai, D. Gazit, L. Gialanella, G. Imbriani, U. Greife, M. Hass, W. C. Haxton, T. Itahashi, K. Kubodera, K. Langanke, D. Leitner, M. Leitner, P. Vetter, L. Winslow, L. E. Marcucci, T. Motobayashi, A. Mukhamedzhanov, R. E. Tribble, Kenneth M. Nollett, F. M. Nunes, T.-S. Park, P. D. Parker, R. Schiavilla, E. C. Simpson, C. Spitaleri, F. Strieder, H.-P. Trautvetter, K. Suemmerer, and S. Typel, "Solar fusion cross sections. II. the *pp* chain and CNO cycles," Rev. Mod. Phys. **83**, 195–245 (2011).
[193] S. Schram and S. E. Koonin, "Pycnonuclear fusion rates," Astrophys. J. **365**, 296–300 (1990).
[194] A. V. Afanasjev, M. Beard, A. I. Chugunov, M. Wiescher, and D. G. Yakovlev, "Large collection of astrophysical *S* factors and their compact representation," Phys. Rev. C **85**, 054615 (2012).
[195] A. S. Umar, V. E. Oberacker, C. J. Horowitz, P.G. Reinhard, and J. A. Maruhn, "Swelling of nuclei embedded in neutron-gas and consequences for fusion," Phys. Rev. C **92**, 025808 (2015).
[196] D. G. Ravenhall, C. J. Pethick, and J. R. Wilson, "Structure of matter below nuclear saturation density," Phys. Rev. Lett. **50**, 2066–2069 (1983).
[197] Masa-aki Hashimoto, Hironori Seki, and Masami Yamada, "Shape of nuclei in the crust of neutron star," Progress of Theoretical Physics **71**, 320 (1984).
[198] H. A. Bethe, "Supernova mechanisms," Rev. Mod. Phys. **62**, 801–866 (1990).
[199] Hans-Thomas Janka, "Explosion mechanisms of core-collapse supernovae," Annual Review of Nuclear and Particle Science **62**, 407–451 (2012).
[200] C. J. Horowitz, M. A. Pérez-García, and J. Piekarewicz, "Neutrino-"pasta" scattering: The opacity of nonuniform neutron-rich matter," Phys. Rev. C **69**, 045804 (2004).
[201] M. D. Alloy and D. P. Menezes, "Nuclear "pasta phase" and its consequences on neutrino opacities," Phys. Rev. C **83**, 035803 (2011).
[202] M. Gearheart, W. G. Newton, J. Hooker, and Bao-An Li, "Upper limits on the observational effects of nuclear pasta in neutron stars," Monthly Notices of the Royal Astronomical Society **418**, 2343 (2011).
[203] Jose A. Pons, Daniele Vigano, and Nanda Rea, "A highly resistive layer within the crust of x-ray pulsars limits their spin periods," Nat Phys **9**, 431–434 (2013).
[204] Yuri Levin and Greg Ushomirsky, "Crust–core coupling and r-mode damping in neutron stars: a toy model," Monthly Notices of the Royal Astronomical Society **324**, 917 (2001).
[205] Minoru Okamoto, Toshiki Maruyama, Kazuhiro Yabana, and Toshitaka Tatsumi, "Nuclear "pasta" structures in low-density nuclear matter and properties of the neutron-star crust," Phys. Rev. C **88**, 025801 (2013).
[206] F. J. Fattoyev, C. J. Horowitz, and B. Schuetrumpf, "Quantum nuclear pasta and nuclear symmetry energy," Phys. Rev. C **95**, 055804 (2017).
[207] B. Schuetrumpf, K. Iida, J. A. Maruhn, and P.-G. Reinhard, "Nuclear "pasta matter" for different proton fractions," Phys. Rev. C **90**, 055802 (2014).
[208] M. Baldo, C. Maieron, P. Schuck, and X. Viñas, "Low densities in nuclear and neutron matters and in the nuclear surface," Nuclear Physics A **736**, 241 – 254 (2004).
[209] G. Audi, A.H. Wapstra, and C. Thibault, "The ame2003 atomic mass evaluation," Nuclear Physics A **729**, 337 – 676 (2003), the 2003 NUBASE and Atomic Mass Evaluations.
[210] T. Niksic, D. Vretenar, and P. Ring, "Relativistic nuclear energy density functionals: Mean-field and beyond," Prog. Part. Nucl. Phys. **66**, 519 (2011).
[211] S. E. Agbemava, A. V. Afanasjev, D. Ray, and P. Ring, "Global performance of covariant energy density functionals: Ground state observables of even-even nuclei and the estimate of theoretical uncertainties," Phys. Rev. C **89**, 054320 (2014).
[212] M. Baranger and M. Véneroni, "An adiabatic time-dependent Hartree-Fock theory of collective motion in finite systems," Ann. Phys. (NY) **114**, 123 – 200 (1978).
[213] D. M. Brink, M. J. Giannoni, and M. Veneroni, "Derivation of an adiabatic time-dependent Hartree-Fock formalism from a variational principle," Nucl. Phys. A **258**, 237–256 (1976).
[214] N. Schunck, J. Dobaczewski, J. McDonnell, J. Moré, W. Nazarewicz, J. Sarich, and M. V. Stoitsov, "One-quasiparticle states in the nuclear energy density functional theory," Phys. Rev. C **81**, 024316 (2010).
[215] J. Engel, "Intrinsic-density functionals," Phys. Rev. C **75**, 014306 (2007).
[216] Nir Barnea, "Density functional theory for self-bound systems," Phys. Rev. C **76**, 067302 (2007).
[217] B. G. Giraud, "Scalar nature of the nuclear density functional," Phys. Rev. C **78**, 014307 (2008).
[218] B. G. Giraud, "Density functionals in the laboratory frame," Phys. Rev. C **77**, 014311 (2008).
[219] B. G. Giraud, B. K. Jennings, and B. R. Barrett, "Existence of a density functional for an intrinsic state," Phys. Rev. A **78**, 032507 (2008).
[220] Jérémie Messud, Michael Bender, and Eric Suraud, "Density functional theory and kohn-sham scheme for self-bound systems," Phys. Rev. C **80**, 054314 (2009).
[221] Jérémie Messud, "Generalization of internal density-functional theory and kohn-sham scheme to multicomponent self-bound systems, and link with traditional density-functional theory," Phys. Rev. A **84**, 052113 (2011).
[222] Jérémie Messud, "Alternate, well-founded way to treat center-of-mass correlations: Proposal of a local center-of-mass correlations potential," Phys. Rev. C **87**, 024302 (2013).
[223] J.L. Egido and L.M. Robledo, "Angular Momentum Projection and Quadrupole Correlations Effects in Atomic Nuclei," in *Extended Density Functionals in Nuclear Structure Physics*, edited by Georgios A. Lalazissis, Peter Ring, and Dario Vretenar (Springer Berlin Heidelberg, Berlin, Heidelberg, 2004) pp. 269–302.
[224] David García-Aldea and J. E. Alvarellos, "Kinetic energy density study of some representative semilocal kinetic energy functionals," J. Chem. Phys. **127**, 144109 (2007).
[225] J. W. Negele and D. Vautherin, "Density-matrix expansion for an effective nuclear hamiltonian," Phys. Rev. C **5**, 1472–1493 (1972).
[226] J. W. Negele and D. Vautherin, "Density-matrix expansion for an effective nuclear hamiltonian. II," Phys. Rev. C **11**, 1031–1041 (1975).
[227] B. Gebremariam, T. Duguet, and S. K. Bogner, "Improved density matrix expansion for spin-unsaturated nuclei," Phys. Rev. C **82**, 014305 (2010).
[228] W. Stocker, J. Bartel, J.R. Nix, and A.J. Sierk, "Anomaly in the nuclear curvature energy," Nucl. Phys. A **489**, 252 – 268

(1988).
[229] M. Brack, B. K. Jennings, and Y. H. Chu, "On the extended Thomas-Fermi approximation to the kinetic energy density," Phys. Lett. B **65**, 1 – 4 (1976).
[230] Aurel Bulgac, "Semilocal approach to nonlocal equations," Nucl. Phys. A **487**, 251 – 268 (1988).
[231] Michael McNeil Forbes and Rishi Sharma, "Validating simple dynamical simulations of the unitary Fermi gas," Phys. Rev. A **90**, 043638 (2014).
[232] X. Viñas, M. Centelles, X. Roca-Maza, and M. Warda, "Density dependence of the symmetry energy from neutron skin thickness in finite nuclei," Eur. Phys. J. A **50**, 27 (2014).
[233] C. J. Horowitz, E. F. Brown, Y. Kim, W. G. Lynch, R. Michaels, A. Ono, J. Piekarewicz, M. B. Tsang, and H. H. Wolter, "A way forward in the study of the symmetry energy: Experiment, theory, and observation," J. Phys. G **41**, 093001 (2014).
[234] B. Alex Brown, "Constraints on the Skyrme equations of state from properties of doubly magic nuclei," Phys. Rev. Lett. **111**, 232502 (2013).
[235] B. Alex Brown and A. Schwenk, "Constraints on Skyrme equations of state from properties of doubly magic nuclei and *ab initio* calculations of low-density neutron matter," Phys. Rev. C **89**, 011307 (2014).
[236] A. F. Fantina, N. Chamel, J. M. Pearson, and S. Goriely, "Constraints on the equation of state of cold dense matter from nuclear physics and astrophysics," EPJ Web Conf. **66**, 07005 (2014).
[237] J. Erler, C. J. Horowitz, W. Nazarewicz, M. Rafalski, and P.-G. Reinhard, "Energy density functional for nuclei and neutron stars," Phys. Rev. C **87**, 044320 (2013).
[238] C. F. Perdrisat, V. Punjabi, and M. Vanderhaeghen, "Nucleon electromagnetic form factors," Progress in Particle and Nuclear Physics **59**, 694 – 764 (2007).
[239] T. R. Gentile and C. B. Crawford, "Neutron charge radius and the neutron electric form factor," Phys. Rev. C **83**, 055203 (2011).